

Discrete intrinsic localized modes in a microelectromechanical resonator

Authors: Adarsh Ganesan, Cuong Do and Ashwin A. Seshia

Intrinsic Localized Modes (ILMs) or Discrete Breathers (DBs) are produced through a non-linear vibration localization phenomenon. While Anderson localization is due to lattice defects, the nonlinearity of lattices provides the basis for ILM excitation. Over the past two decades, these ILMs have been realized in a wide range of physical systems including photonic crystals, nonlinear atomic lattices, anti-ferromagnets, coupled Josephson junction arrays and coupled cantilevers. This paper brings out the feasibility of exciting ILMs in a standalone mechanical resonator. Through piezoelectric driving and optical visualization, various intriguing features of ILMs have been recorded. The ILMs in our system are observed as spectral bushes and their frequencies are much lower than that of the drive frequency. The excitation of ILMs is mediated through large amplitude instability following autoparametric excitation of a sub-harmonic mode. The spatial prevalence of discrete ILM excitations is at antinodes of the sub-harmonic mode. Further, the ILMs have been observed to be time-variant and various events including attraction-repulsion (or splitting-merging) of ILMs and hopping occur during the time evolution of ILMs.

Intrinsic localized modes (ILM) or Discrete Breathers (DBs) have been a subject of interest for the last two decades ever since the pioneering generalization by Takeno and co-workers [1-3]. Such nonlinear vibration energy localization phenomenon has had much impact in condensed matter physics [4-6] and led to the understanding and control of physical processes [7-10] involving high density vibration energy. The key features concerning ILMs are nonlinearity [1-3] and discreteness [11-12]. Also, these ILMs are not externally imposed as in the case of Anderson localization [13-14] rather due to intrinsic nonlinearity. More recently, the presence of ILMs in a wide range of physical systems including photonic crystals [15], nonlinear atomic lattices [16], anti-ferromagnets [17] and coupled Josephson junction arrays [18] has been demonstrated. Particularly, in the mechanical domain, ILMs have been experimentally realized through the elastic coupling of cantilevers [19]. Regardless of these empirical evidences for the existence of ILMs in various physical systems, ILMs have largely been a subject of 'theoretical' physics. This can be attributed to the lack of experimental techniques for the controlled probing of both the nonlinearity and discreteness of ILMs.

This paper brings out the feasibility of exciting travelling ILMs in a standalone microelectromechanical resonator. Using the combination of Laser Doppler Vibrometry (LDV) and piezoelectric driving, we observed the two-dimensional transport of ILMs on mechanical structure

and many interesting features of ILMs are recorded. This seemingly simple device (and other similar devices) can therefore form an experimental testbed for the future experimental investigations of ILMs. Such devices can be fabricated using conventional semiconductor micromachining techniques. Also, the complementary visualization of ILM transport within a single resonator element at microscopic resolution can lead to intriguing and surprising concepts concerning the behaviour of ILMs. The concept concerning the ILM excitation in a micromechanical resonator is presented next.

Theory- Our single mechanical resonator can be modelled as a nonlinear lattice. The equations of motion of each element in the resonator can then be written as [2],

$$\ddot{u}_n + Q^{-1}\dot{u}_n + [1 - H\cos(\omega_d t)]u_n + \alpha u_n^3 + \hat{\eta}u_n^2\dot{u}_n - \frac{1}{2}D(u_{n+1} - 2u_n + u_{n-1}) = 0 \quad (1)$$

where u_n describes the displacement of n^{th} oscillator from the initial position with $n = 0, 1, 2, \dots, N$ and fixed boundary conditions $u_0 = u_{N+1} = 0$; Q is the quality factor of mechanical resonance; H represents the parametric excitation threshold; ω_d is the drive frequency; α captures the cubic nonlinearity of individual oscillators and $\hat{\eta}$ is the nonlinear damping coefficient; D describes the coupling between oscillators. Under weak random noise, the dynamics presented in eq. (1) have been solved in [20] and found to result in spatio-temporally evolving ILM excitation.

For the experimental realization of ILMs, a 1-D extensional-compressional mechanical mode (Figure S1) (eigen-frequency 3.86 MHz) of free-free beam structure of dimensions $1100 \mu m \times 350 \mu m \times 11 \mu m$ (Figure 1A) is considered. A $0.5 \mu m$ thick AlN layer is harnessed for the piezoelectric excitation of the structure (Figure S1). An electrical signal for driving the mechanical mode is fed through one of the split electrodes. Through optical visualization using LDV, an insightful assessment of ILM behaviour can be carried out. Due to the capture area limitation with our vibrometry setup, only one half of the device is imaged. The measurements are carried out at a spatial resolution of $35 \mu m$ and $125 Hz$ spectral resolution which leads to a reasonable temporal resolution of 1 minute. Higher temporal resolution can be reached by compromising the spatial or spectral resolution to probe fast moving ILMs.

At the drive power level $0 dBm$, the frequency spectrum consists of just the drive tone. In contrast, at $10 dBm$, the excitation of low frequency ILMs and the sub-harmonic mode is also observed along with the drive tone (Figure 1B). The sub-harmonic mode is auto-parametrically excited through coupling to the drive mode. Also, during this process, an apparent increase in the background noise floor is observed in the frequency spectrum. This observation of an elevated noise floor (Figure 1B) is qualitatively linked to the observation of ILM excitation. Figure 1C shows elevated displacement amplitudes at frequencies ω_i (ILM) and $\omega_d/2$ upon crossing the drive power threshold for auto-

parametric excitation. The displacement profiles at the tones ω_d and $\omega_d/2$ are shown in figure 1D. Figure 1D also provides evidence for hysteresis observed in the displacement response of the sub-harmonic mode. Despite this, ILM displacements of forward and backward amplitude sweep are almost equal. This may be due to either reduced displacement of sub-harmonic and driven modes or a stochastic ILM destruction process. The RMS displacement profile (Figure 1E), in the spectral range 35 – 75 kHz, indicate the presence of ILMs at a discrete point. The weighted distribution of all spectral lines corresponding to ILM excitation in the range 35 – 75 kHz indicates the presence of two spectral bushes. The dominant and weak spectral bushes are observed in the frequency ranges 50 – 70 kHz and 40 – 50 kHz respectively.

It is also to note that the spatial average frequency spectrum (Figure 2A) at the drive power level presents an ensemble of three sub-processes: auto-parametric excitation of sub-harmonic mode (Figure 2a1); excitation of low frequency ILMs (Figures 2a2 and 2a3) and the individual inherent coupling of ILMs with sub-harmonic (Figure 2a4) and driven modes (Figure 2a5). The coupling results in the splitting of sub-harmonic and driven modes at the location of ILM excitation (Figure 2a2) and the resultant spectral lines are spaced away by twice the frequency of ILMs (Figures 2a4 and 2a5). Due to sub-harmonic excitation, the overall vibration mode shape is a merger of sub-harmonic and driven mode shapes. Since the sub-harmonic excitation is significantly higher in magnitude, the vibration mode shape simply corresponds to sub-harmonic mode shape (Figure 2b1). Hence, the maximal displacements are associated with both the antinodes of sub-harmonic mode. The displacement profiles corresponding to a large set of ILM experiments (Supplementary S2) indicate the prevalence of ILM excitations at the spatial locations of maximal displacement (Figure 2b2). In order to understand the drive frequency and amplitude dependence on ILMs and the corresponding modulation of drive tone, frequency detuning and amplitude control measurements were taken. The drive amplitude does not influence the shape of frequency spectrum (3.7 – 4 MHz) and hence, also the ILMs (Figures 2c1-2c3). The drive frequency similarly did not influence the ILMs (Figures 2c4-2c6) observed and the additional tones $\omega_d \pm \omega_i$ follow the drive tone ω_d . Although the ILM behaviour is not drastically influenced by drive amplitude and frequency, there is some minor modulation around $\omega_d \pm \omega_i$ due to ILMs (ω_i) (Figures 2c1-2c6). This can be due to the temporal changes in ILMs during the course of experiments.

In order to validate the temporal dependence of ILMs, the displacements in the spectral range 35 – 75 kHz were imaged every minute for about 30-60 minutes from the time when the drive signal is introduced. This entire process was carried out several times. (The entire set of experimental data is provided in the supplementary material S2.) The RMS displacement patterns

(supplementary S2) provide the evidence for variations in spatial locations corresponding to ILMs. During these measurements, a number of interesting features of ILMs were recorded and a few are presented below.

1 – Spatial stabilization – In run 2, from 32th minute, there is an evidence for locking of ILMs at a spatial location *a1* for a long period of atleast 20 minutes (Figure 3-A).

2 – Hopping – In run 3, from 35th to 37th minute, the ILMs are seen to hop from points *b1* and *b2* to *b3* respectively (Figure 3-B).

3 – Attraction-repulsion of breathers – In run 4, from 7th to 9th minute, the ILMs at the points *c1* and *c3* tend to coalesce and separate due to attraction and repulsion respectively and as a result, the displacement at *c3* increases and decreases and corresponding decrease and increase in the displacement is observed at *c4* (Figure 3-C). This behaviour may also be conceived as ‘ILM Splitting’ [20].

In summary, we have experimentally observed both the discreteness and nonlinearity of ILMs in a micromechanical resonator. Unlike the ILMs in coupled cantilevers [19], the ILMs in our system are observed as spectral bushes and their frequencies are much smaller than that of the drive. The excitation of ILMs in our mechanical resonator is mediated via autoparametric excitation of a sub-harmonic mode and the concomitant apparent increase in noise floor around the carrier. The inherent property of noise sensitive ILM excitation, can also present a basis for in-depth fundamental investigations and characterization of stochastic processes through ILM responses. Our results also showcase different compulsive features of ILMs including hopping, attraction-repulsion and single and spatial stabilization. Such features can be individual subjects for future experimental investigations. The various physical aspects of ILMs reported in this letter also motivate the development of a predictive first-principles model.

Acknowledgements

Funding from the Cambridge Trusts is gratefully acknowledged.

Authors’ contributions

AG and CD designed the device and performed the experiments; AG and AAS analyzed the results and wrote the manuscript; AAS supervised the research.

References

- [1] A. S. Dolgov, *Sov. Phys. Solid State* 28, 907 (1986)
- [2] A. J. Sievers and S. Takeno, *Phys. Rev. Lett.* 61, 970 (1988)
- [3] J. B. Page, *Phys. Rev. B* 41, 7835 (1990)
- [4] P. M. Chaikin and T. C. Lubensky, *Principles of Condensed Matter Physics* (Cambridge University Press, Cambridge, England, 1995), Chap. 10.
- [5] A. M. Kosevich, B. A. Ivanov, and A. S. Kovalev, *Phys. Rep.* 194, 117 (1990).
- [6] H.-J. Mikeska and M. Steiner, *Adv. Phys.* 40, 191 (1991).
- [7] A. S. Davydov, *Physica scripta* 20, 387 (1979).
- [8] A. S. Davydov, *Biology and Quantum Mechanics* (Pergamon, New York, 1982)
- [9] H. Kellouai *et al.*, *Journal of biological physics* 21, 25 (1995).
- [10] *Davydov's Soliton Revisited: Self-Trapping of Vibrational Energy in Protein*, edited by P. L. Christiansen and A. C. Scott (Plenum Press, New York, 1990), Sec. IV.
- [11] S. Flach, K. Kladko, and R. S. MacKay, *Phys. Rev. Lett.* 78, 1207 (1997)
- [12] W.-Z. Wang *et al.*, *Phys. Rev. Lett.* 76, 3598 (1996)
- [13] E. Abrahams *et al.*, *Phys. Rev. Lett.* 42, 673 (1979).
- [14] J. Billy *et al.*, *Nature* 453, 891 (2008).
- [15] J. W. Fleischer *et al.*, *Nature* 422, 147 (2003).
- [16] B. I. Swanson *et al.*, *Phys. Rev. Lett.* 82, 3288 (1999).
- [17] M. Sato, and A. J. Sievers, *Nature* 432, 486 (2004).
- [18] E. Trias, J. J. Mazo, and T. P. Orlando, *Phys. Rev. Lett.* 84, 741 (2000).
- [19] M. Sato *et al.*, *Phys. Rev. Lett.* 90, 044102 (2003).
- [20] E. Kenig *et al.*, *Phys. Rev. E* 80, 046202 (2009).

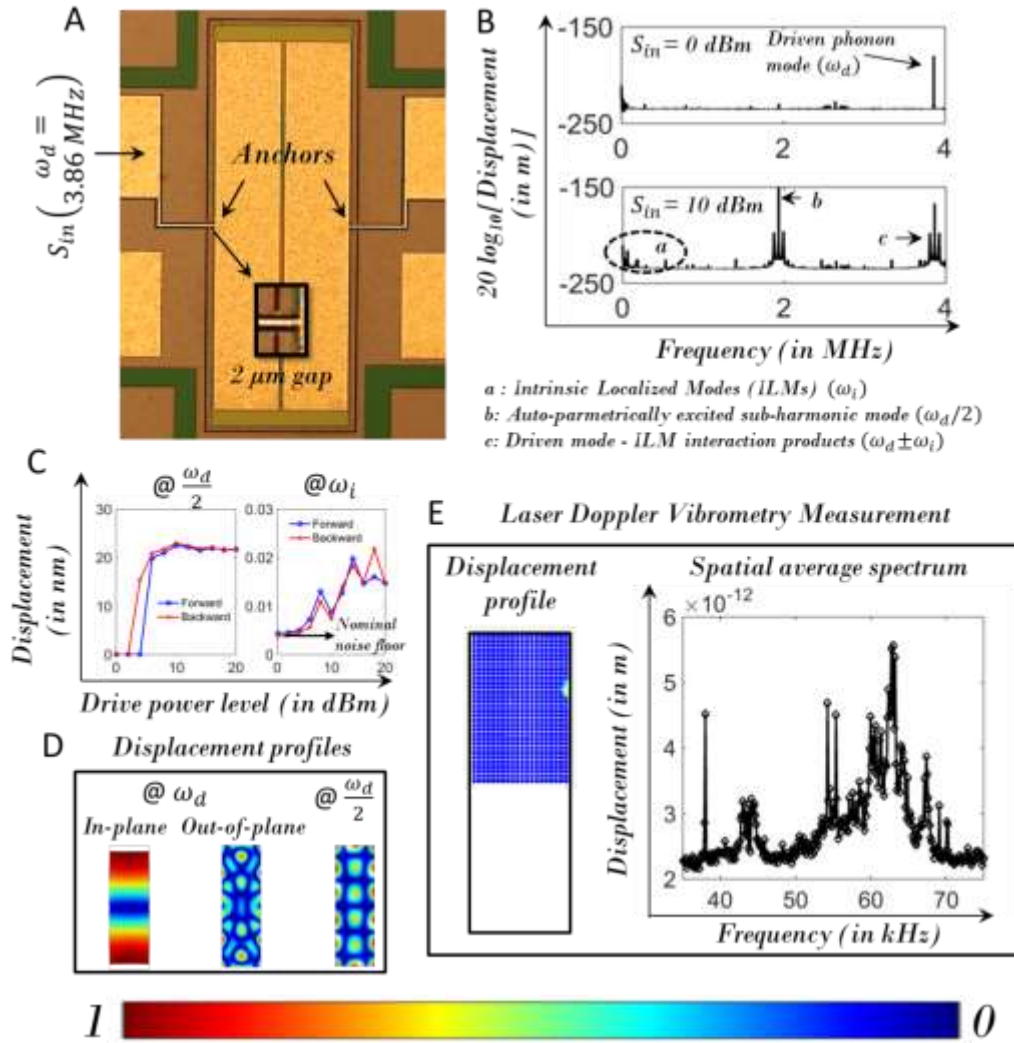


Figure 1: **Observation of Intrinsic Localized Modes.** A: Signal $S_{in}(\omega_d = 3.86 \text{ MHz})$ is applied on a free-free beam microstructure; B: At $S_{in} = 0 \text{ dBm}$, the spectral line is present at 3.86 MHz and at $S_{in} = 10 \text{ dBm}$, additional spectral lines are observed at ω_i , $\omega_d \pm \omega_i$, $\frac{\omega_d}{2}$, $\frac{\omega_d}{2} \pm \omega_i$; C: Displacement levels at the frequencies ω_i (corresponding to the maximum displacement in the spectral range $35 - 75 \text{ kHz}$) and $\frac{\omega_d}{2} = 1.93 \text{ MHz}$ for forward and backward amplitude sweep; D: Displacement profiles at the frequencies $\omega_d = 3.86 \text{ MHz}$ and $\frac{\omega_d}{2} = 1.93 \text{ MHz}$; E: Left: RMS displacement profile (averaged over the spectral range $35 - 75 \text{ kHz}$); E: Right: The spatial average frequency spectrum over a specific one minute interval. Note: The displacement profiles are normalized to the maximum displacement in the structure as color-coded.

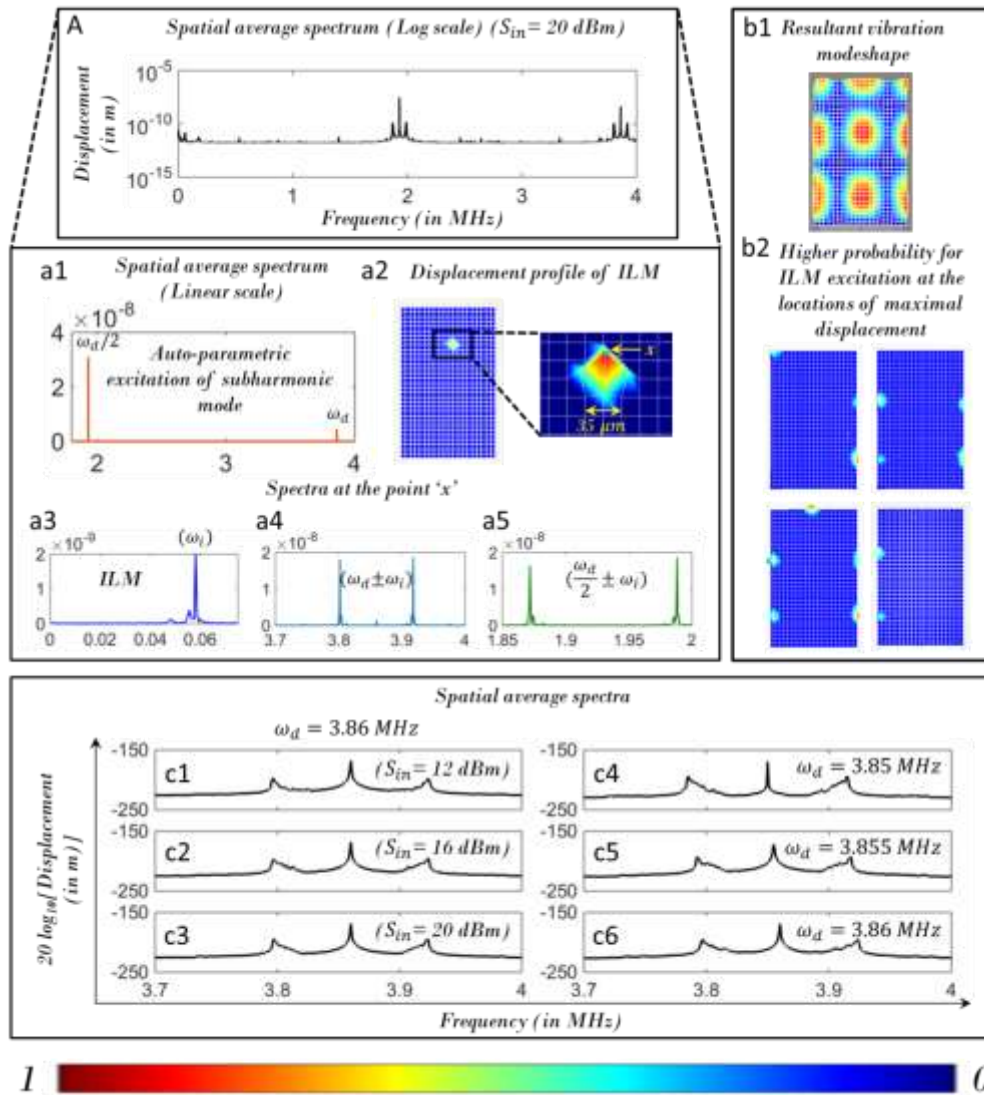


Figure 2: **Spatio-spectral features of Intrinsic Localized Modes.** A: Spatial average spectrum (Log scale) at the drive power level $S_{in}(\omega_d = 3.86 \text{ MHz}) = 20 \text{ dBm}$; a1: Spatial average spectrum (Linear scale) indicating the significant excitation of sub-harmonic mode via auto-parametric resonance; a2: Displacement profile of ILM at frequency 57.6 kHz indicating the elevated displacement at the point x ; a3-a4: Spectrum at the point x , zoomed into the frequency ranges $0 - 70 \text{ kHz}$; $3.7 - 4 \text{ MHz}$ and $1.85 - 2 \text{ MHz}$ respectively; b1: Resultant vibration pattern (averaged over the spectral range $0 - 5 \text{ MHz}$) of the beam; b2: The RMS displacement profiles (averaged over the spectral range $35 - 75 \text{ kHz}$) at the 12^{th} , 14^{th} and 16^{th} minutes of run 2 and at the 10^{th} minute of run 3 indicating the spatial prevalence of ILMs; c1-c3: The spatial average spectra for the drive power levels $S_{in}(\omega_d = 3.86 \text{ MHz}) = 12, 16$ and 20 dBm respectively; c4-c6: The spatial average spectra for the drive frequencies $\omega_d = 3.85, 3.855$ and 3.86 MHz respectively. Note: The displacement profiles are normalized to the maximum displacement in the structure- i.e. Red corresponds to 1 and blue corresponds to 0.

RMS Displacement profiles

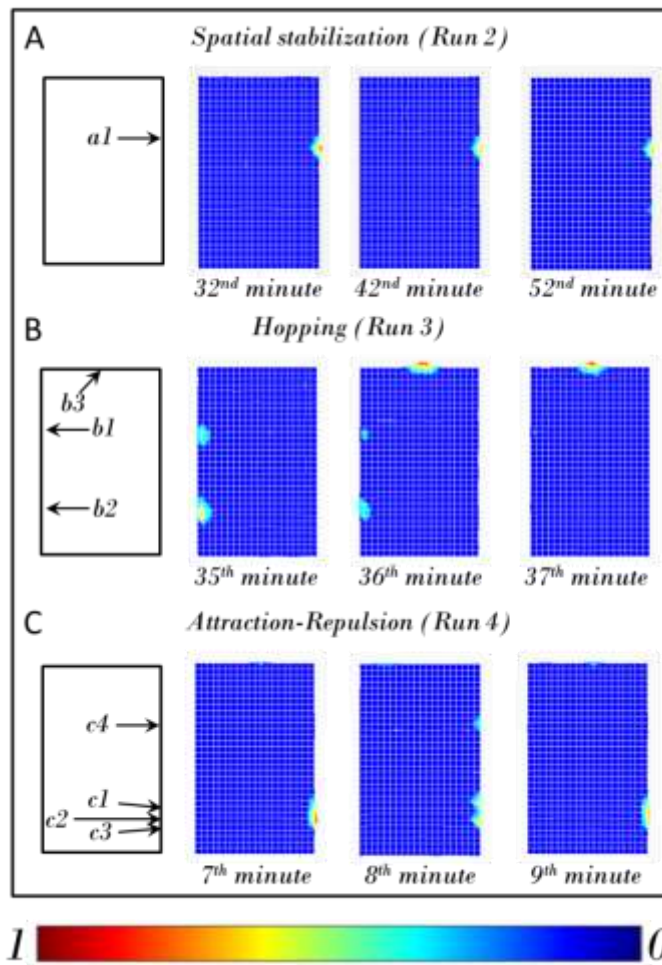


Figure 3: **Temporal dependence of Intrinsic Localized Modes.** A correspond to spatial stabilization feature; B correspond to the attraction-repulsion feature; C correspond to the hopping feature. Note 1: The RMS displacement profiles (averaged over the spectral range 35 – 75 kHz) are normalized to the maximum displacement in the structure. Note 2: The RMS displacement profiles are selected from the supplementary section S2.

Supplementary Information

Discrete intrinsic localized modes in a microelectromechanical resonator

Authors: Adarsh Ganesan¹, Cuong Do¹, Ashwin Seshia¹

1. Nanoscience Centre, University of Cambridge, Cambridge, UK

Supplementary section S1

Operation of piezoelectrically driven micromechanical resonator

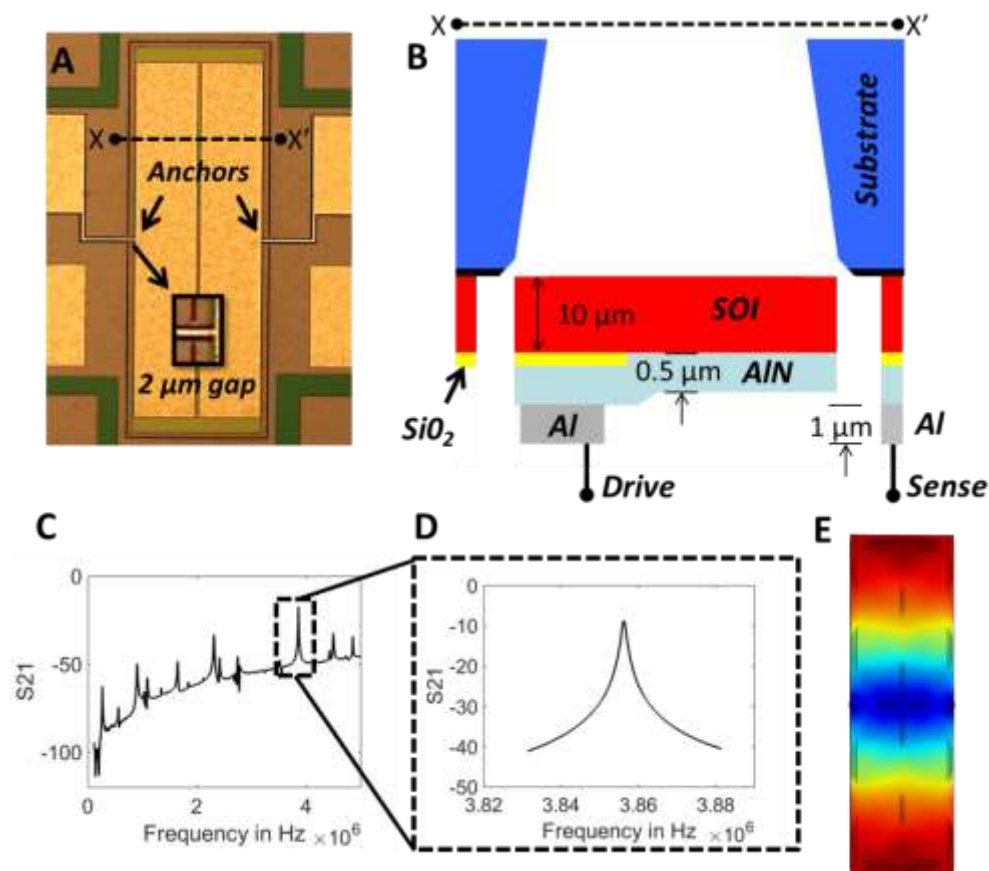
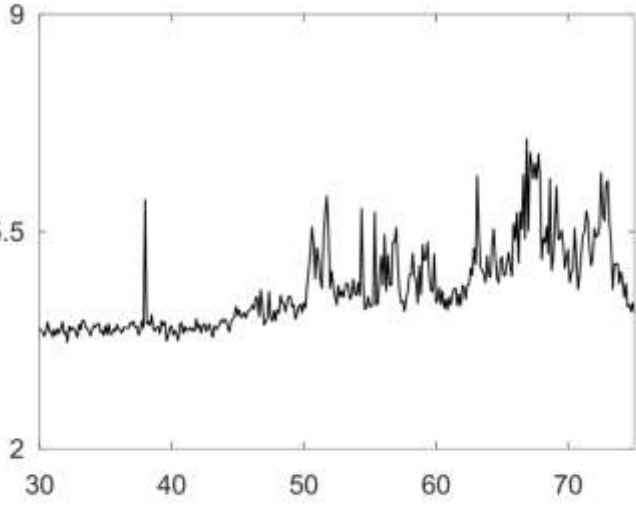
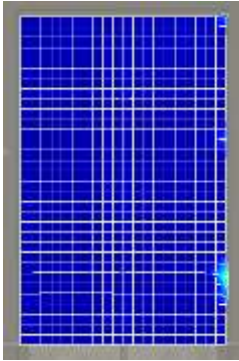
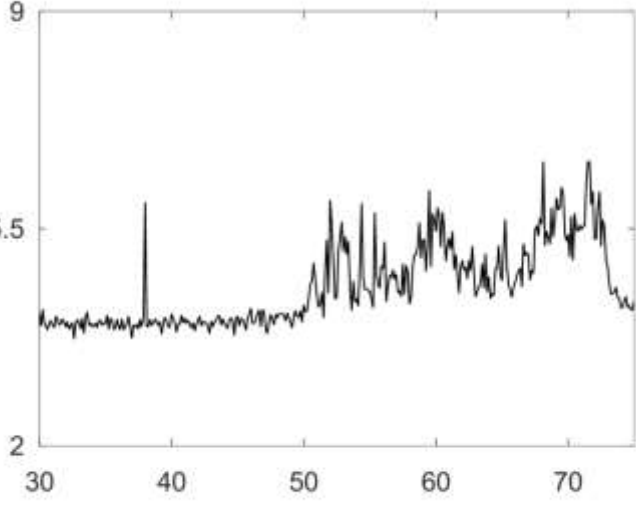
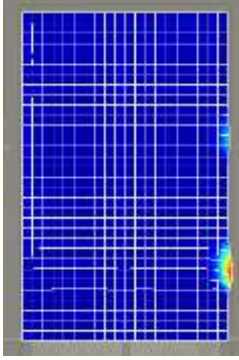


Figure S1: Operation of piezoelectrically driven micromechanical resonator: **A:** Free-free beam topology with 2 μm air gap for in-plane mode excitation; **B:** 1 μm thick Al electrodes patterned on 0.5 μm thick AlN piezoelectric film which is in-turn patterned on SOI substrate; the 10 μm thick SOI layer is then released through back-side etch to realize mechanical functionality; **C:** The scattering parameter S₂₁ denoting forward transmission gain across a broad range of frequencies from 0-4.5 MHz; **D:** across a smaller range of frequencies 3.83-3.88 MHz; **E:** Resonant mode shape of ~3.86 MHz vibrations from eigen-frequency analysis in COMSOL and Doppler shift vibrometry.

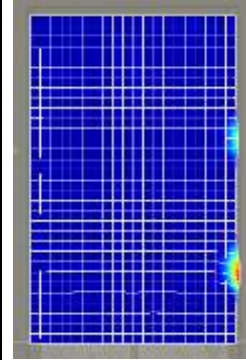
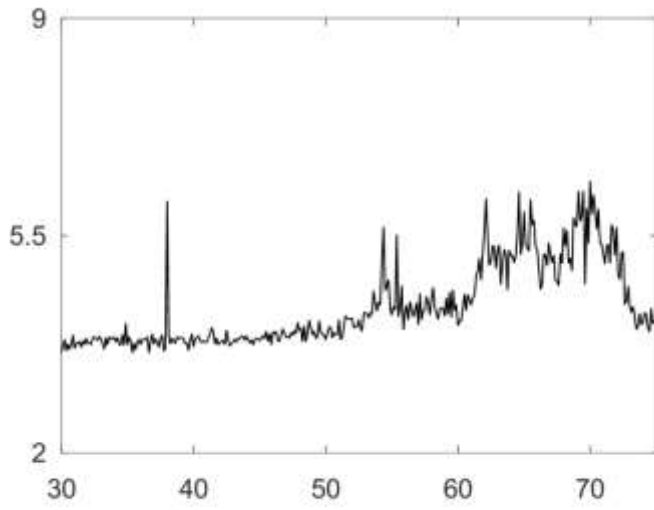
Supplementary section S2

Frequency responses and RMS surface displacement profiles obtained using Laser Doppler Vibrometry at different drive conditions

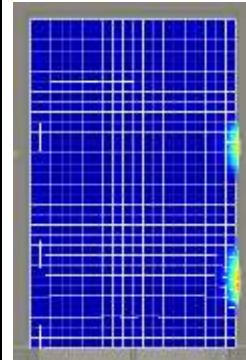
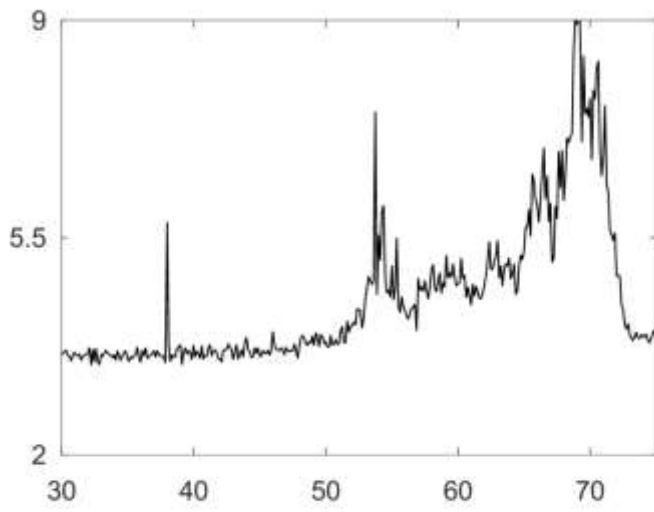
Run 1

Time	Displacement (in pm) vs. Frequency (in kHz)	RMS Surface Displacement 1.2 nm  0 nm
1		
2		

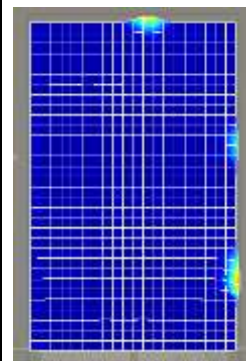
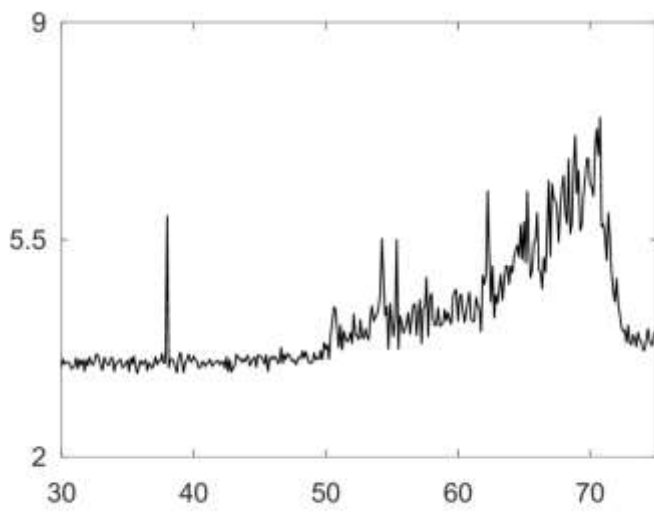
3



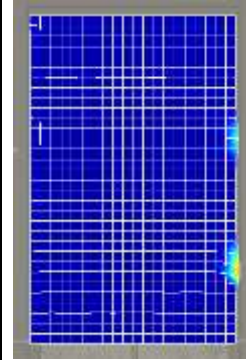
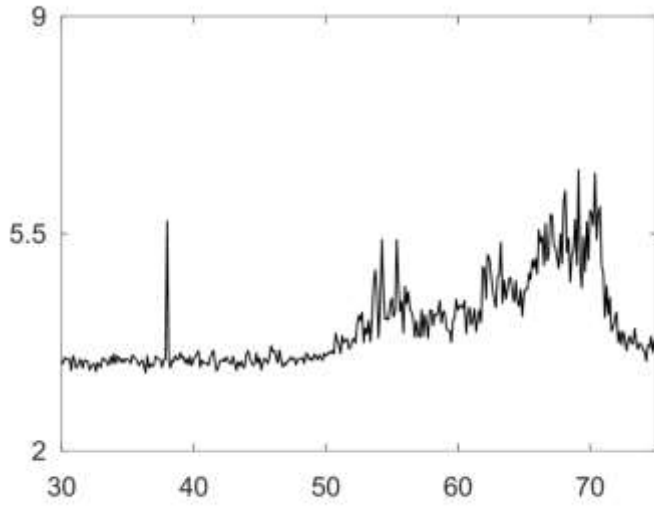
4



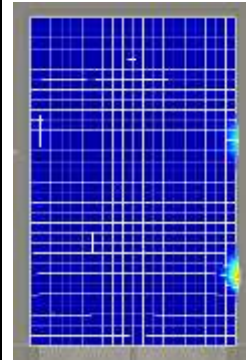
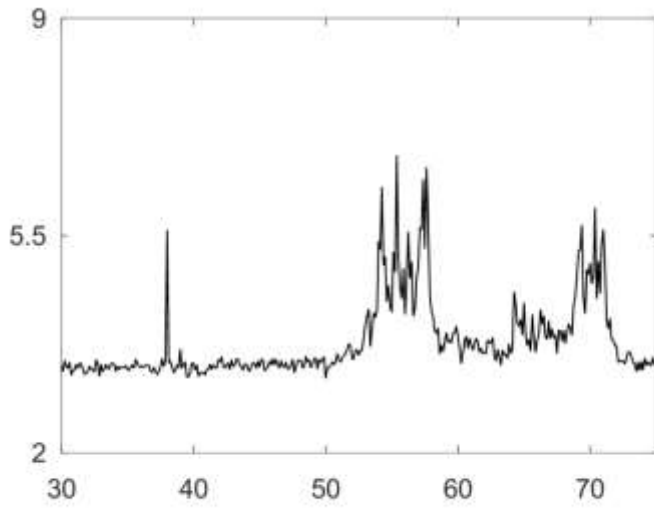
5



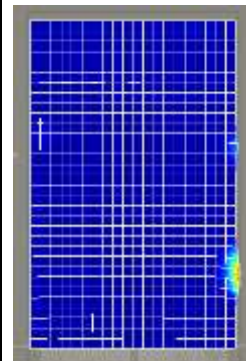
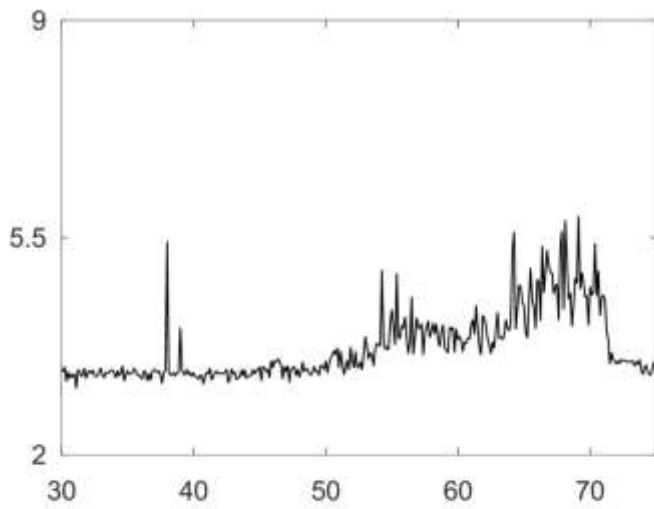
6



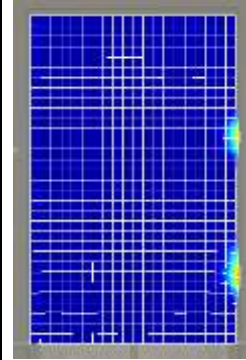
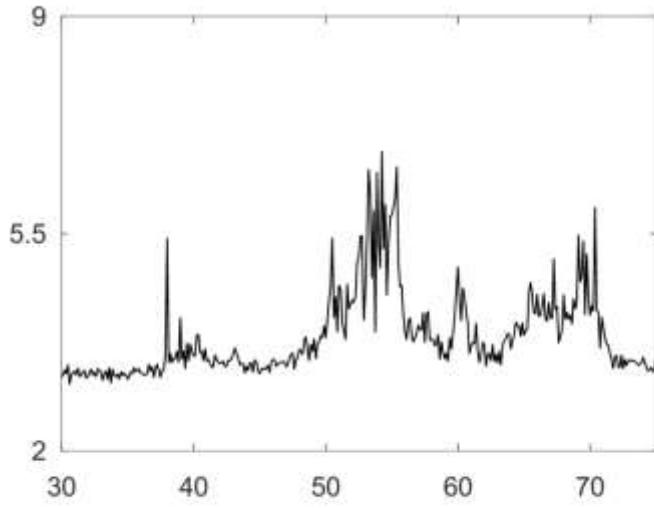
7



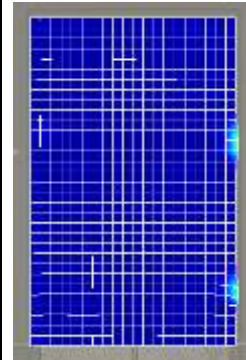
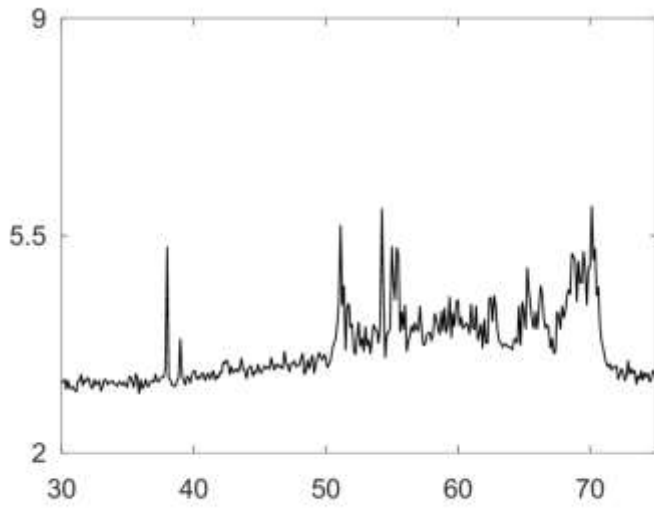
8



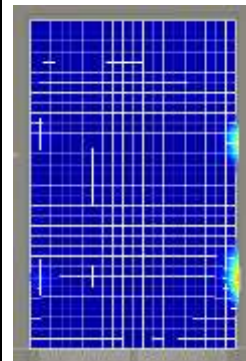
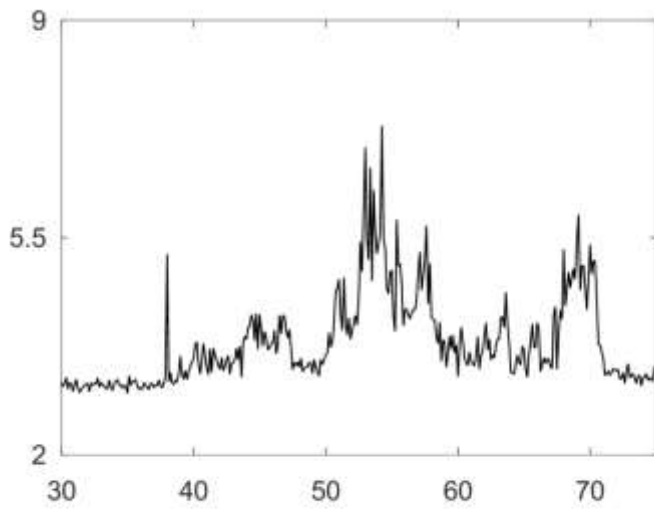
9



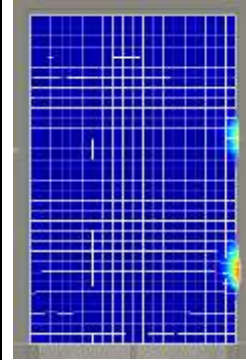
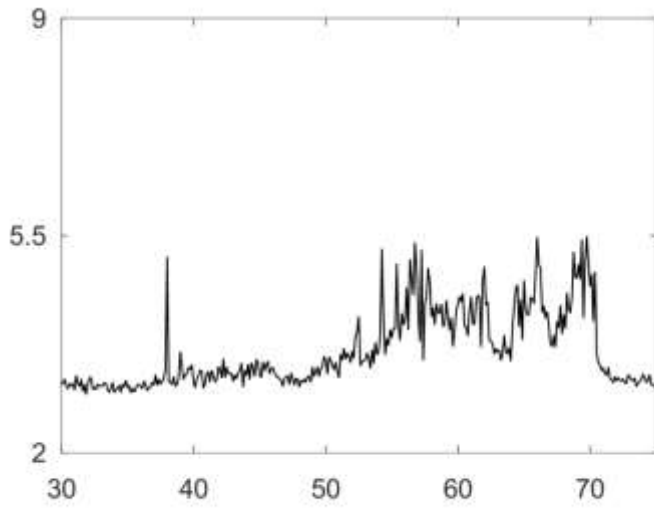
10



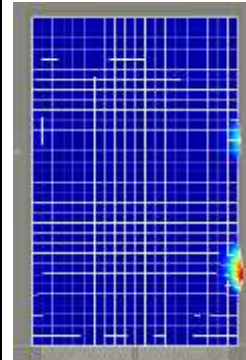
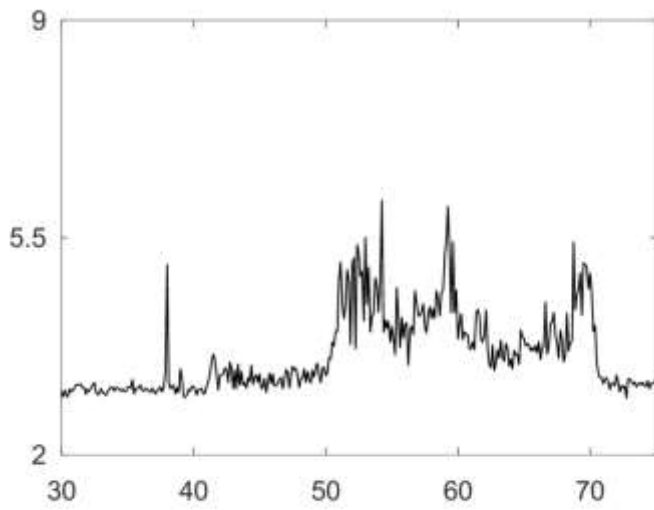
11



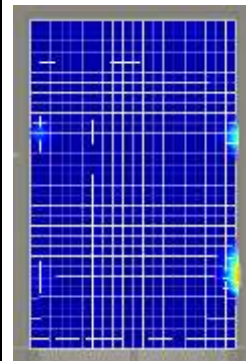
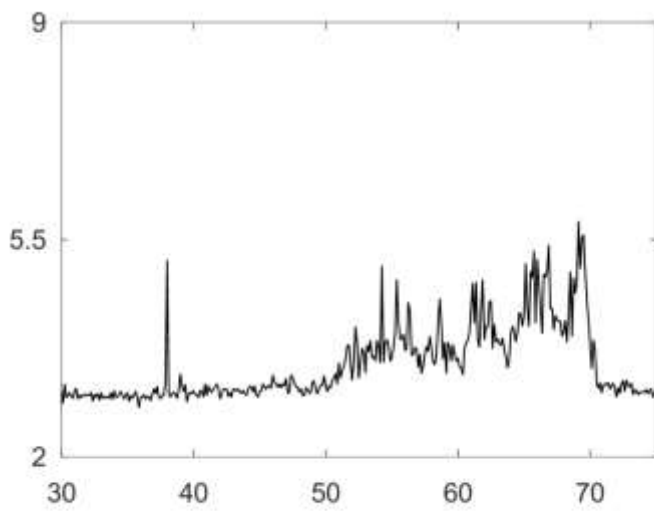
12



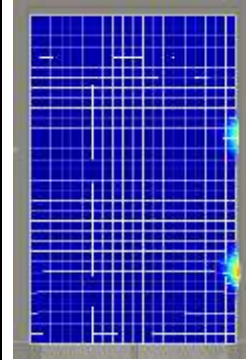
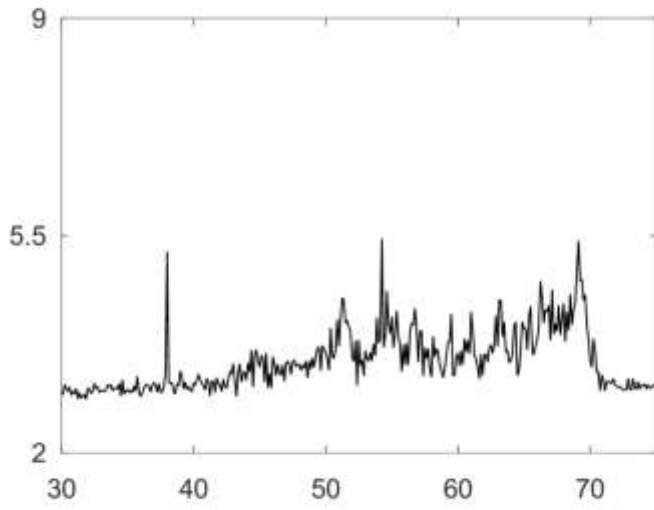
13



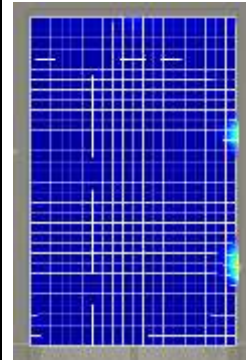
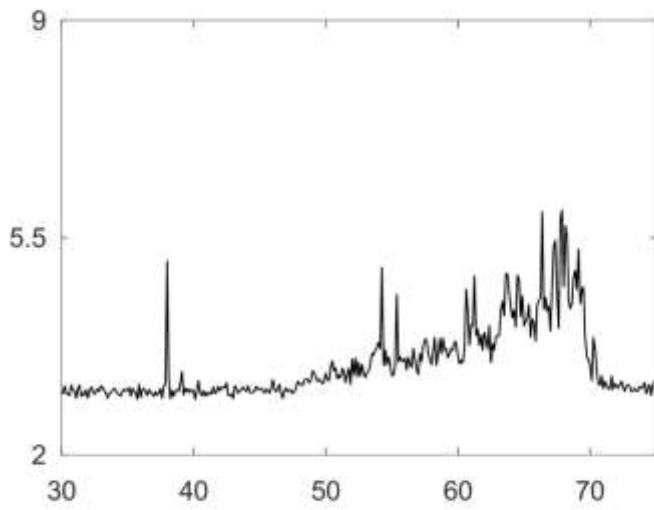
14



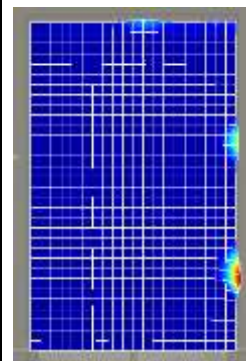
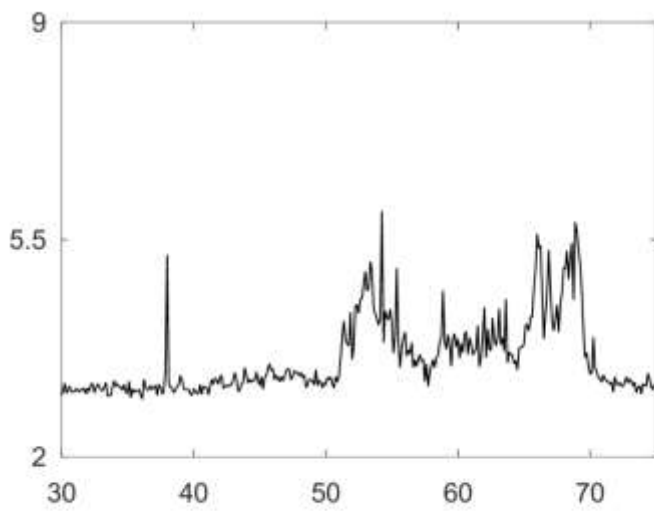
15



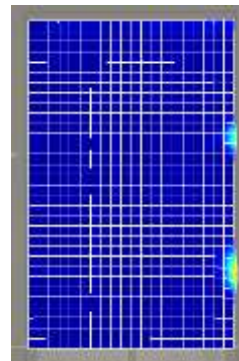
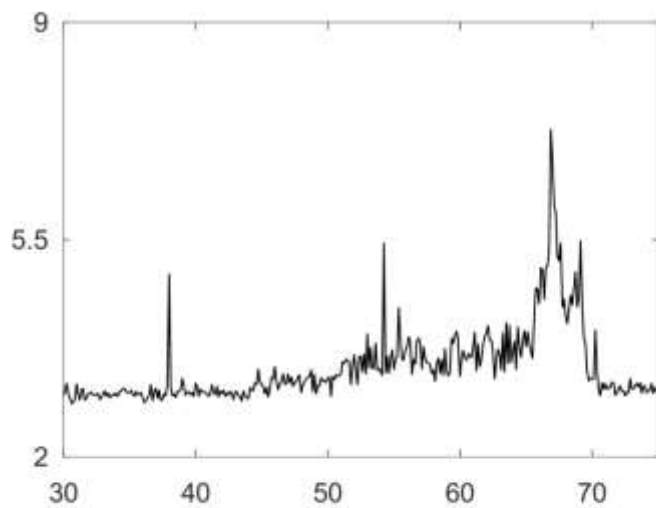
16



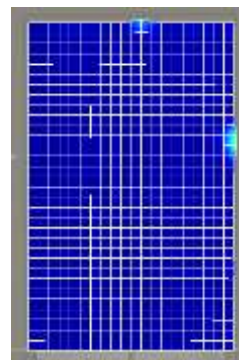
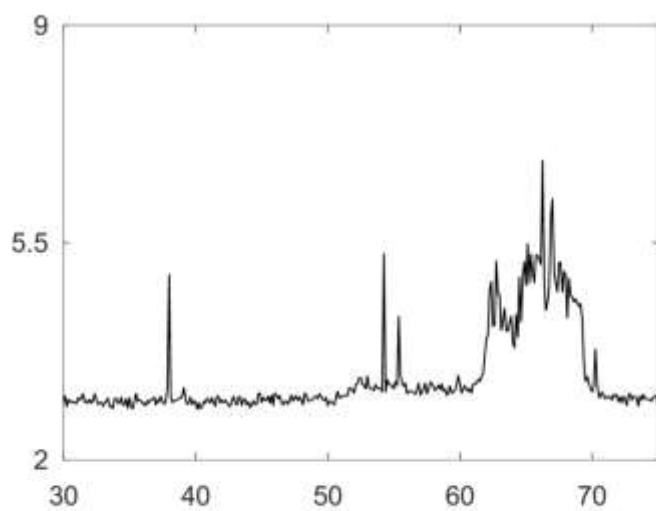
17



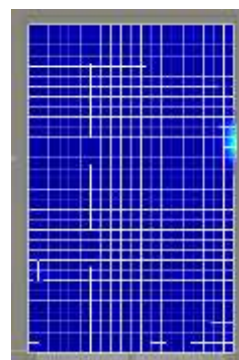
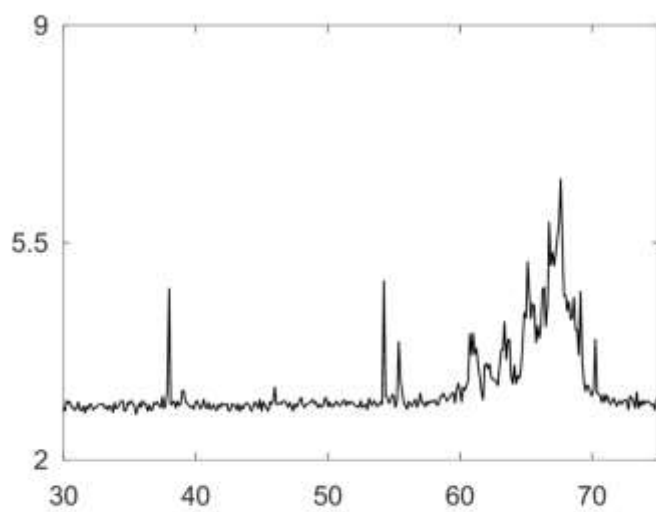
18



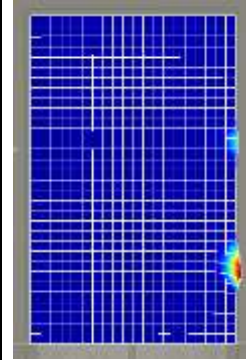
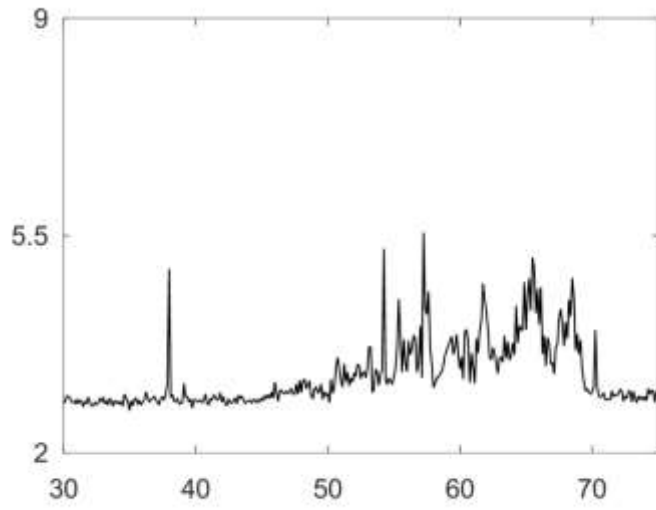
19



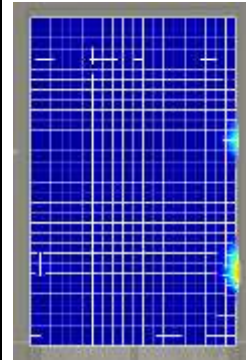
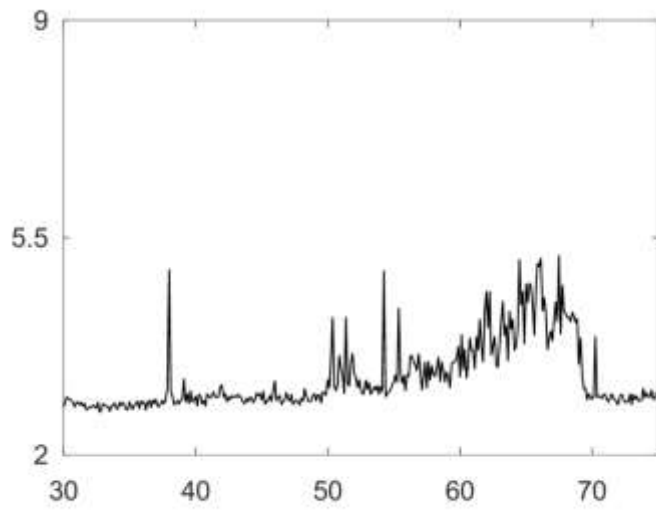
20



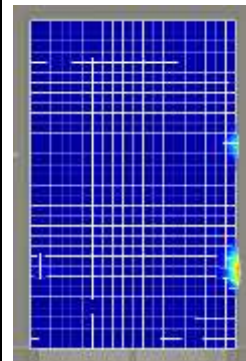
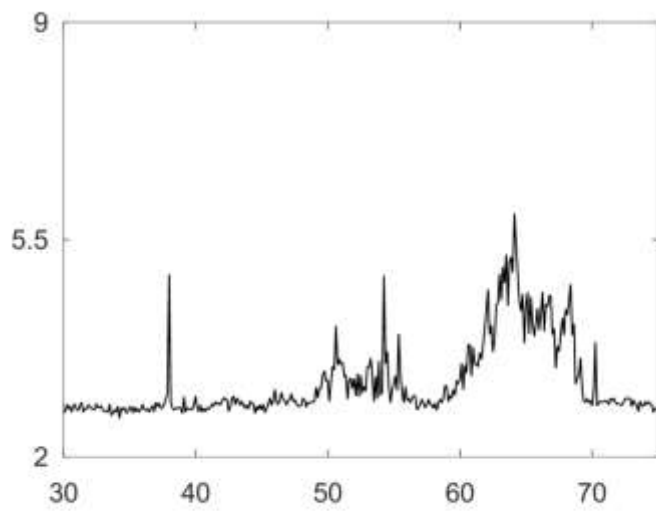
21



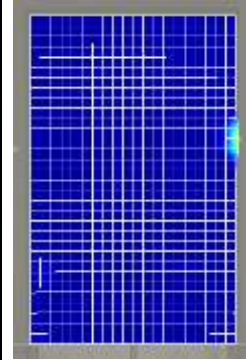
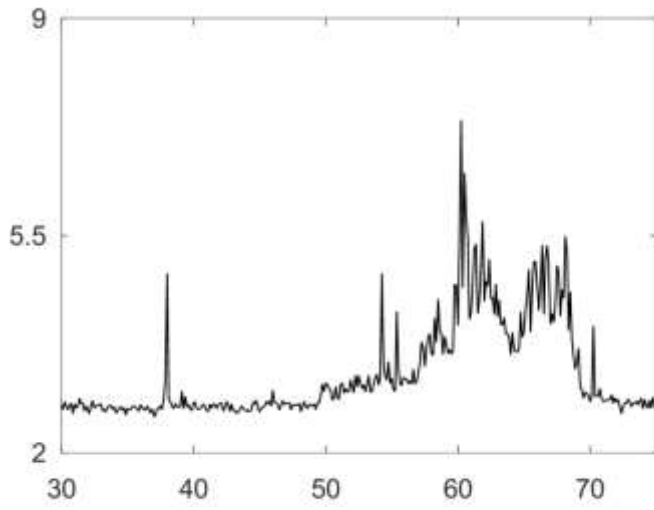
22



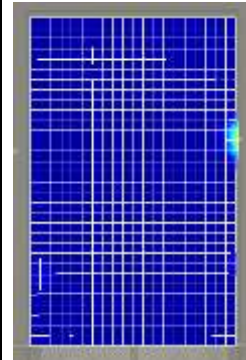
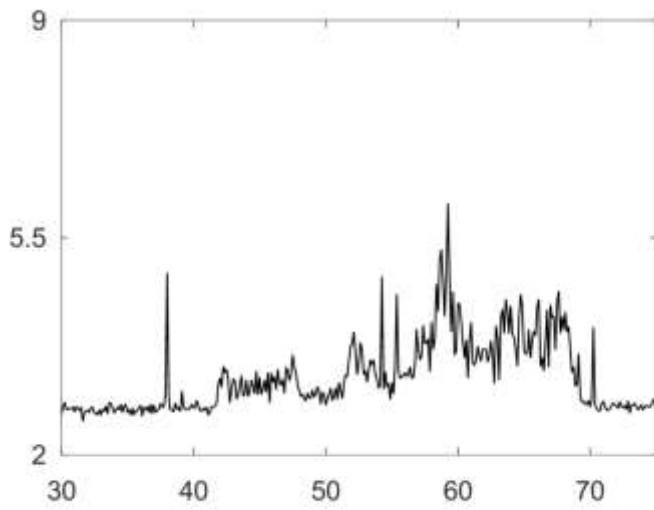
23



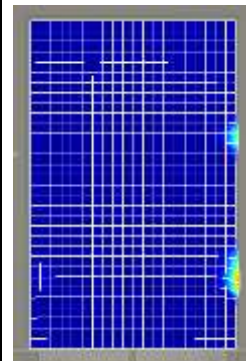
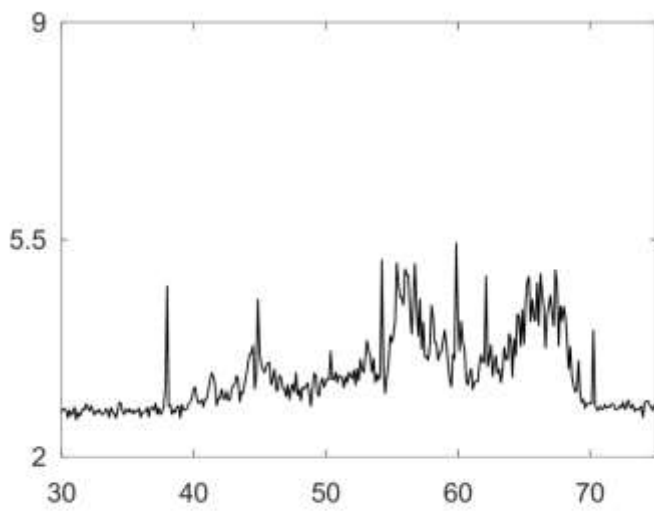
24



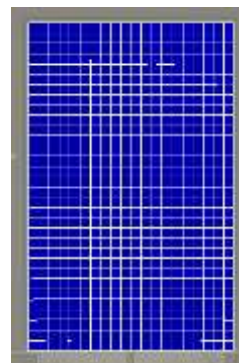
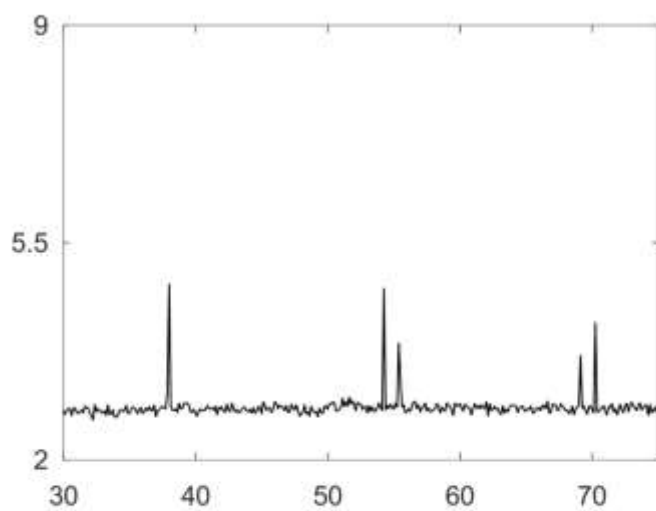
25



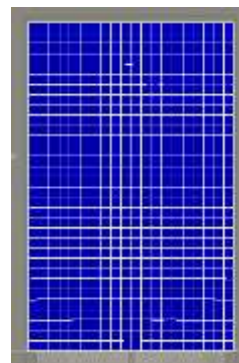
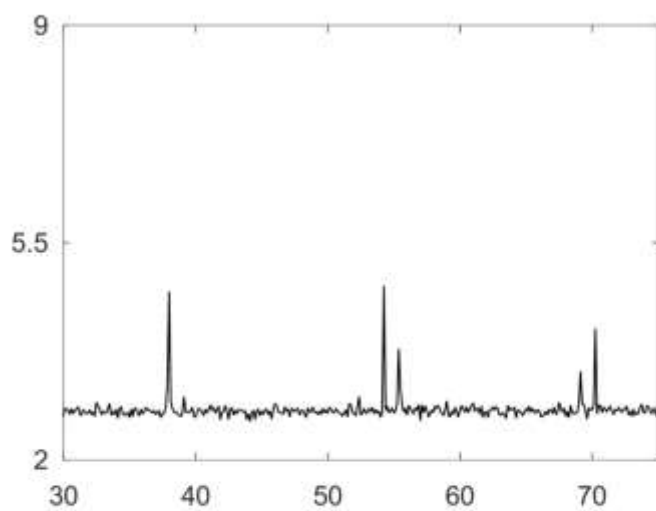
26



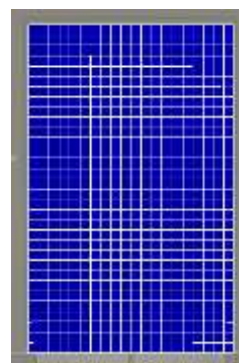
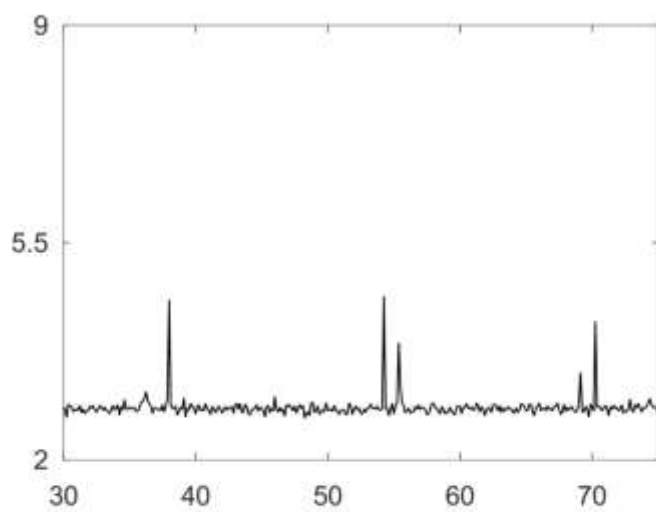
27

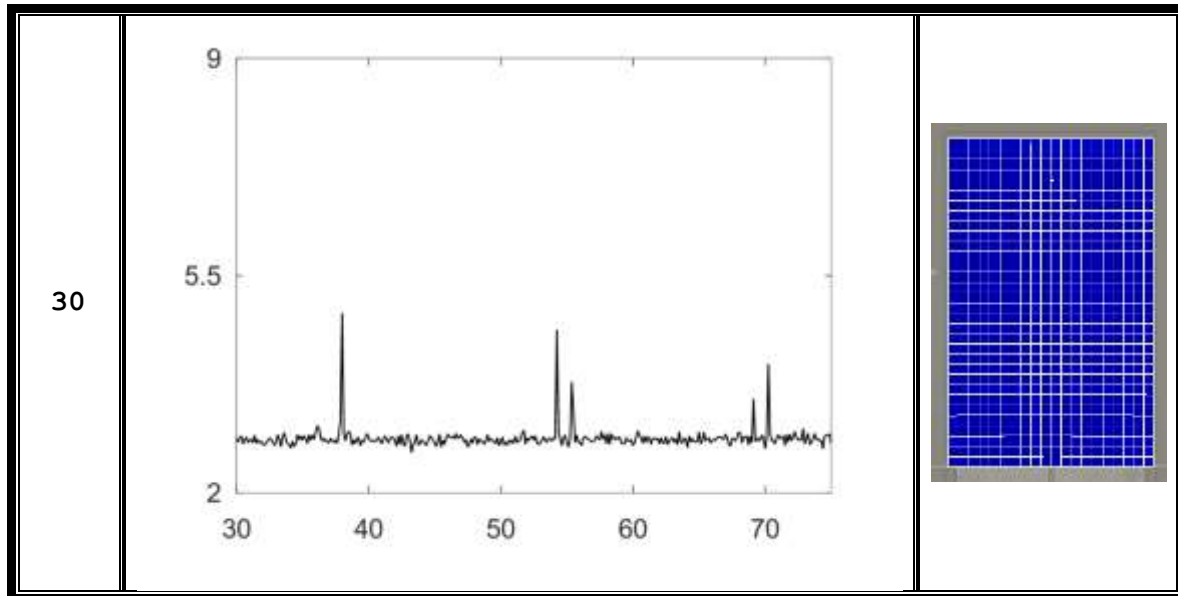


28

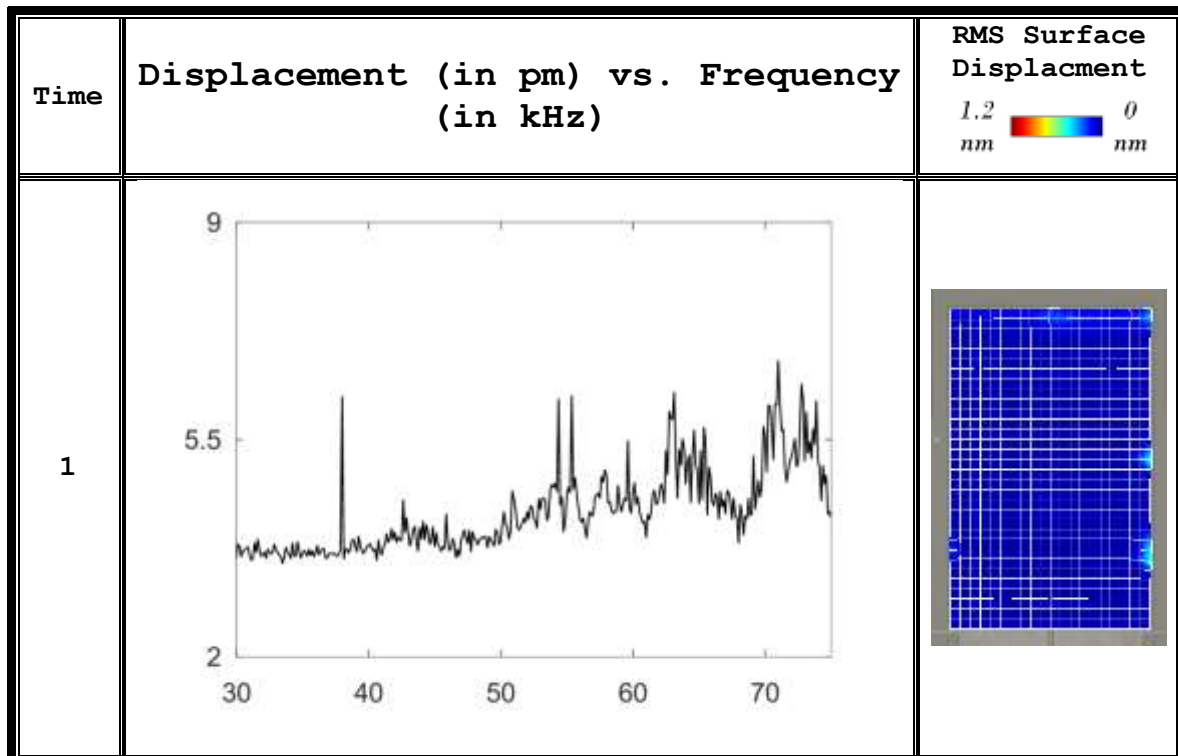


29

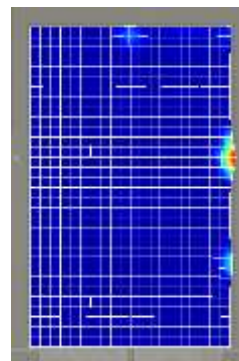
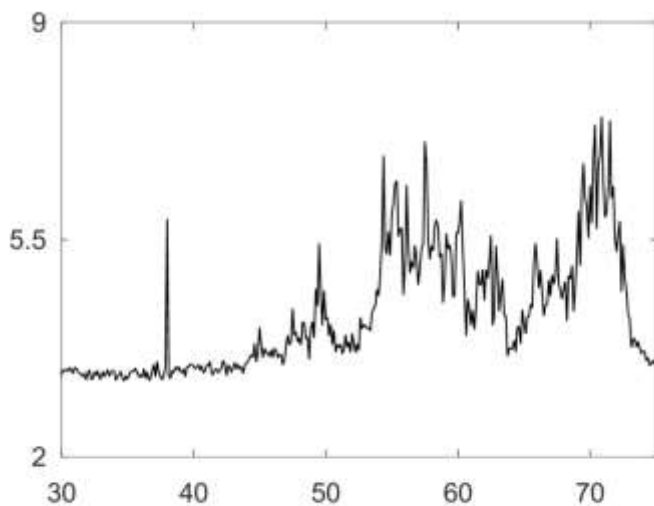




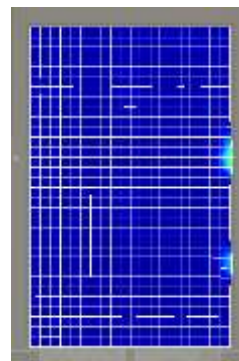
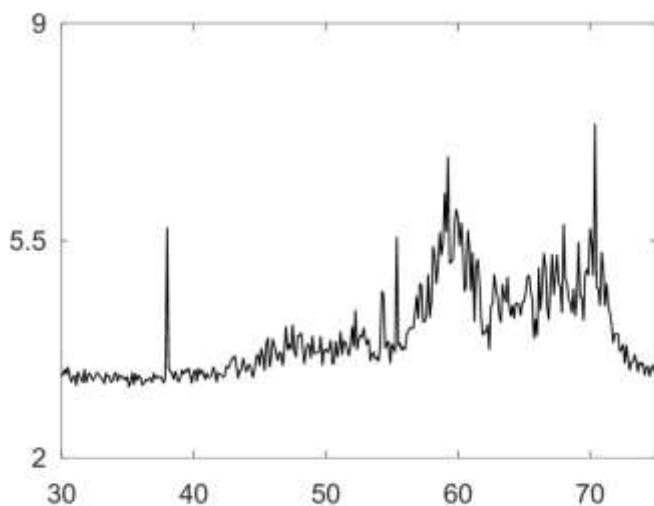
Run 2



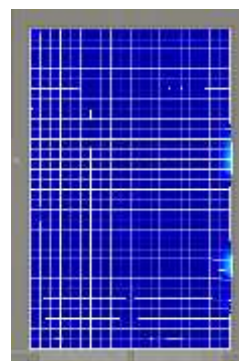
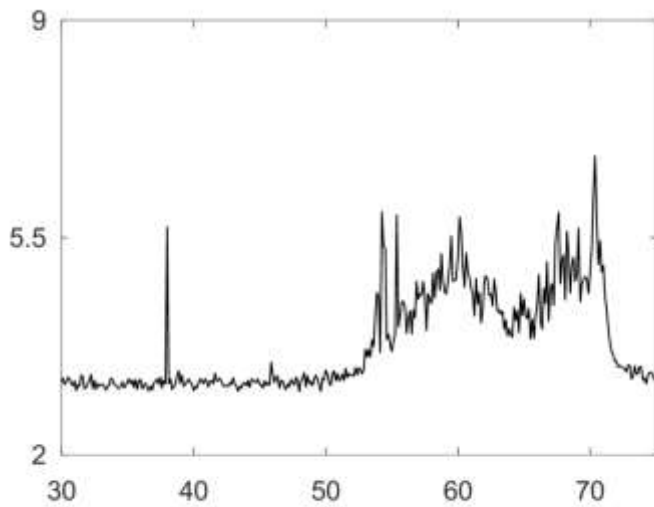
2



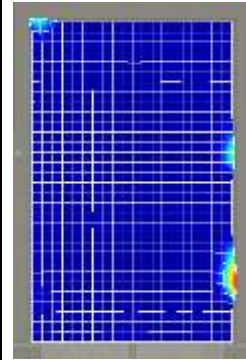
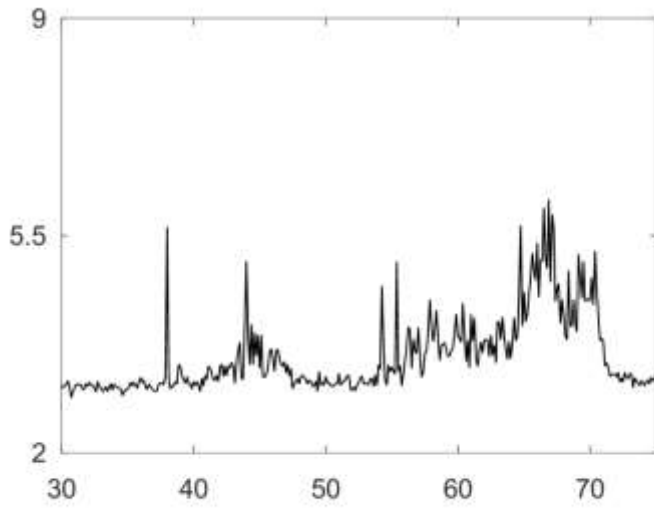
3



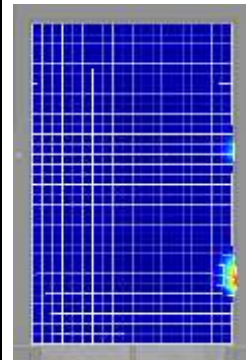
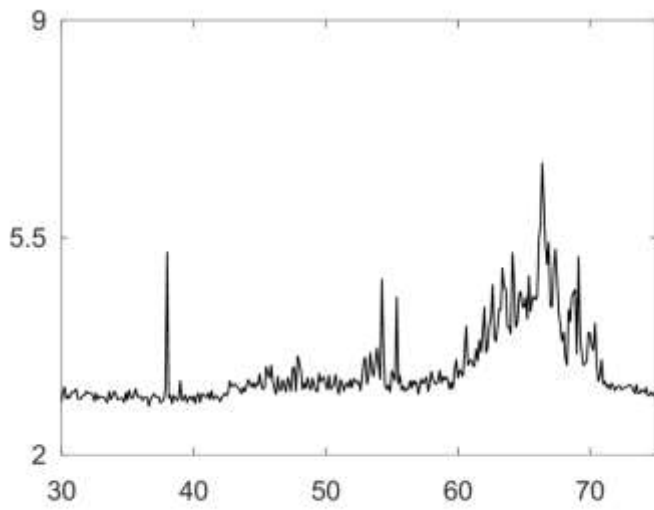
4



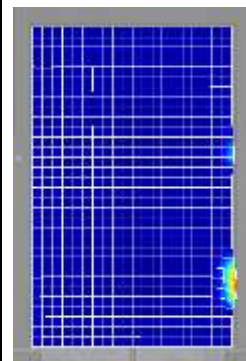
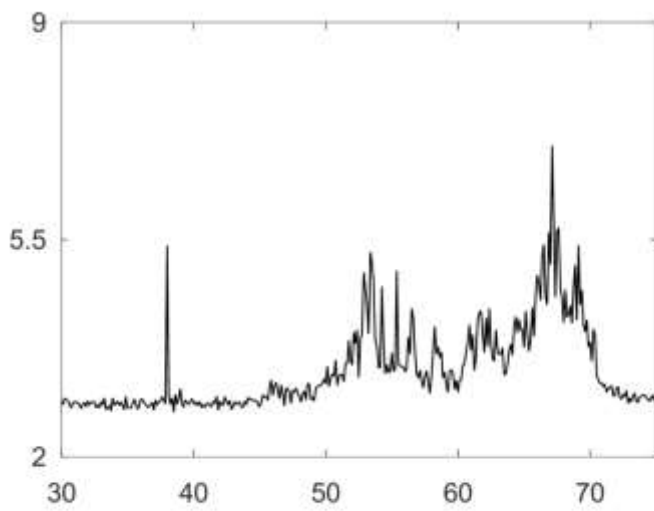
5



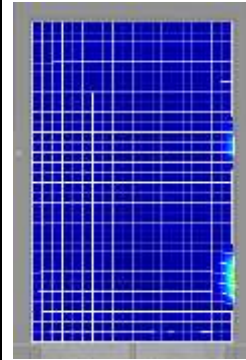
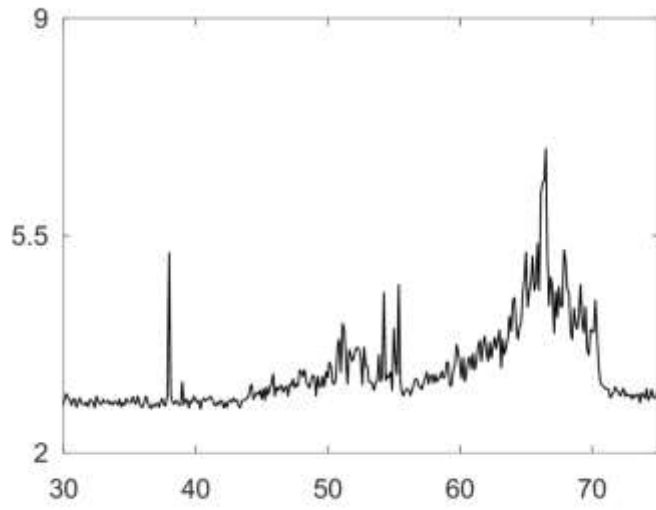
6



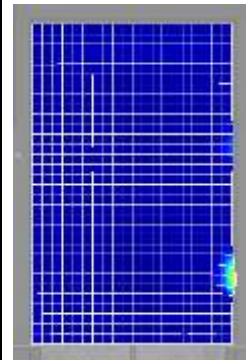
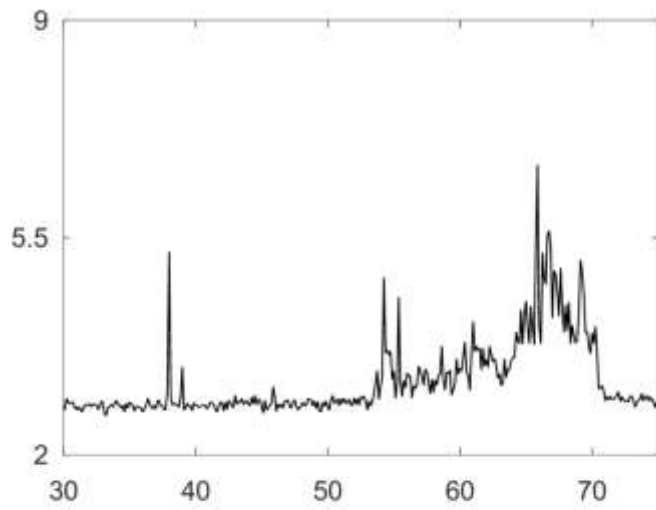
7



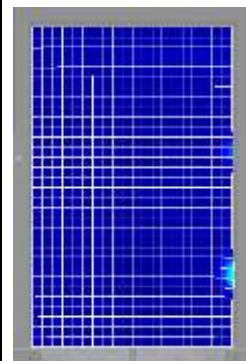
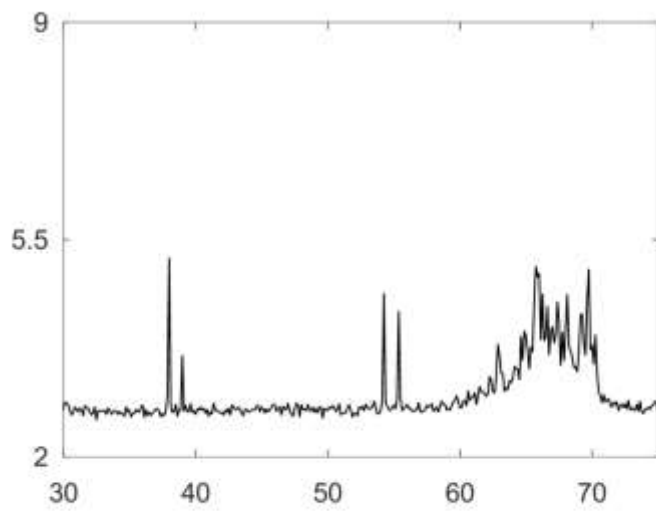
8



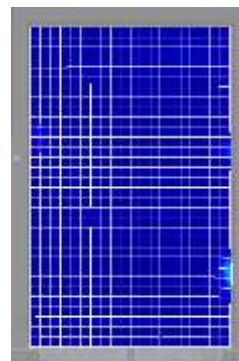
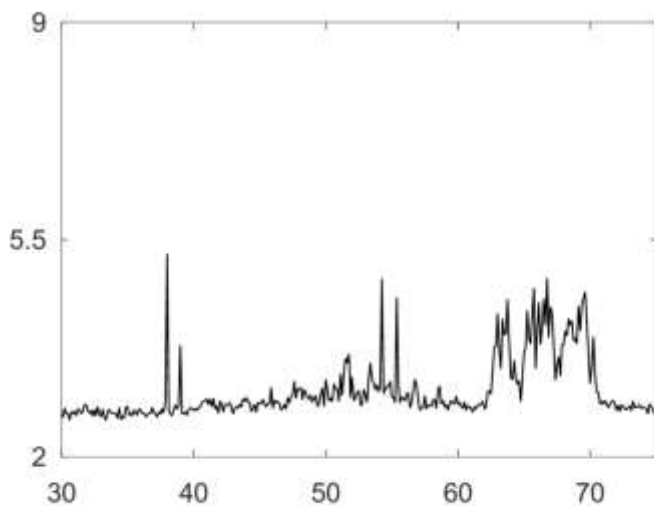
9



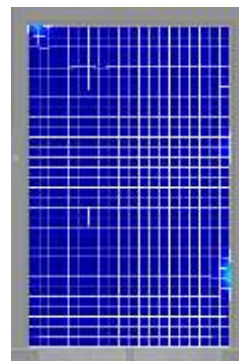
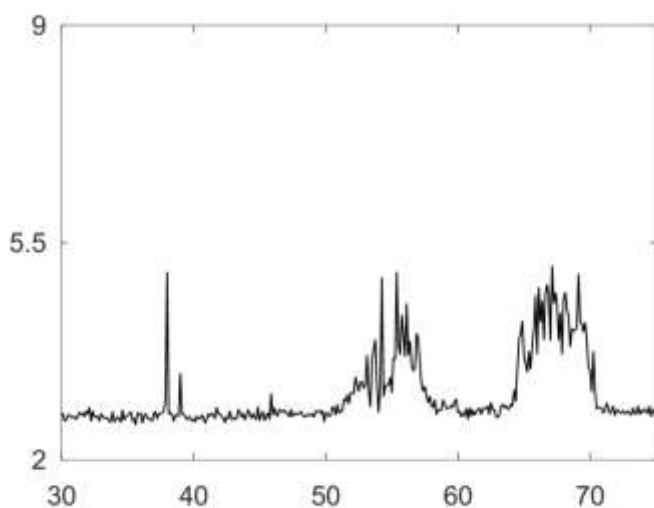
10



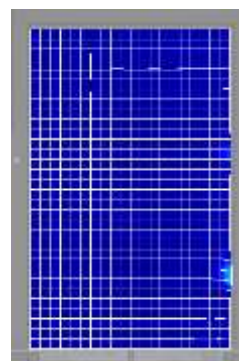
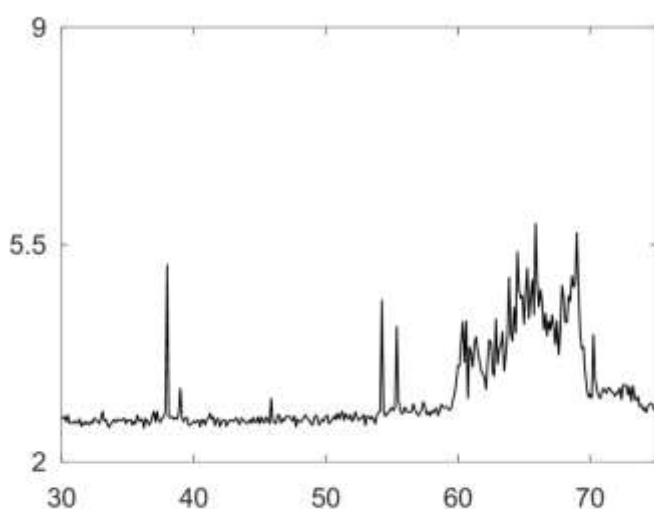
11



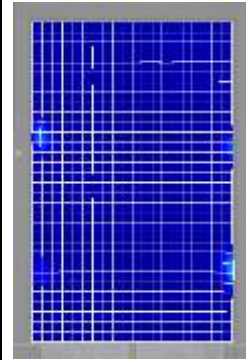
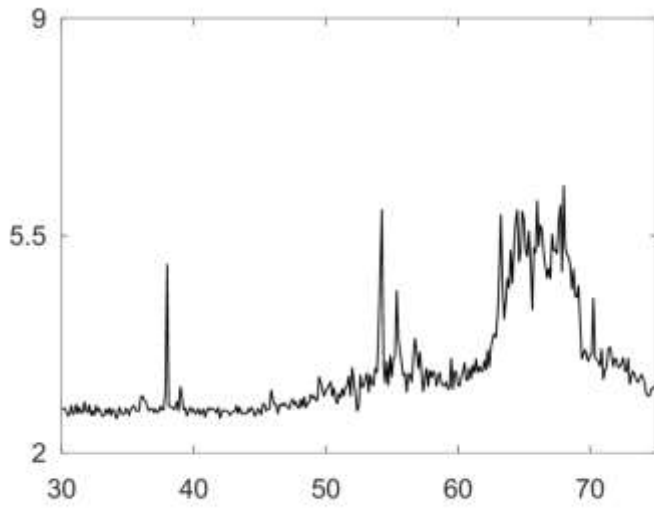
12



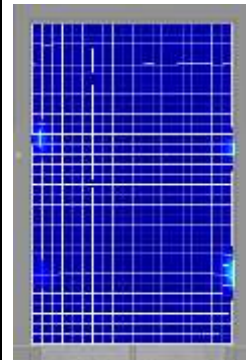
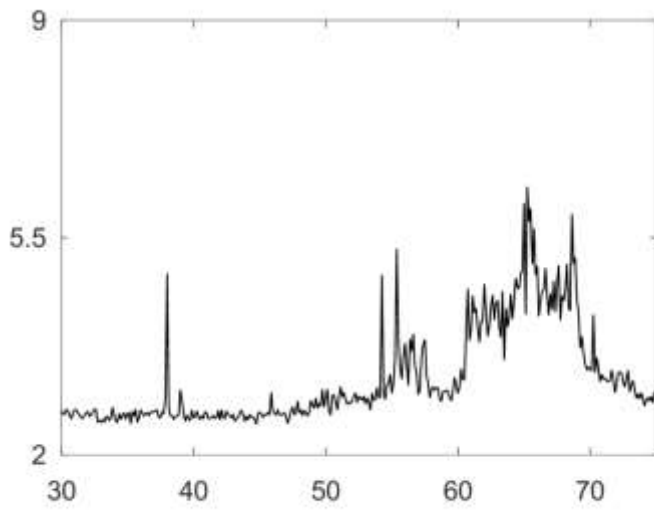
13



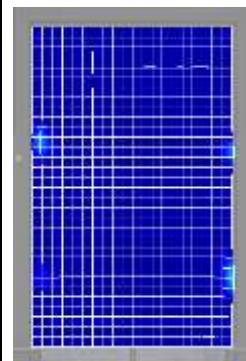
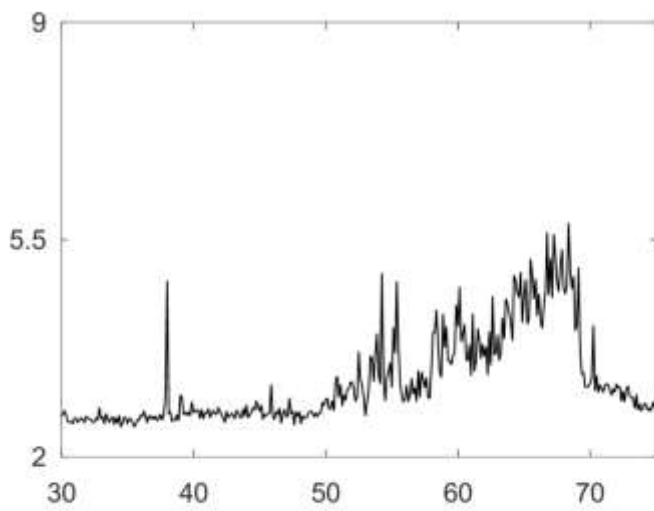
14



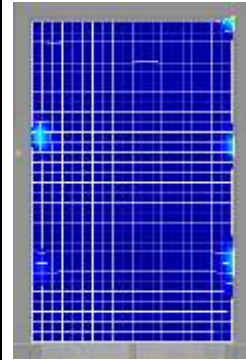
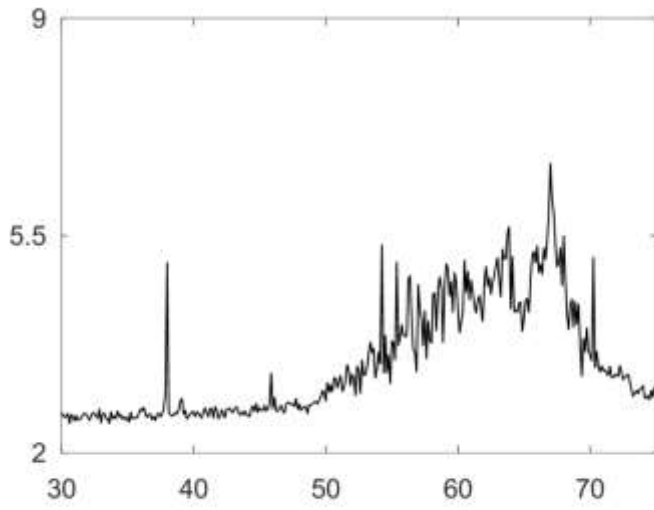
15



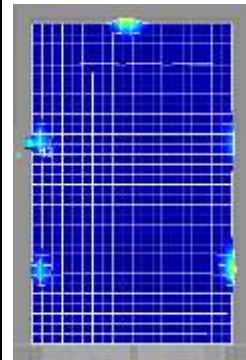
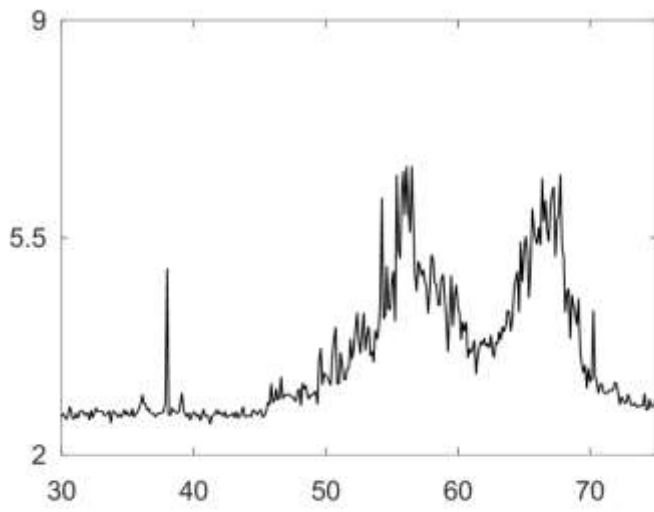
16



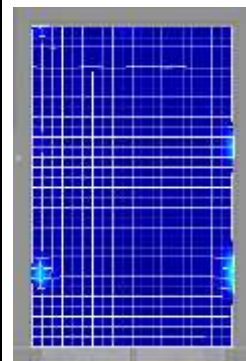
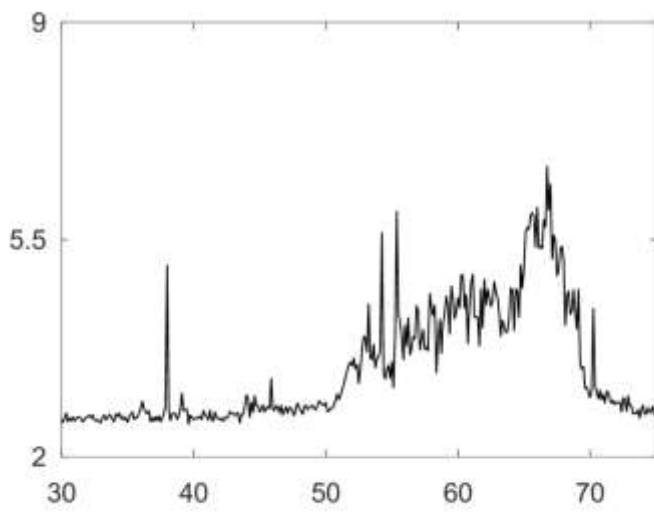
17



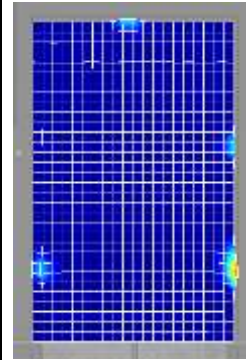
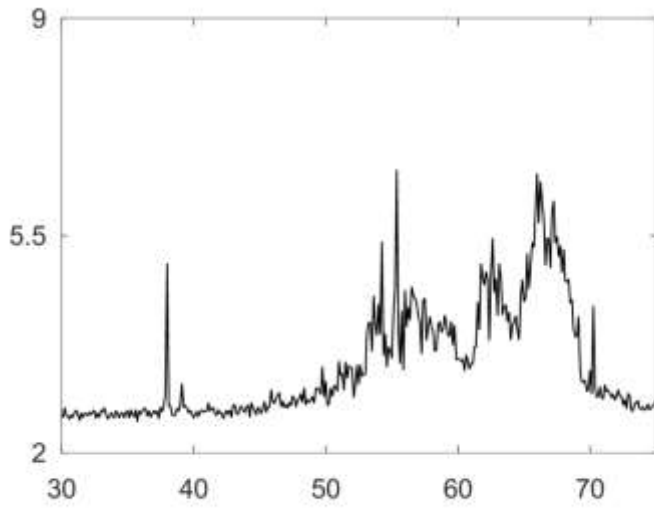
18



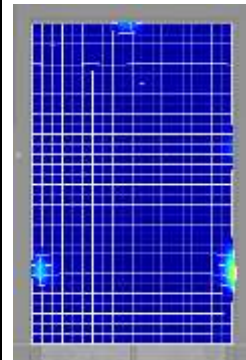
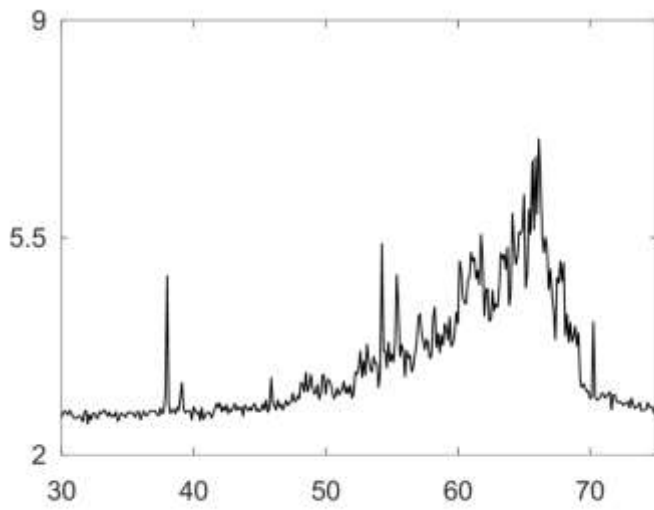
19



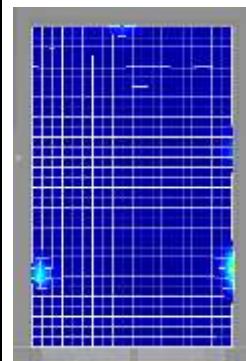
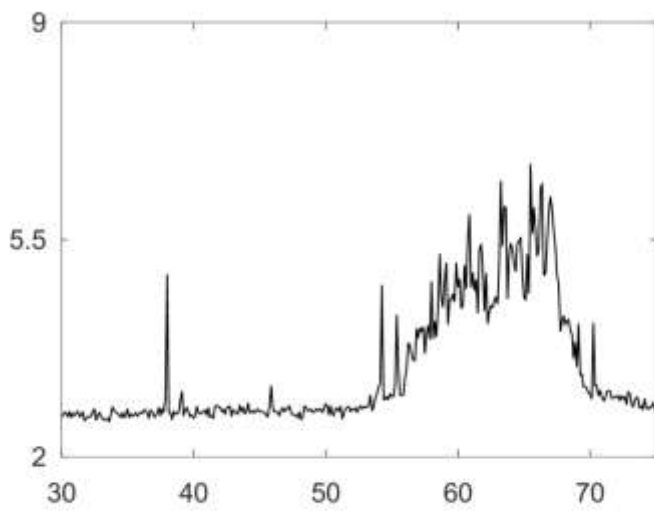
20



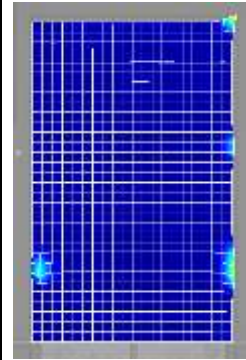
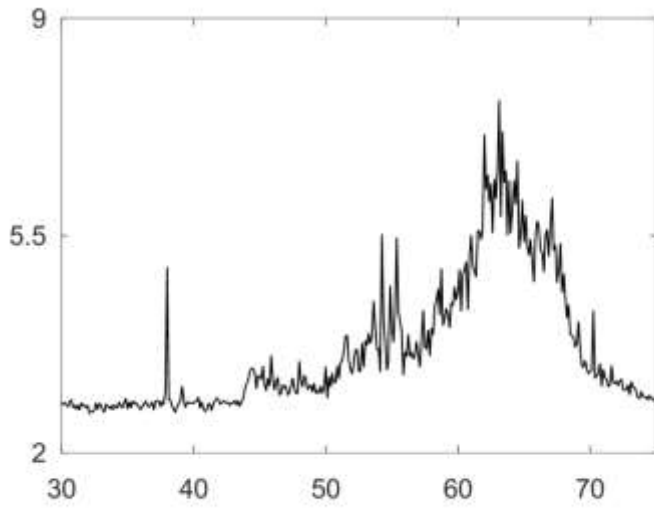
21



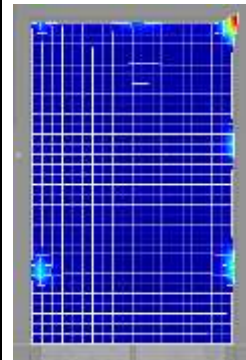
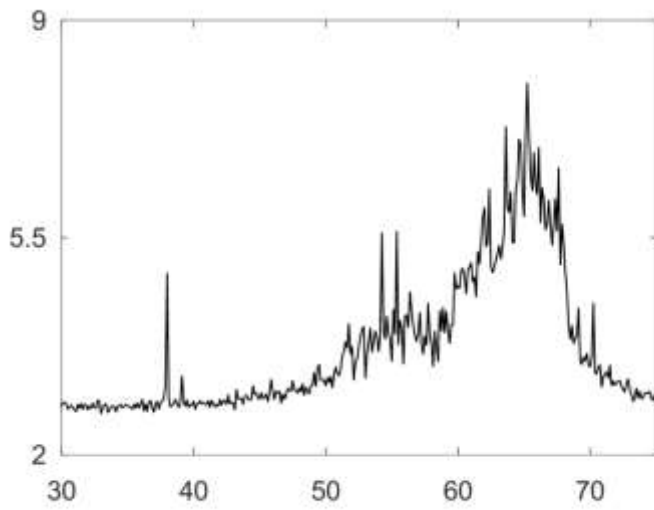
22



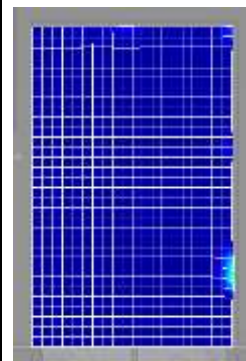
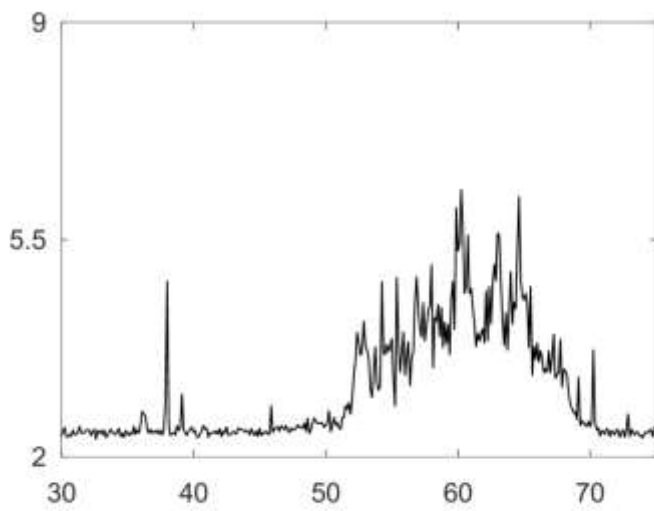
23



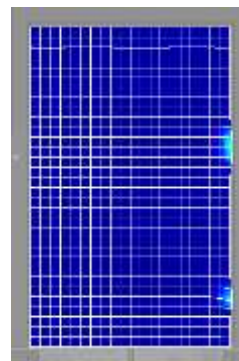
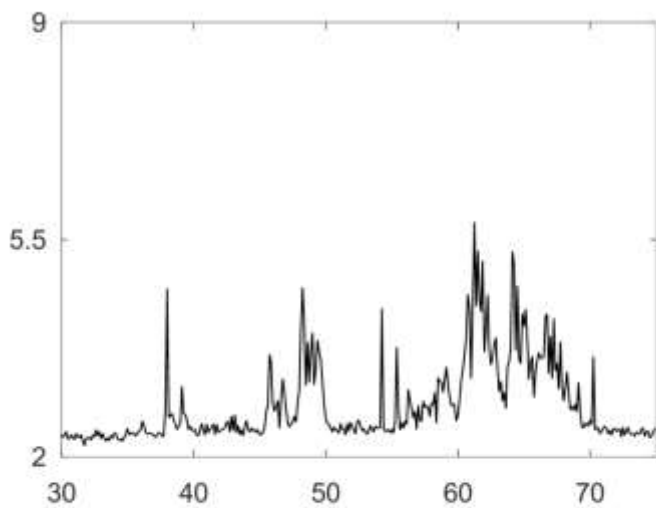
24



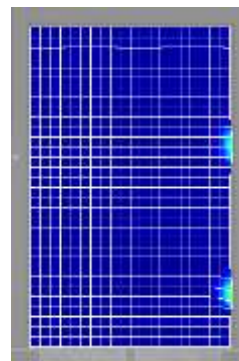
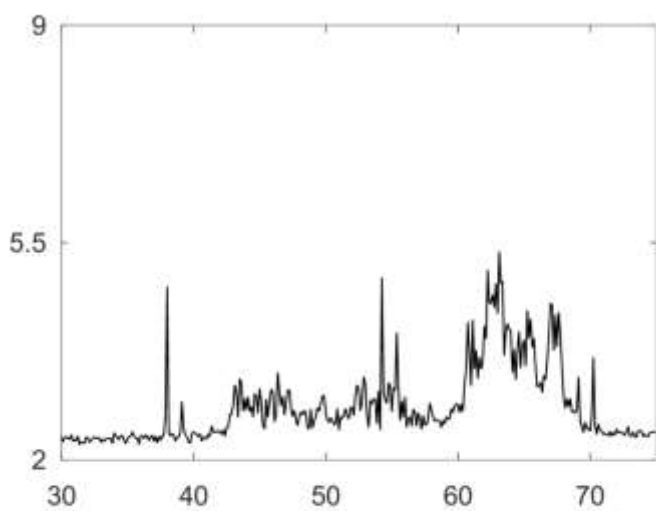
25



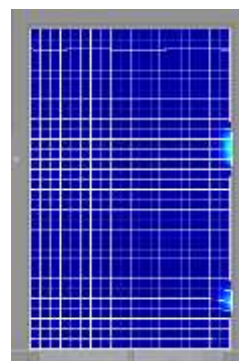
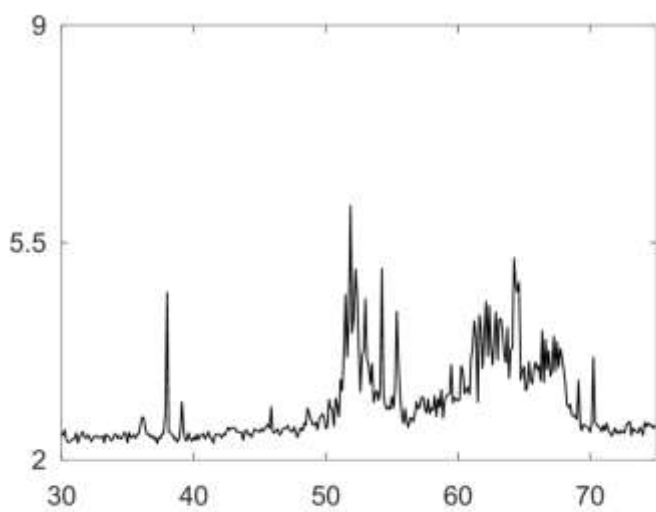
26



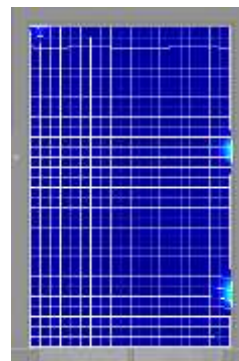
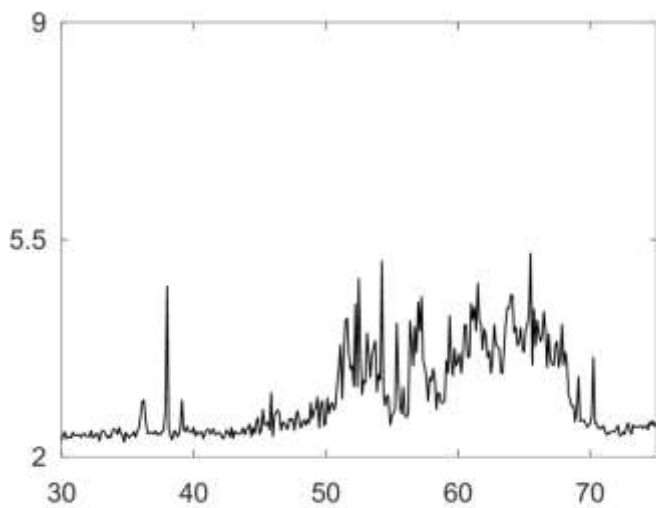
27



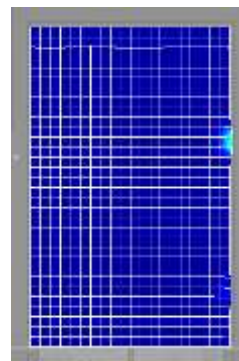
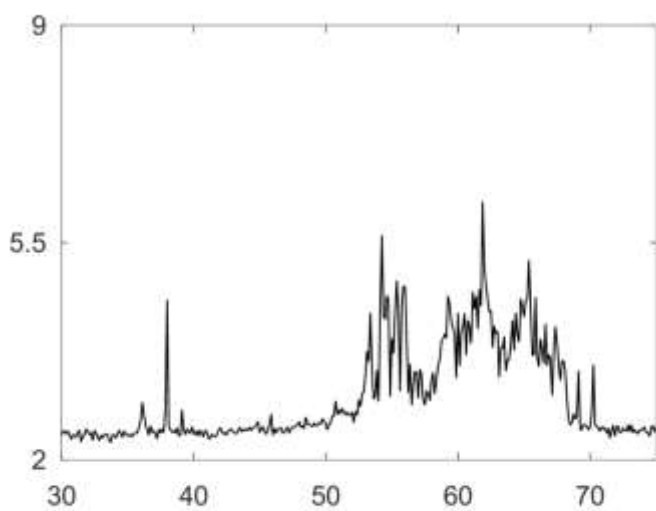
28



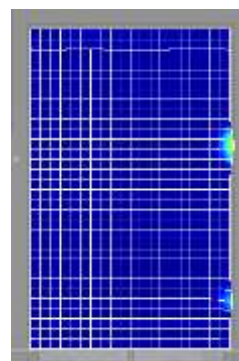
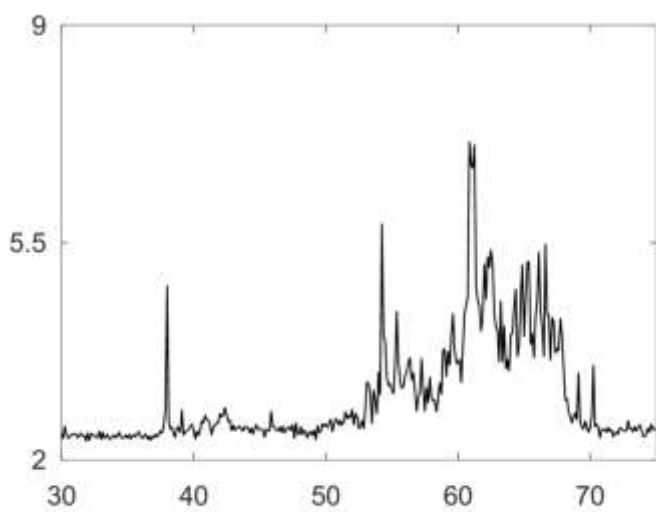
29



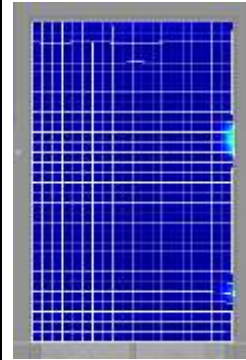
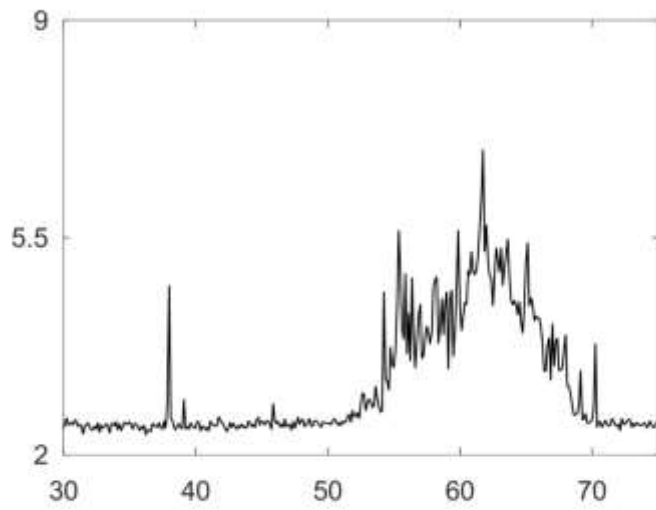
30



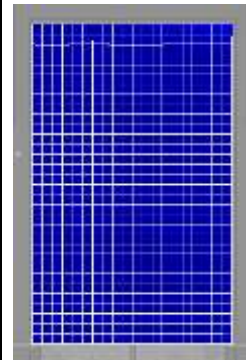
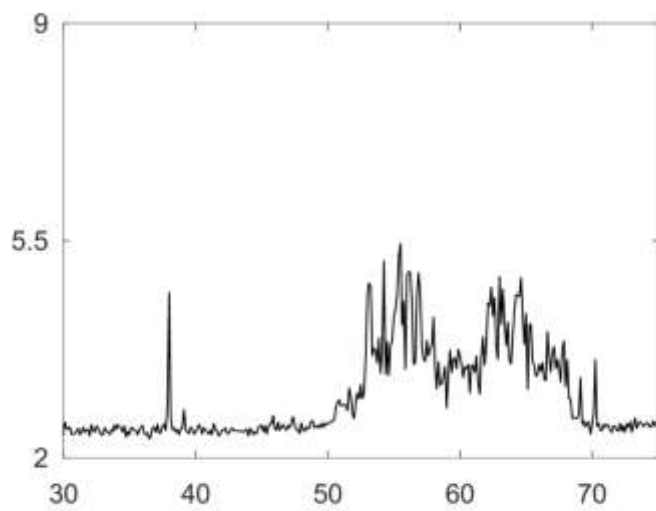
31



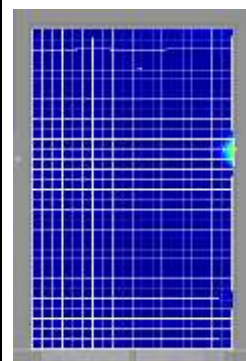
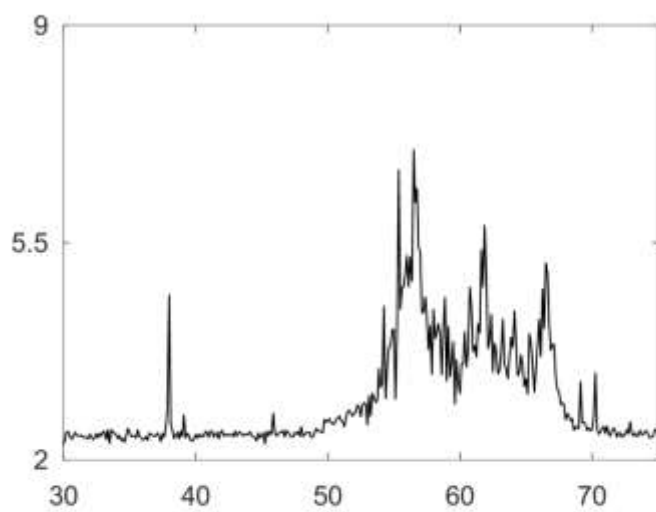
32



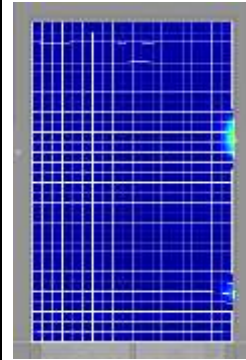
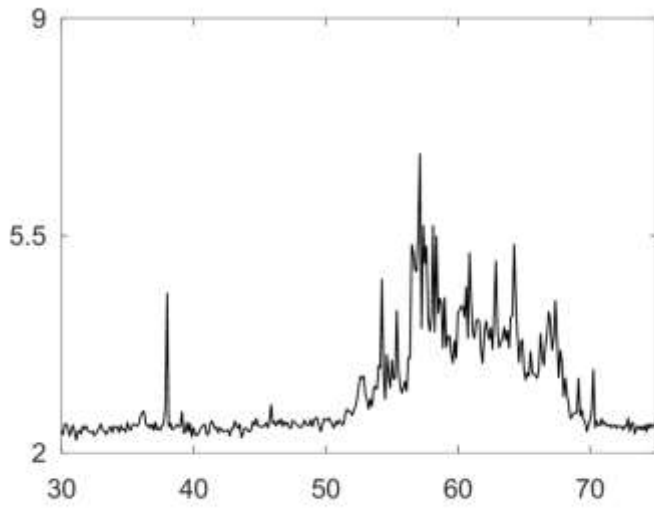
33



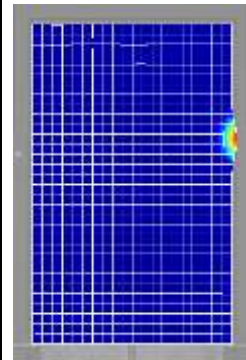
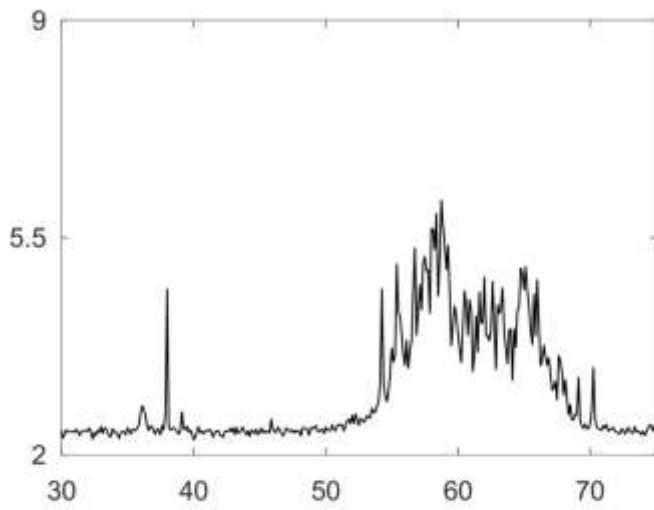
34



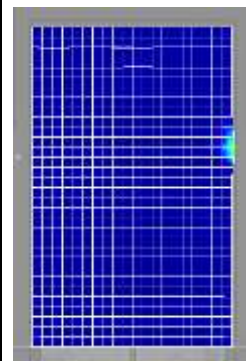
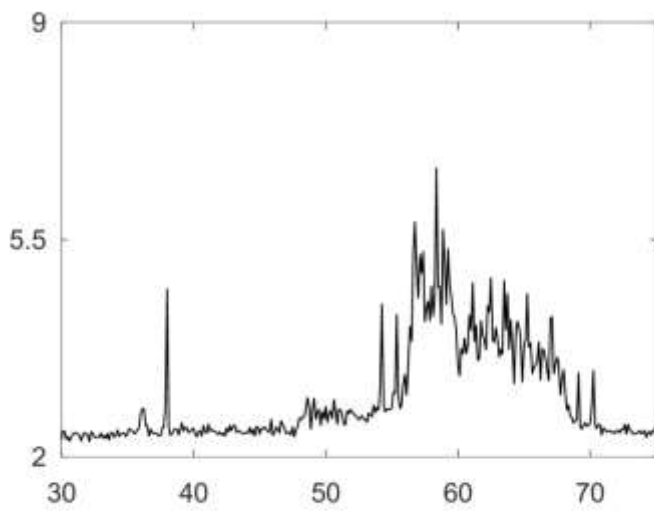
35



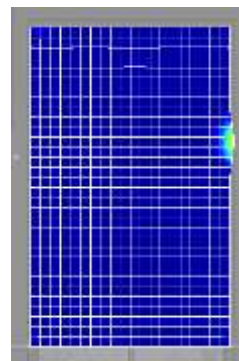
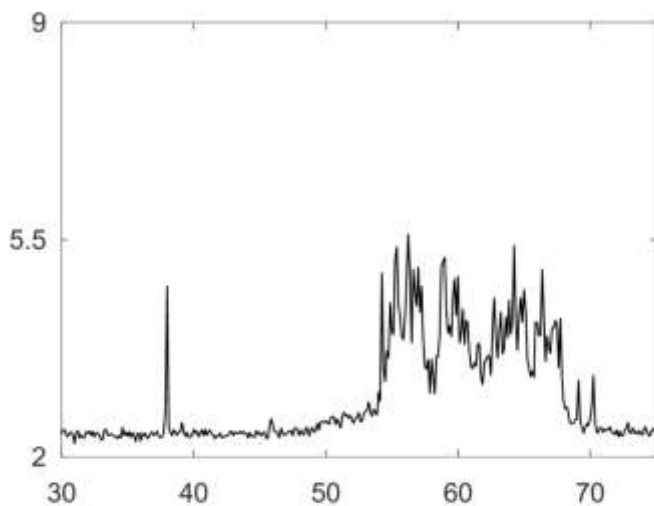
36



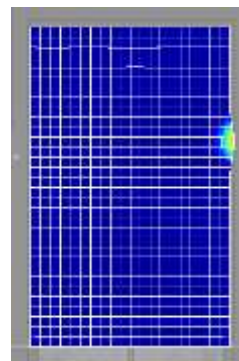
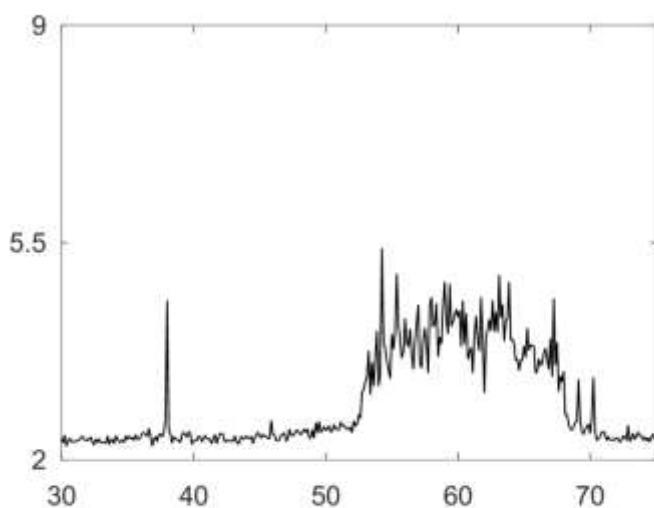
37



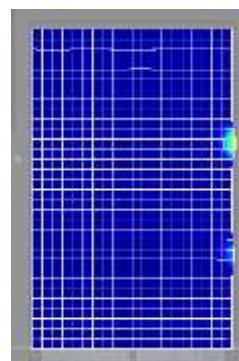
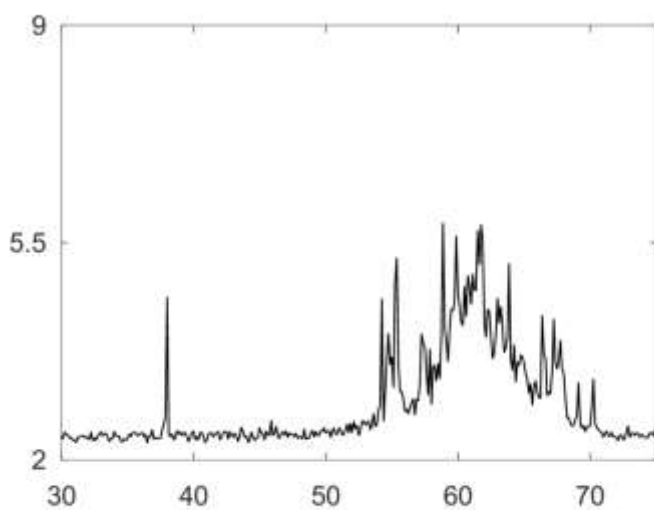
38



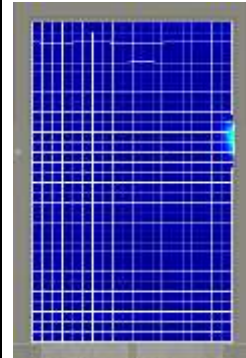
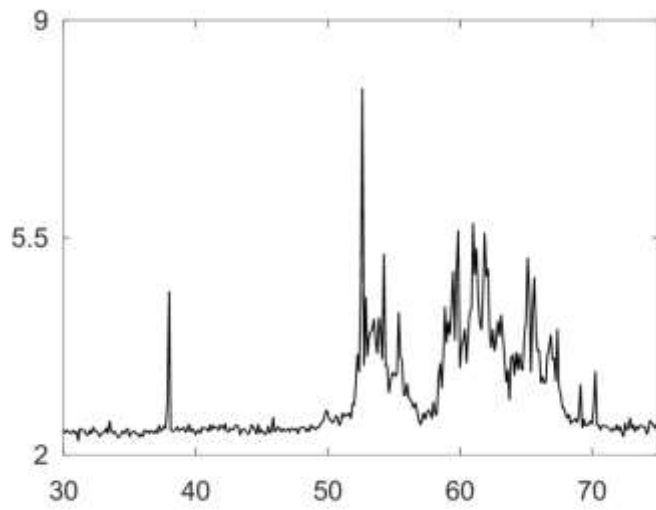
39



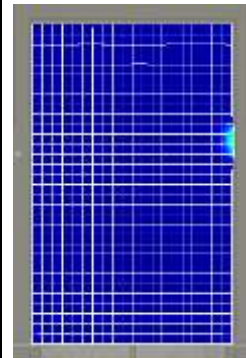
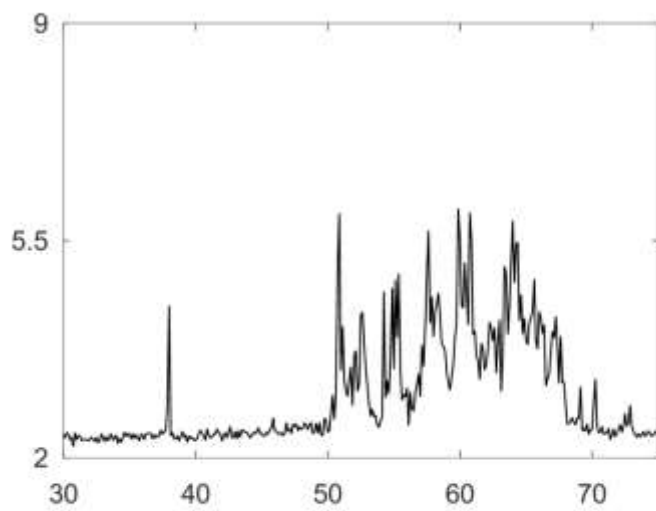
40



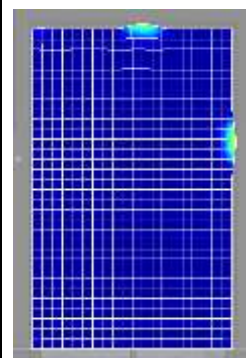
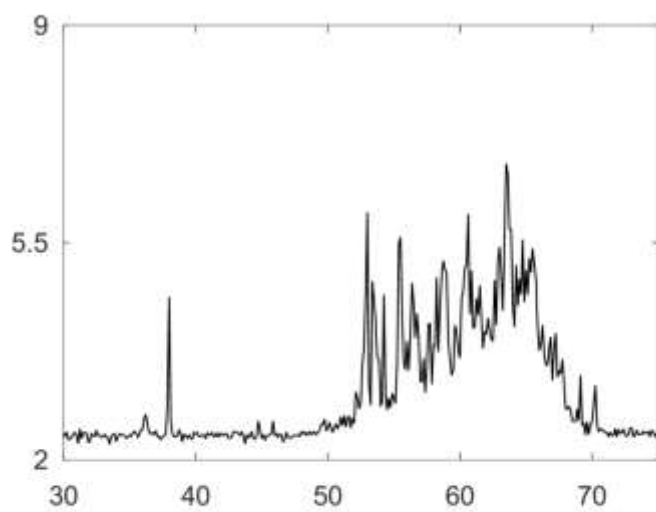
41



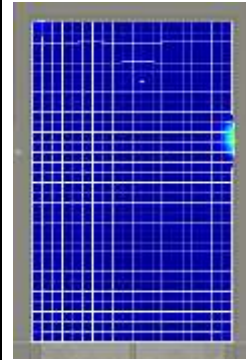
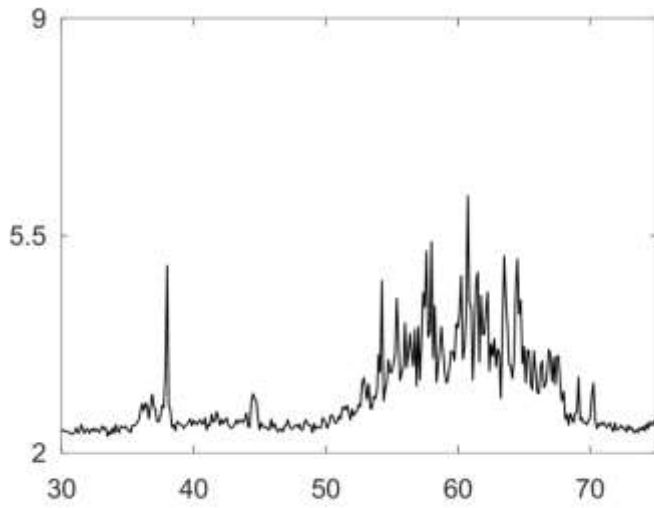
42



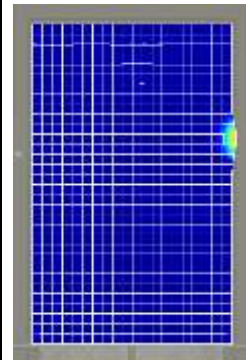
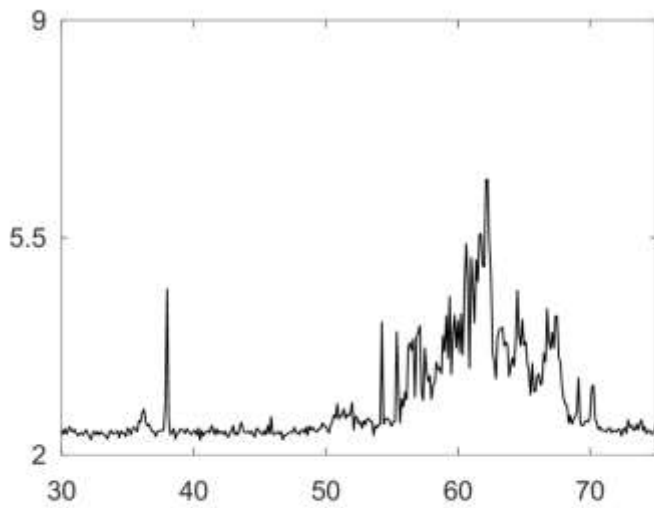
43



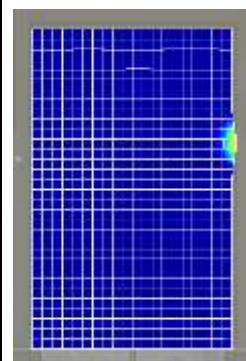
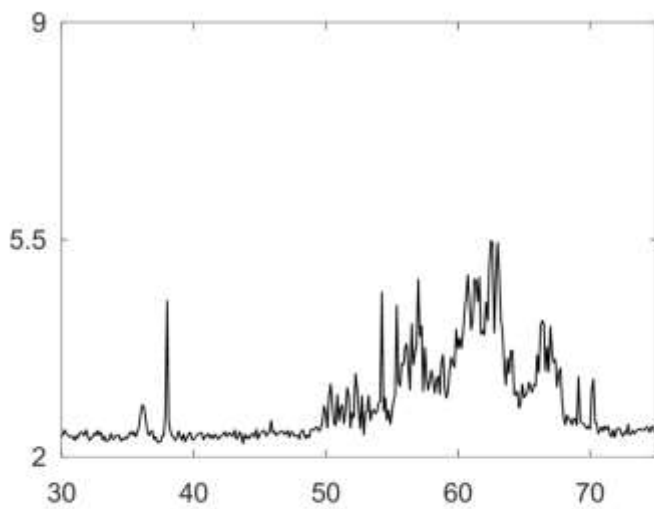
44



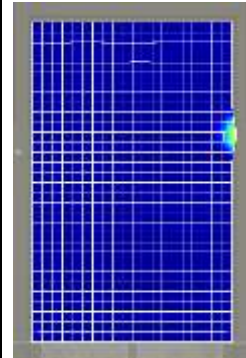
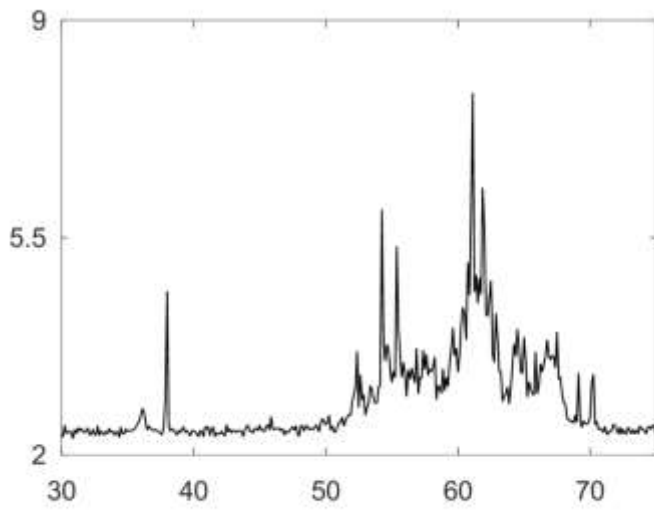
45



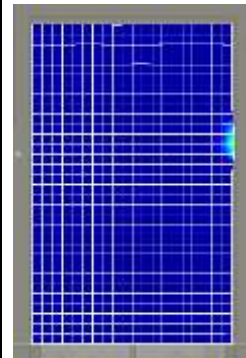
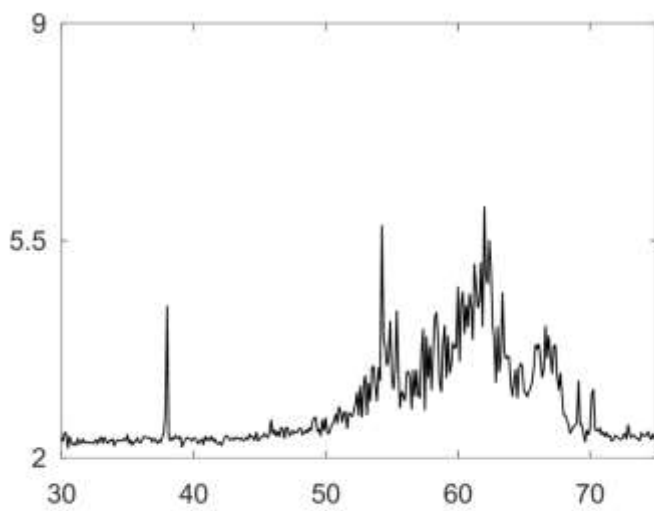
46



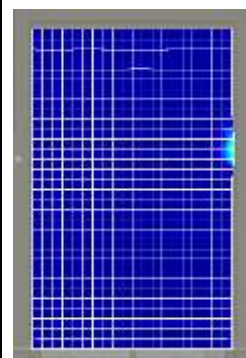
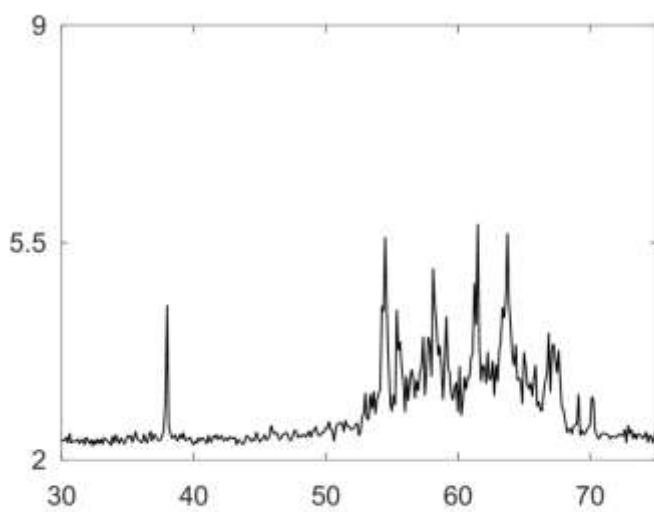
47



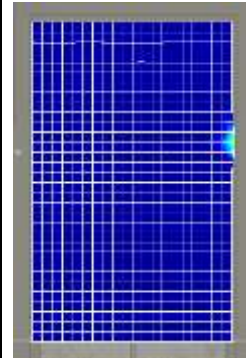
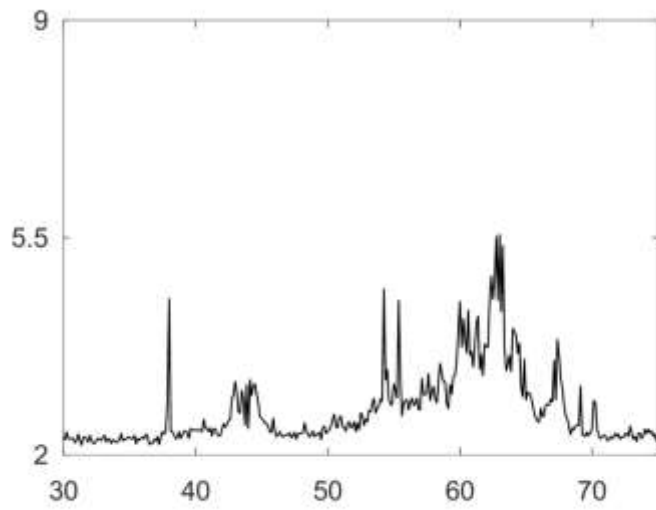
48



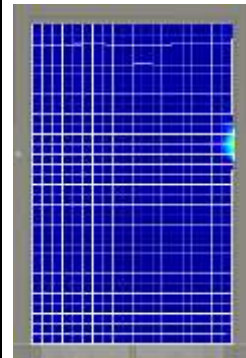
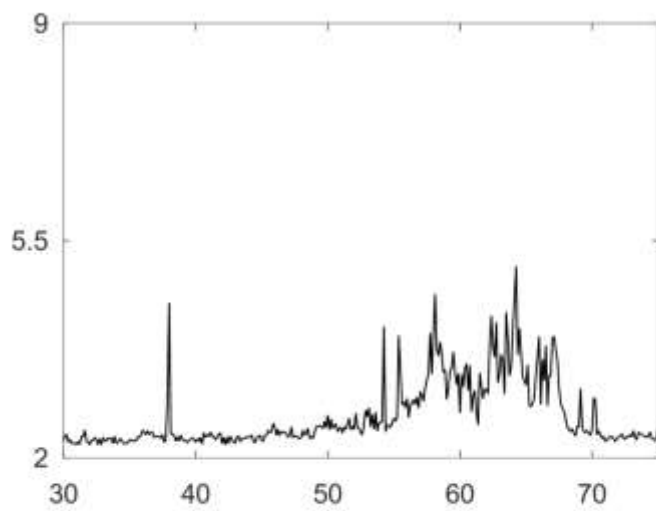
49



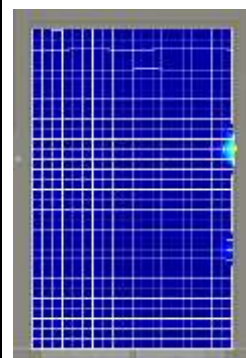
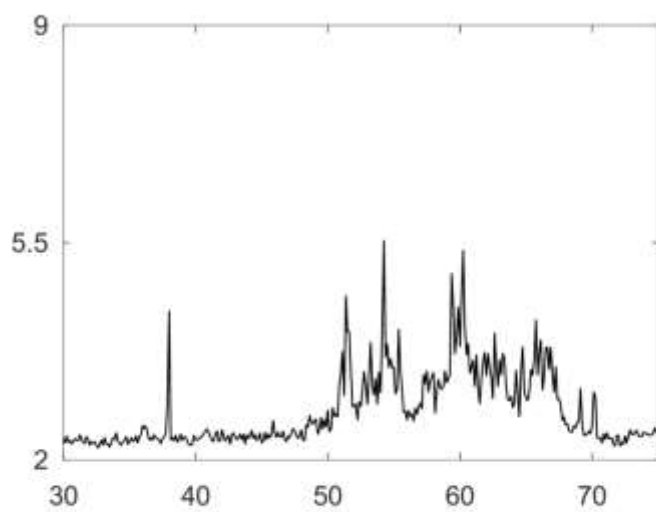
50



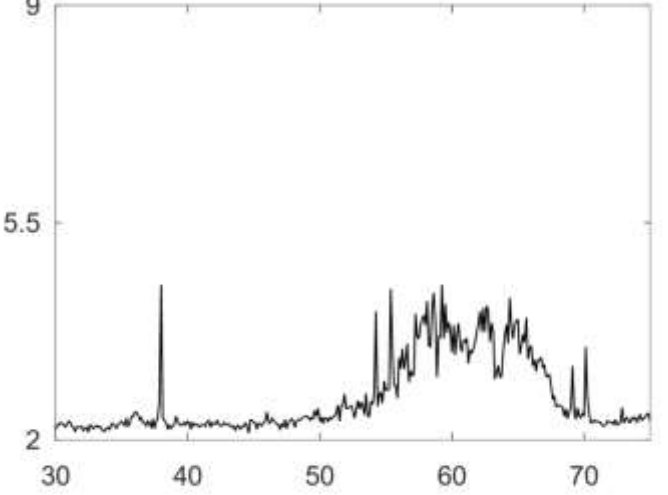
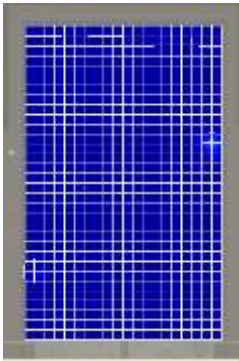
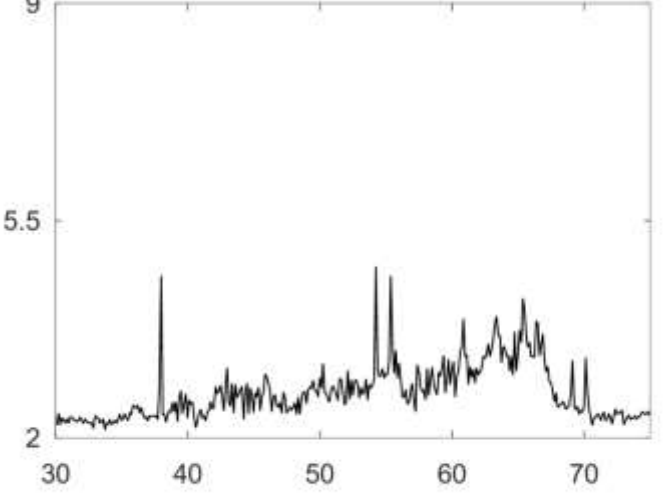
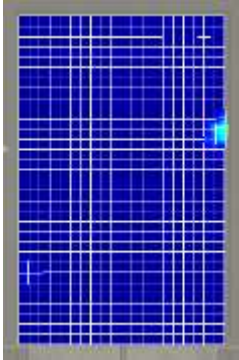
51



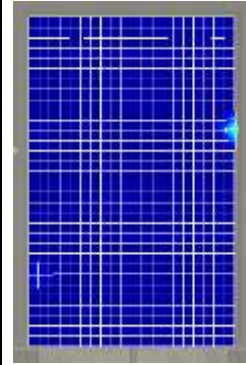
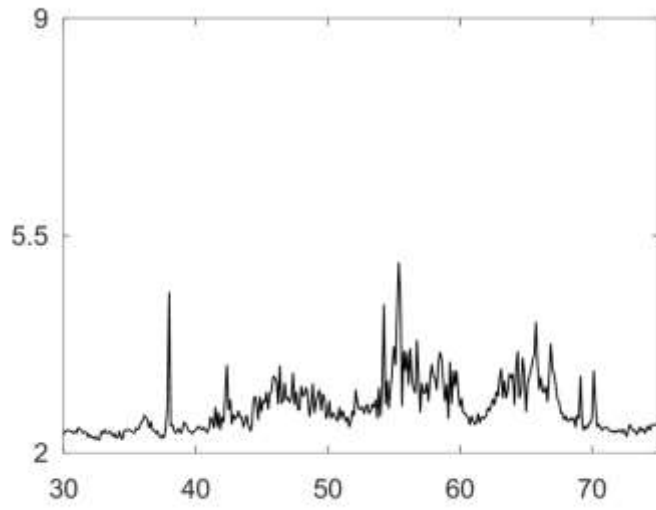
52



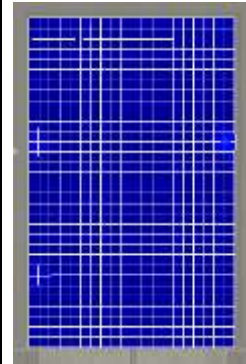
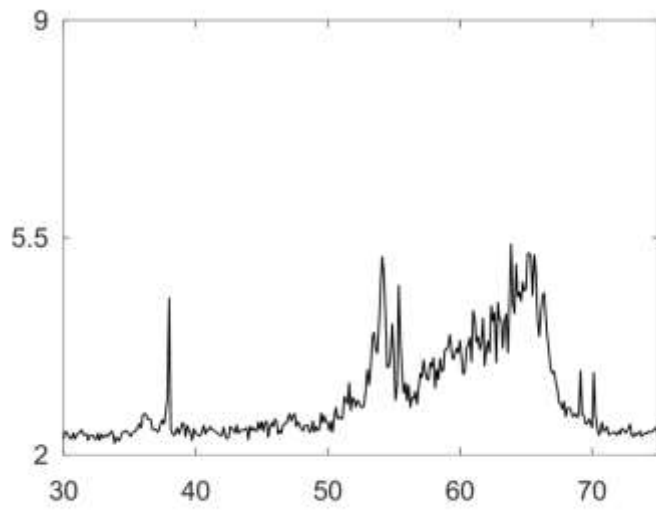
Run 3

Time	Displacement (in pm) vs. Frequency (in kHz)	RMS Surface Displacement 1.2 nm  0 nm
1	 <p>The plot shows displacement in pm on the y-axis (ranging from 2 to 9) versus frequency in kHz on the x-axis (ranging from 30 to 70). A prominent peak is visible at approximately 38 kHz, reaching a displacement of about 4.5 pm. A broader, more complex peak structure is observed between 50 kHz and 70 kHz, with the highest displacement reaching approximately 8.5 pm.</p>	 <p>The heatmap shows a grid of blue squares, indicating low displacement. A small, localized area of higher displacement (yellow/red) is visible on the right side of the grid, corresponding to the peak at 38 kHz.</p>
2	 <p>The plot shows displacement in pm on the y-axis (ranging from 2 to 9) versus frequency in kHz on the x-axis (ranging from 30 to 70). A prominent peak is visible at approximately 38 kHz, reaching a displacement of about 4.5 pm. A broader, more complex peak structure is observed between 50 kHz and 70 kHz, with the highest displacement reaching approximately 8.5 pm.</p>	 <p>The heatmap shows a grid of blue squares, indicating low displacement. A small, localized area of higher displacement (yellow/red) is visible on the right side of the grid, corresponding to the peak at 38 kHz.</p>

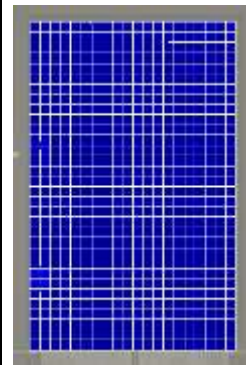
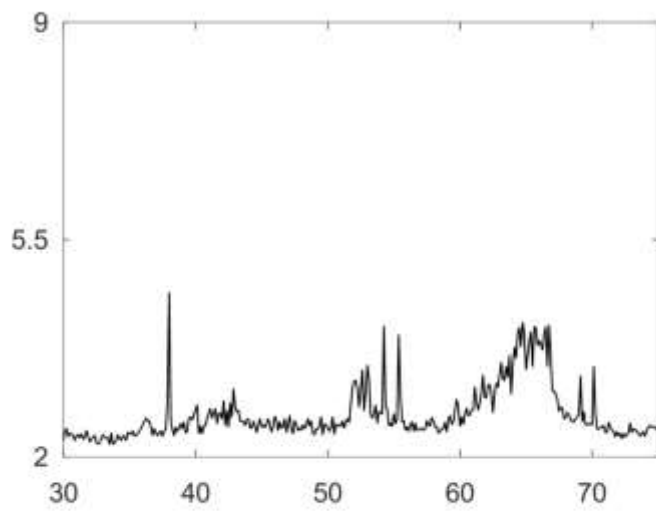
3



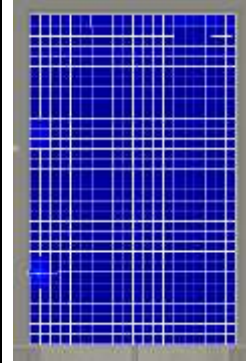
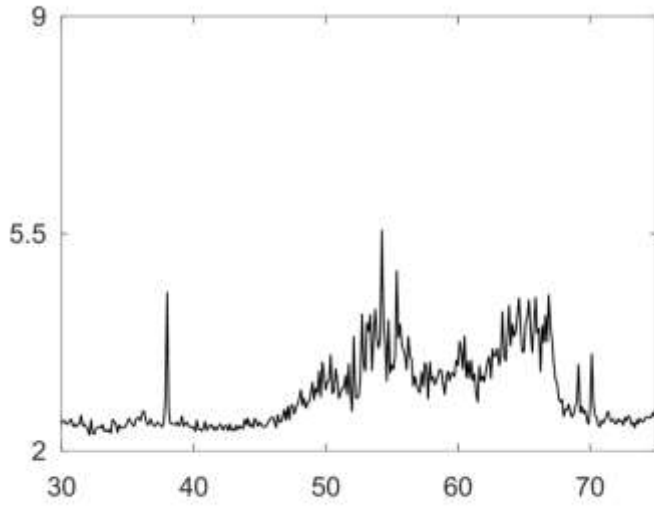
4



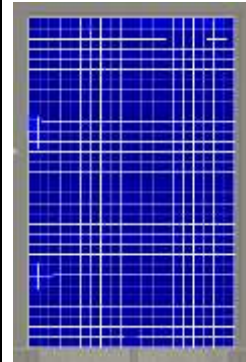
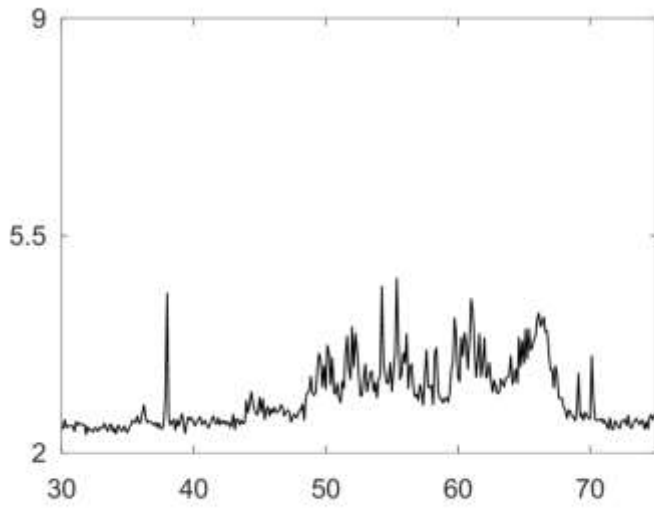
5



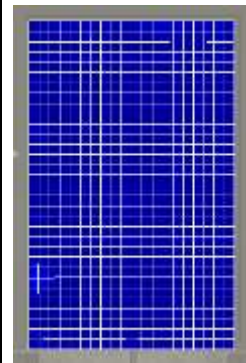
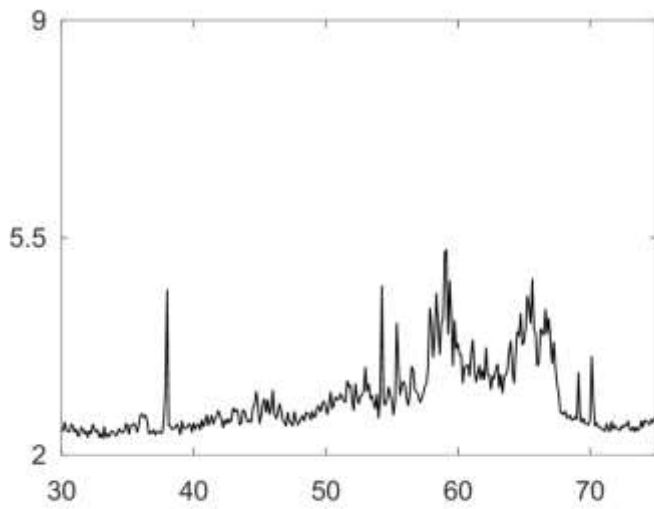
6



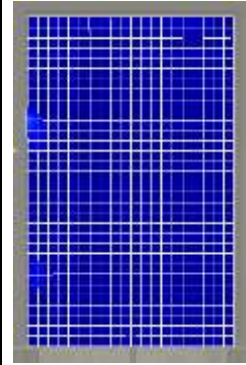
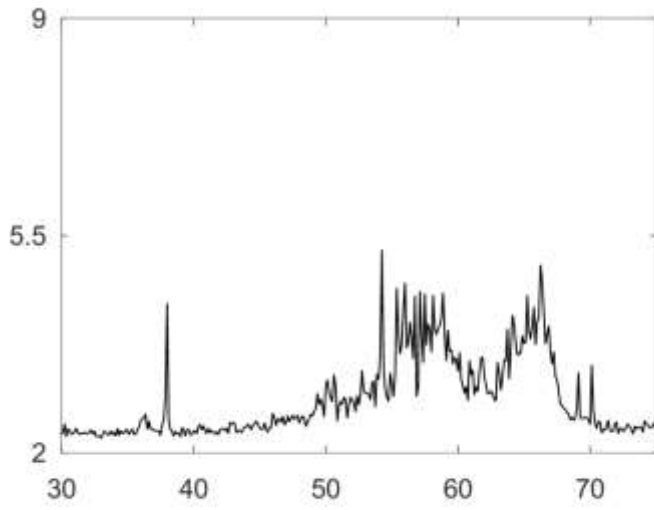
7



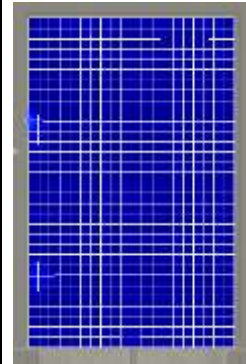
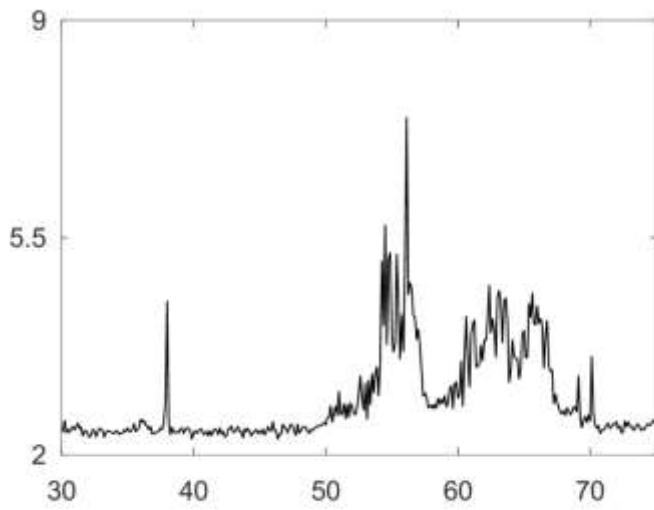
8



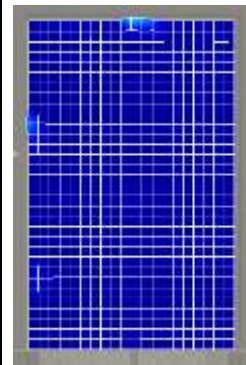
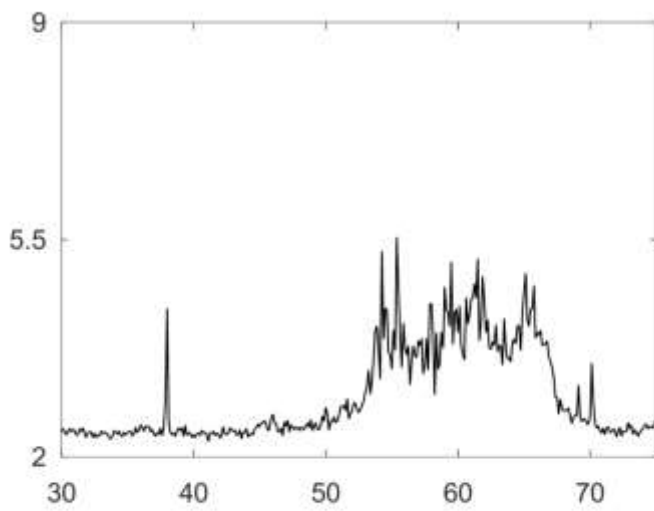
9



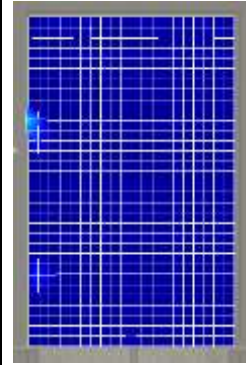
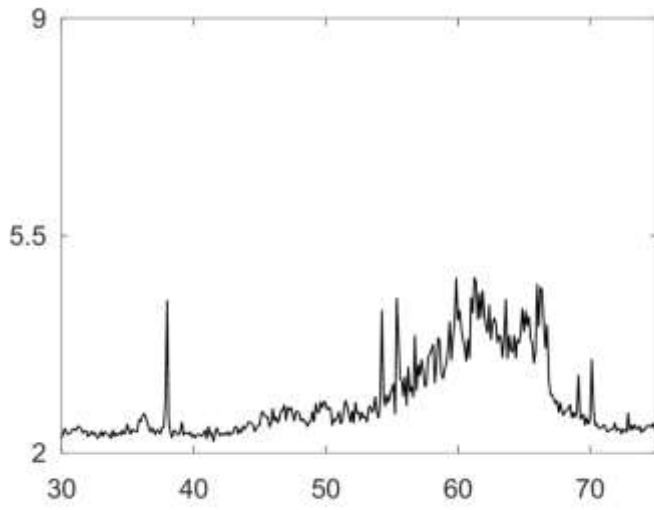
10



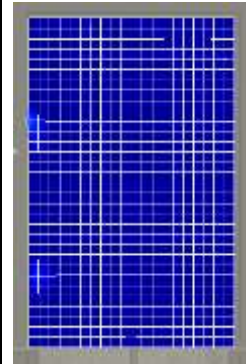
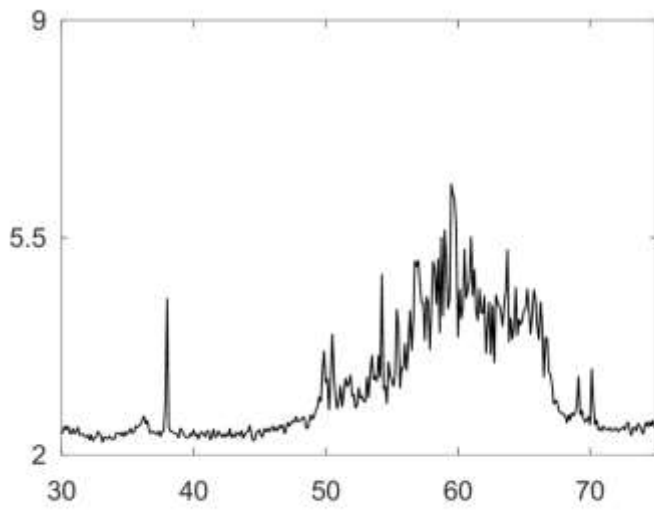
11



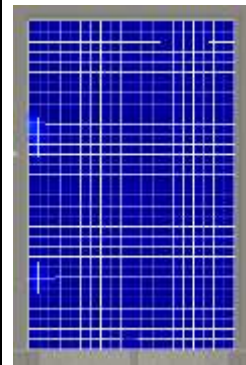
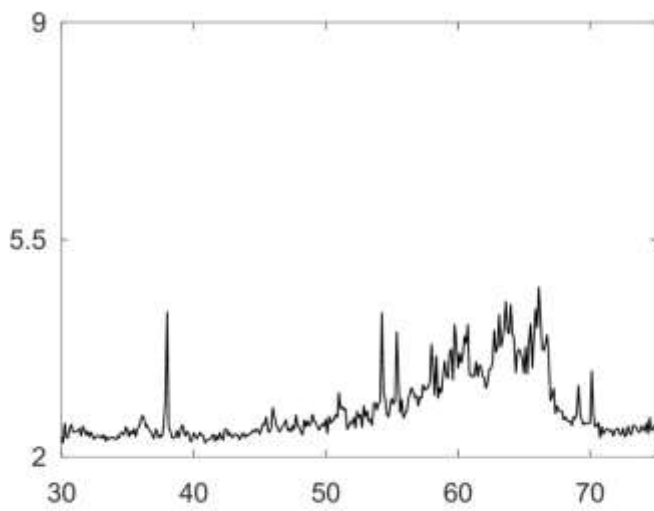
12



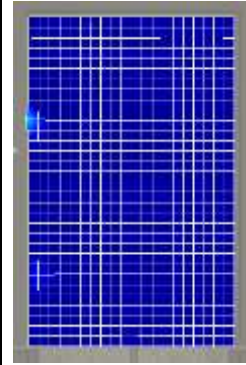
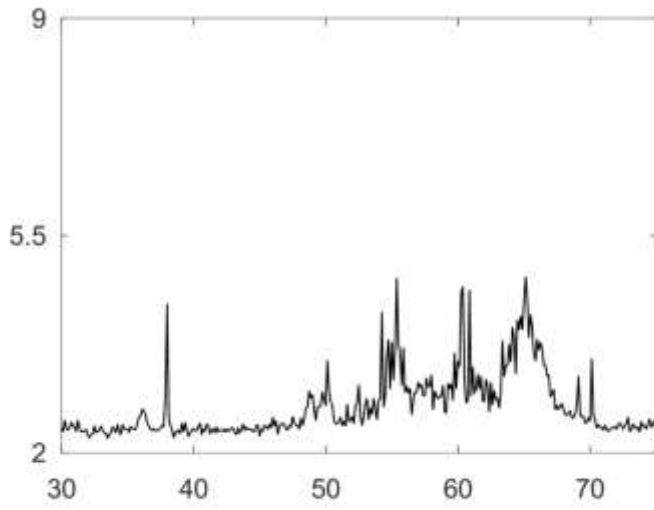
13



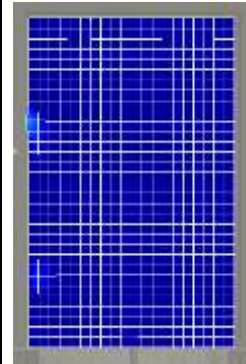
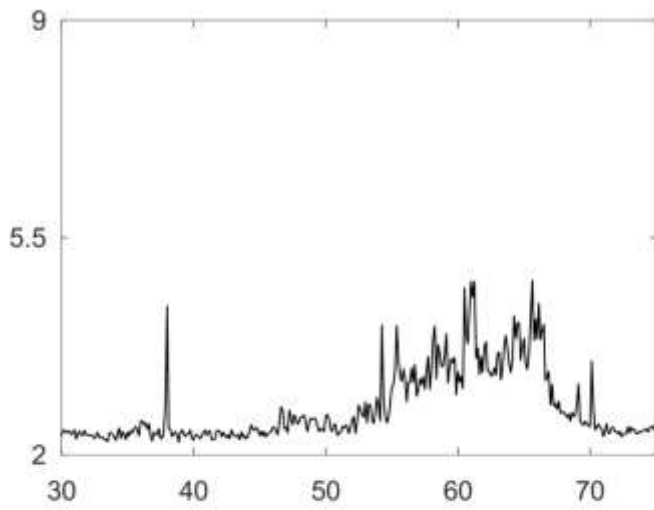
14



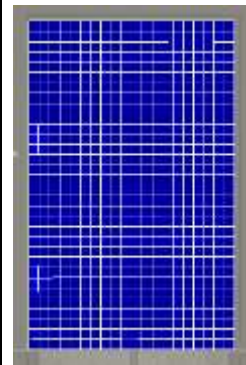
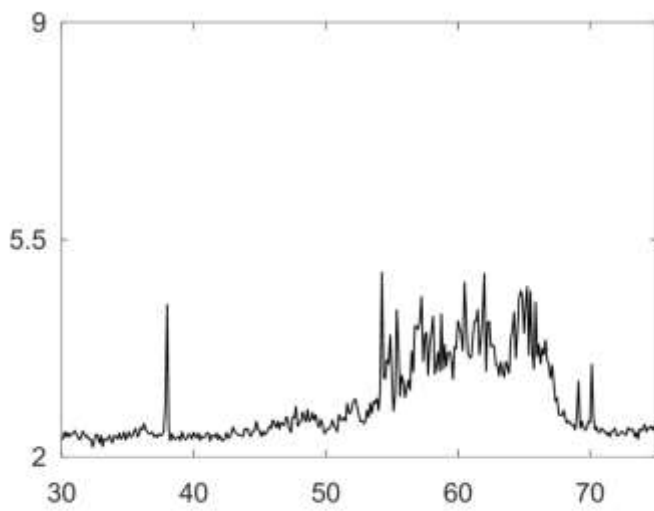
15



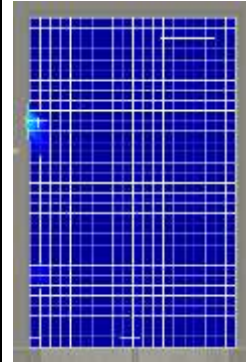
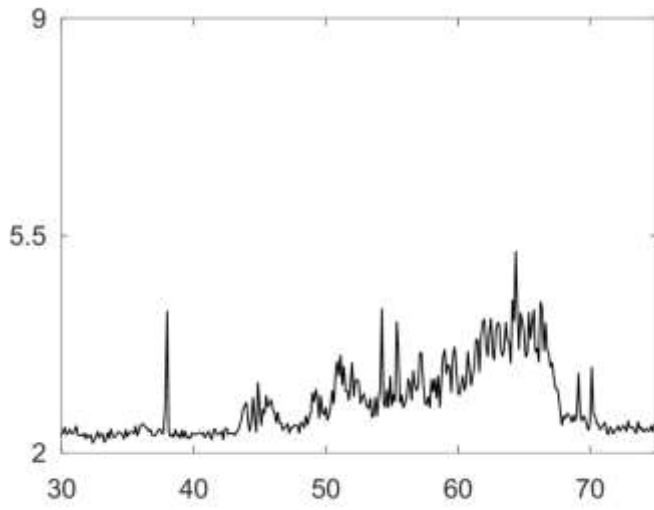
16



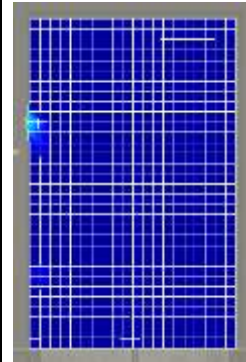
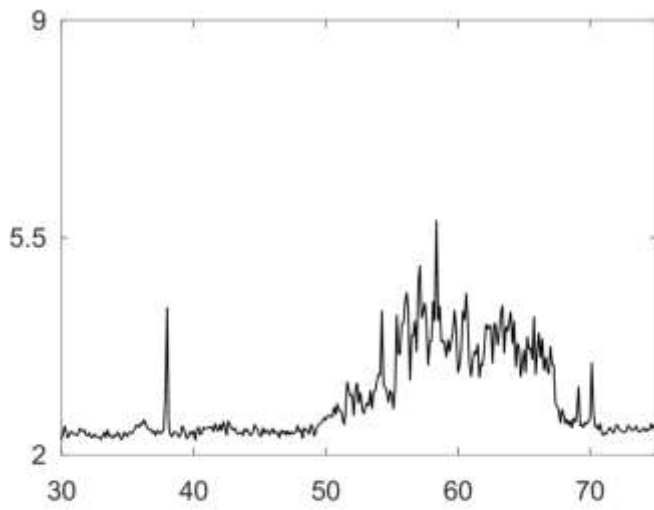
17



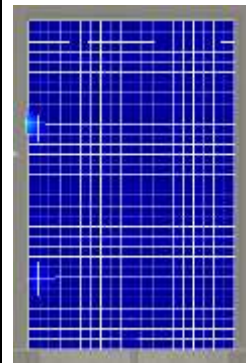
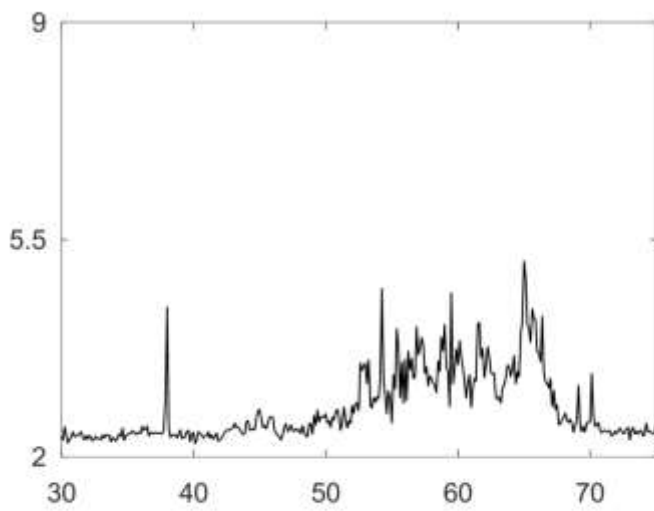
18



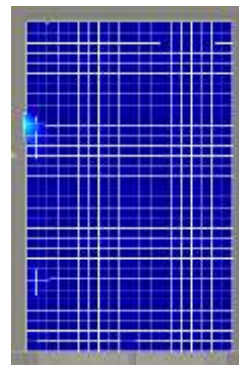
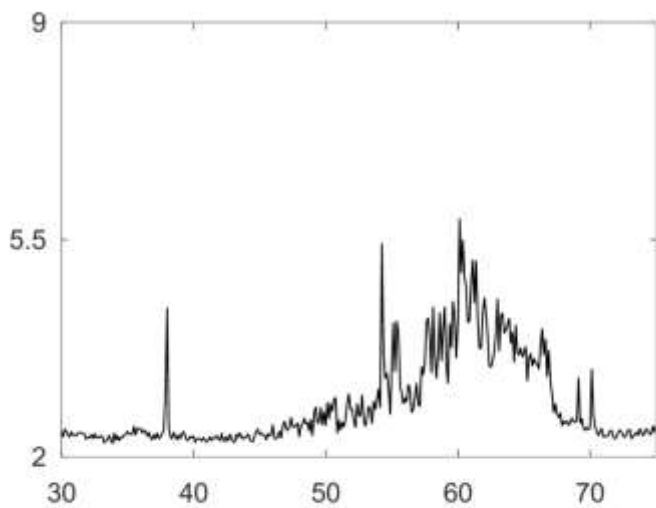
19



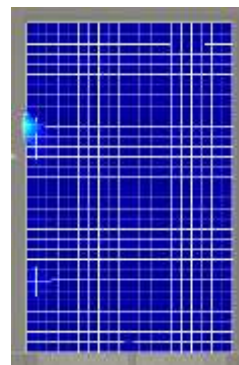
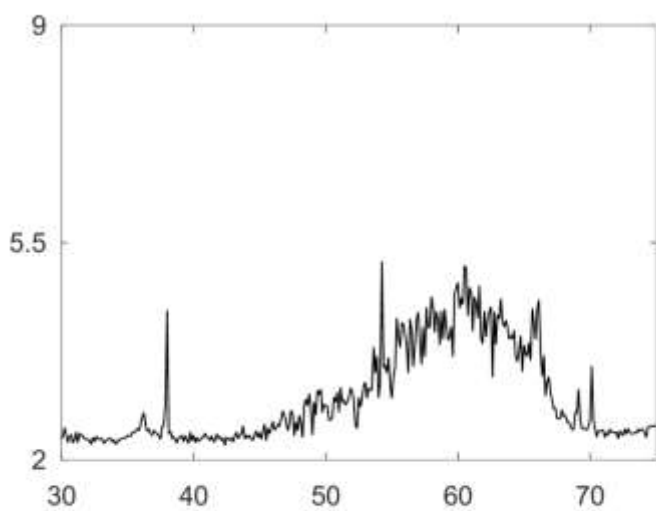
20



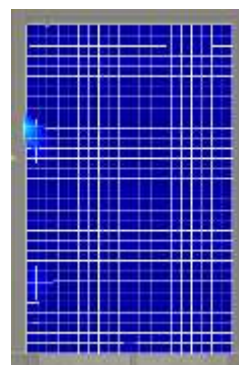
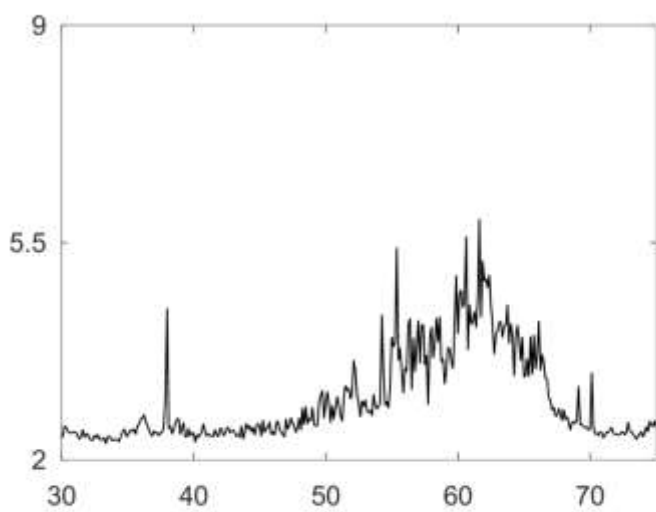
21



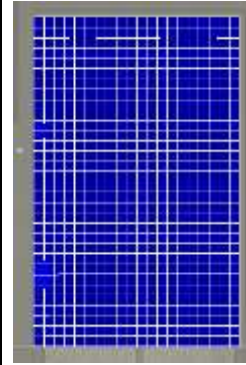
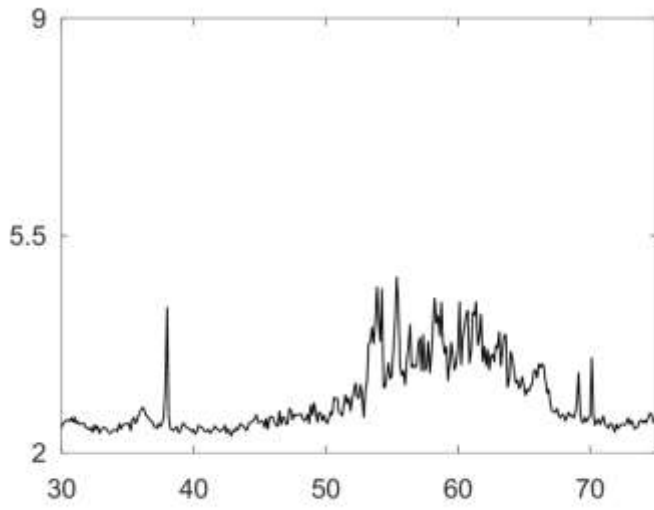
22



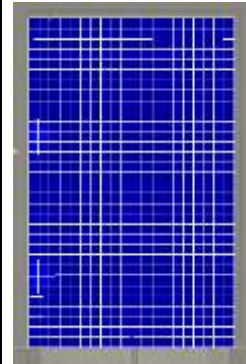
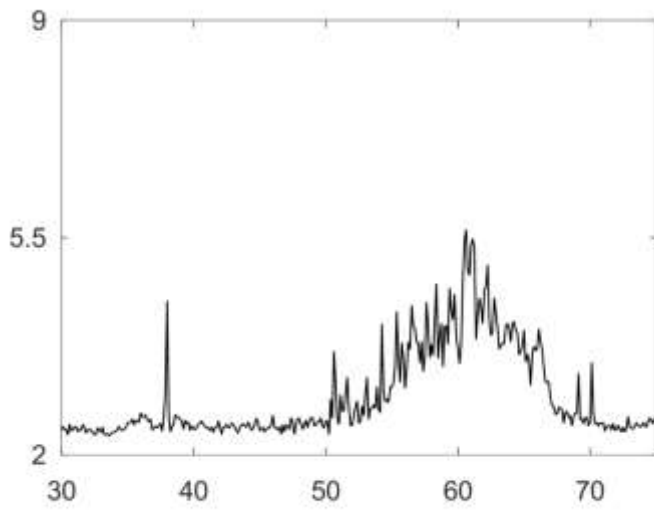
23



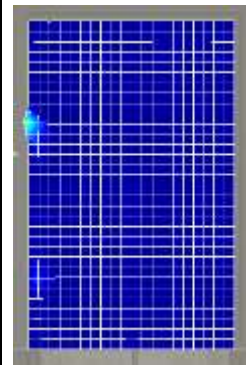
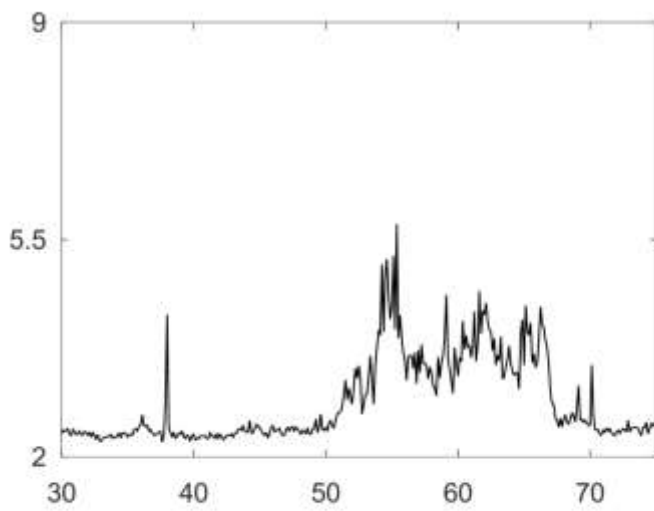
24



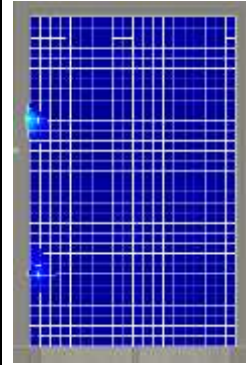
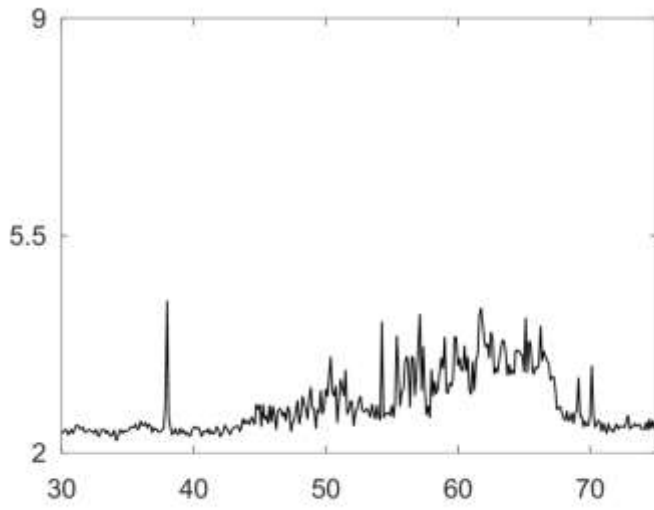
25



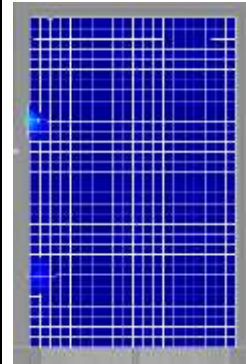
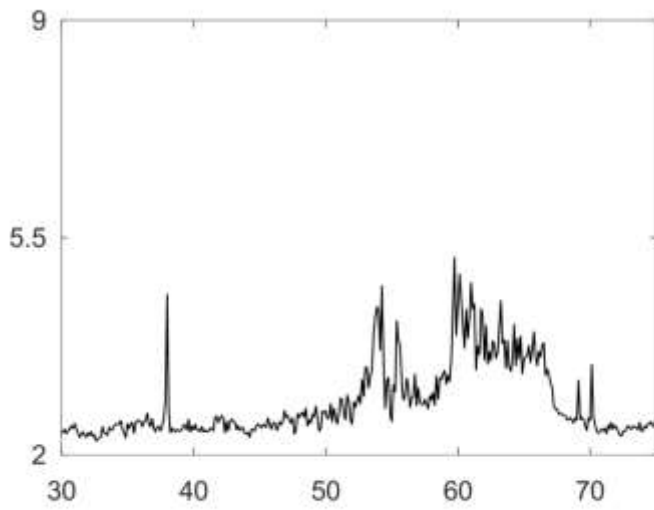
26



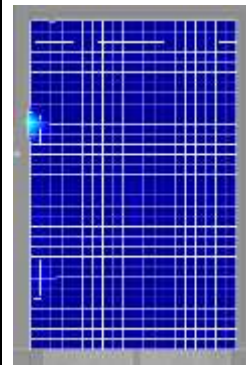
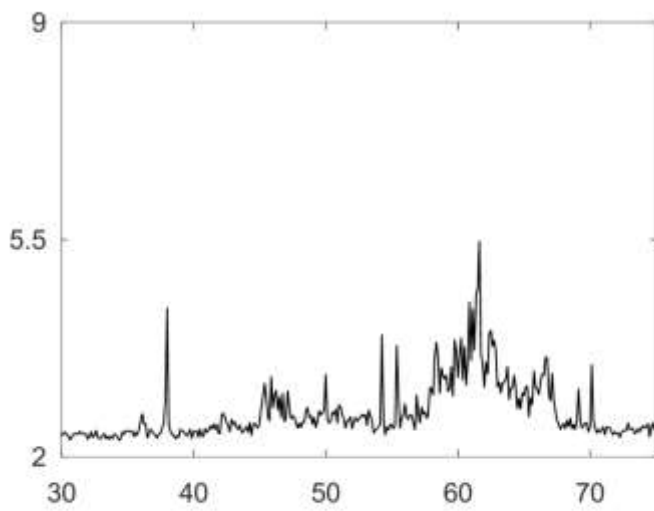
27



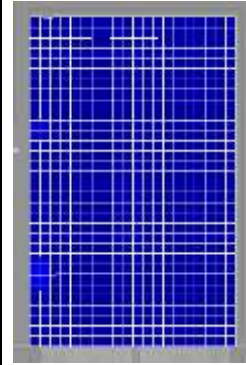
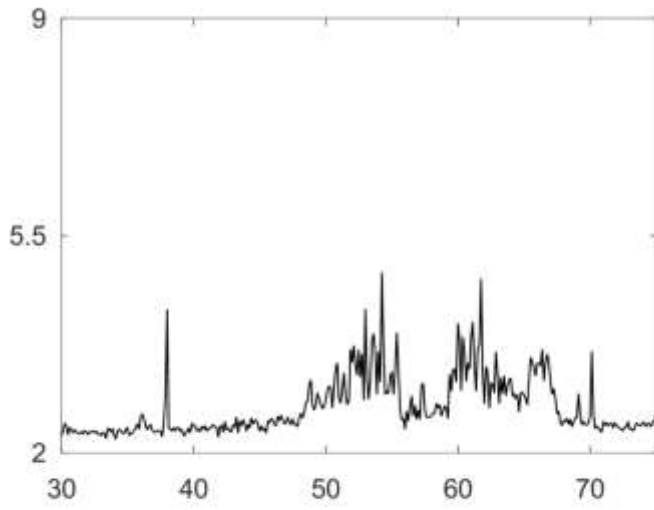
28



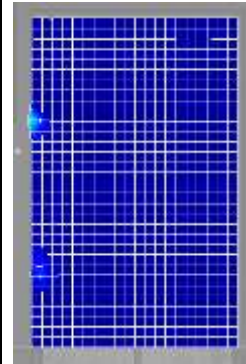
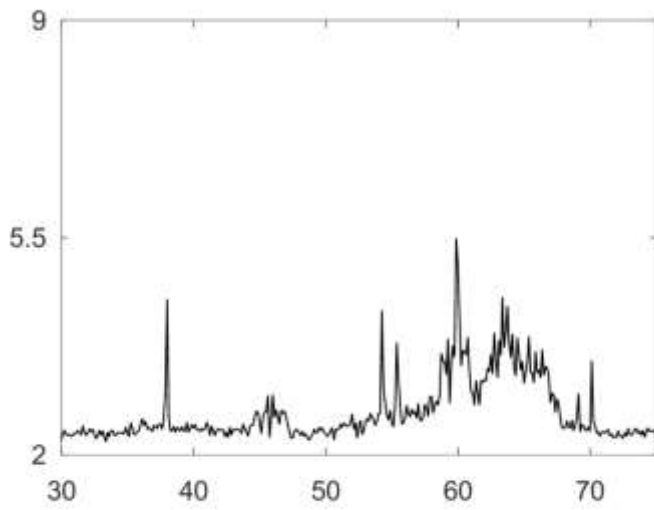
29



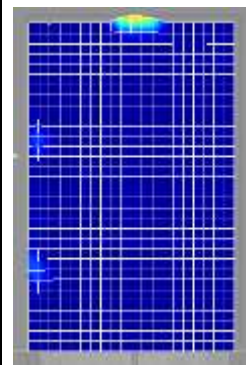
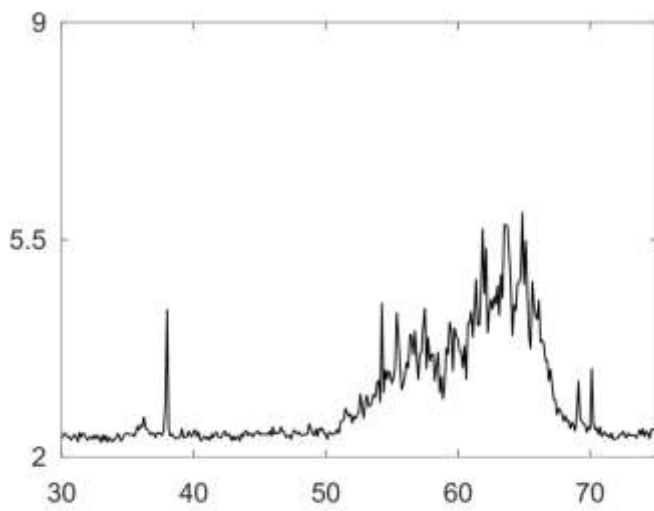
30



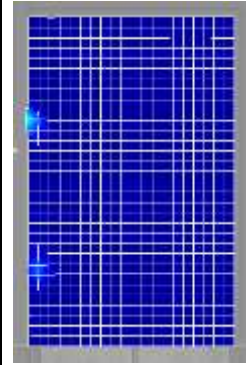
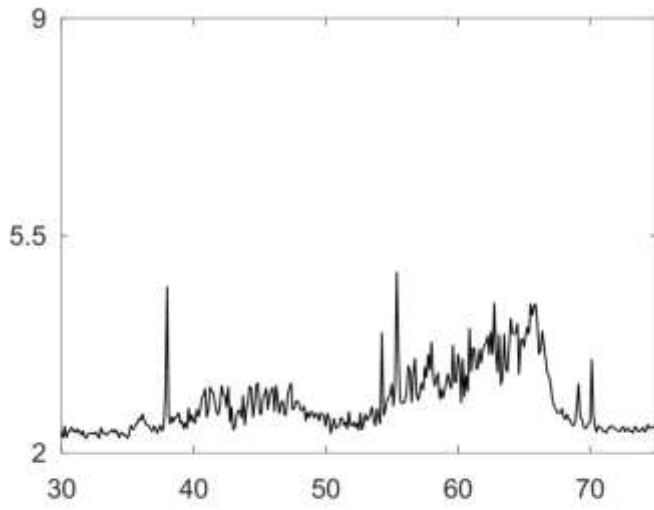
31



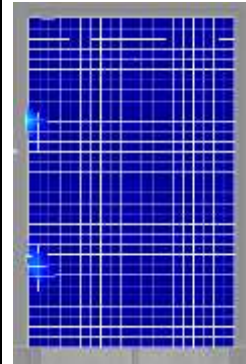
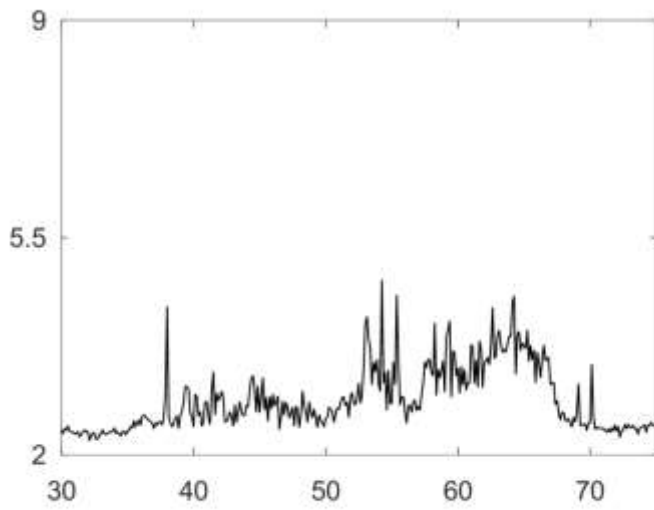
32



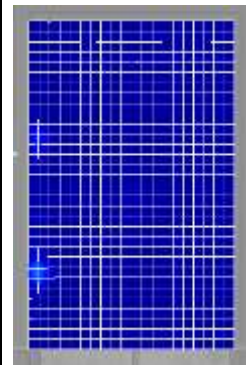
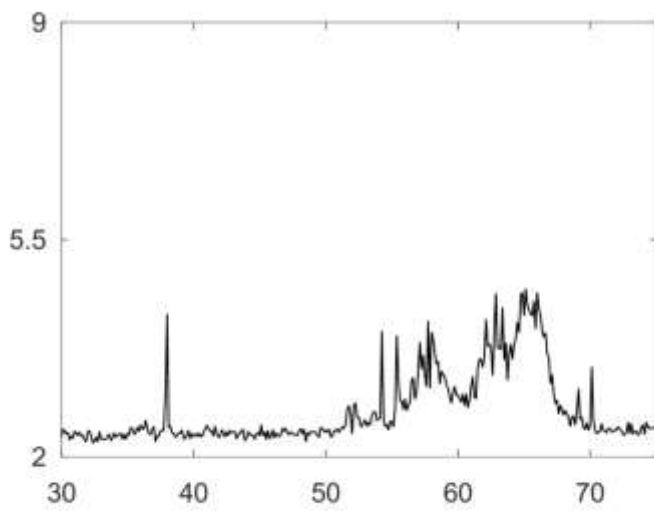
33



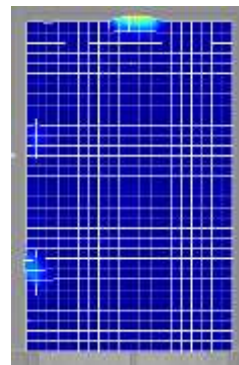
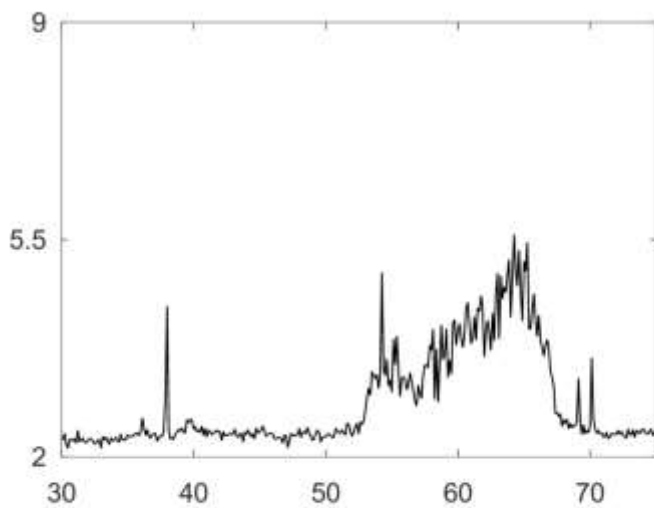
34



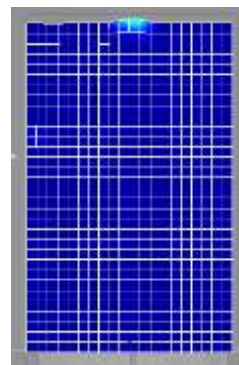
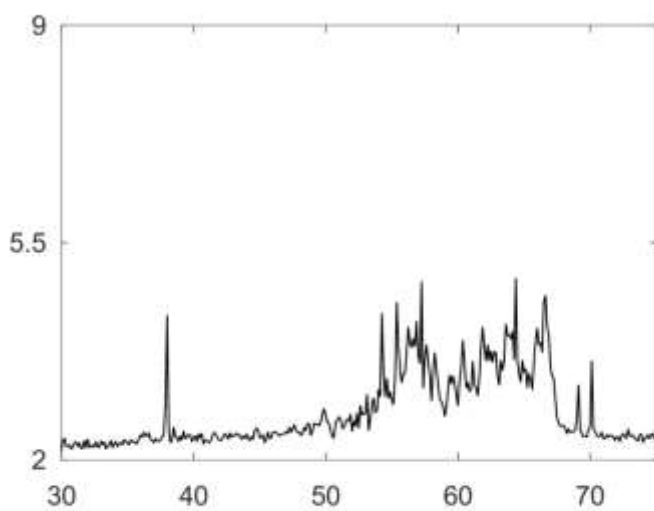
35



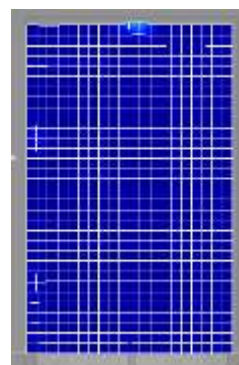
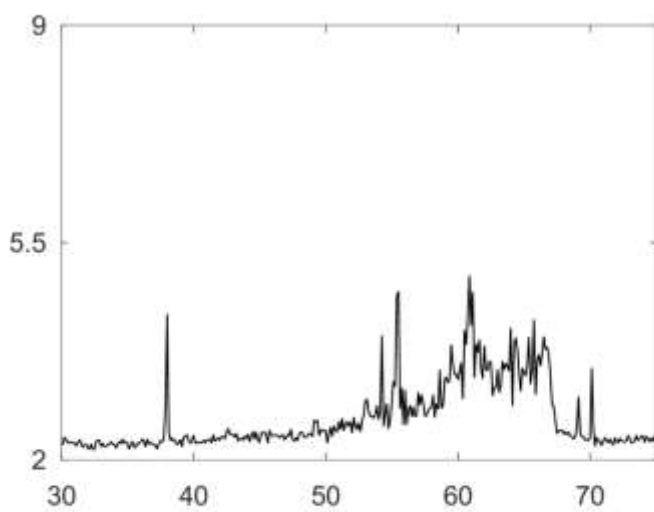
36



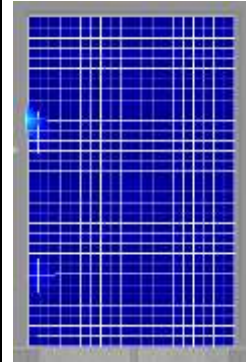
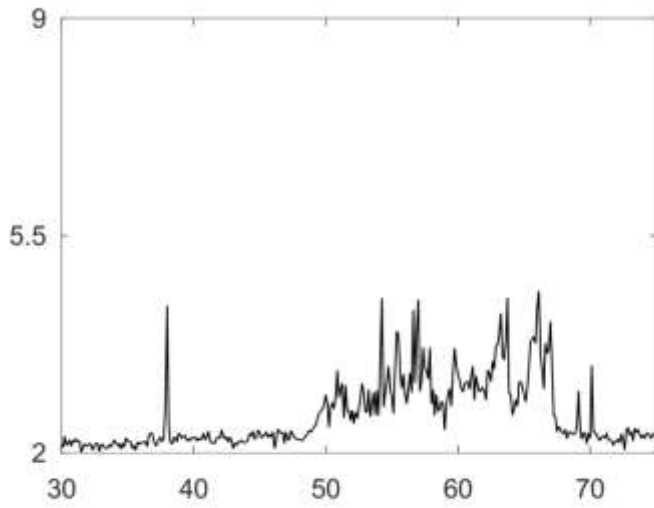
37



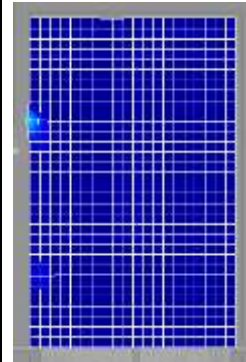
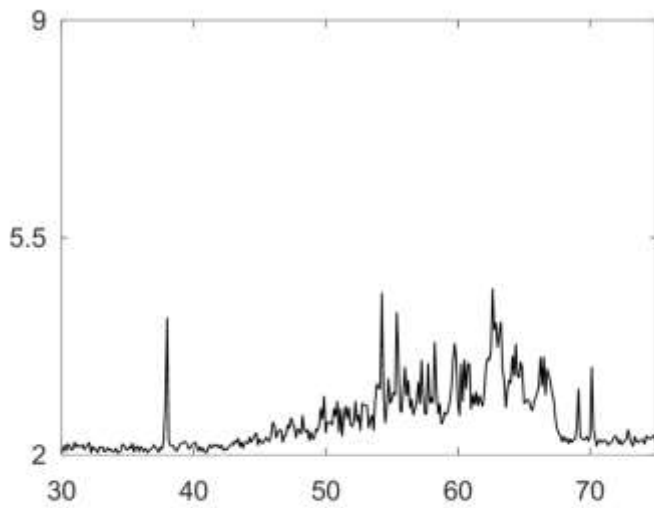
38



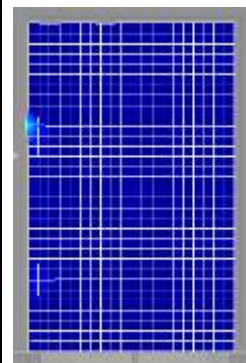
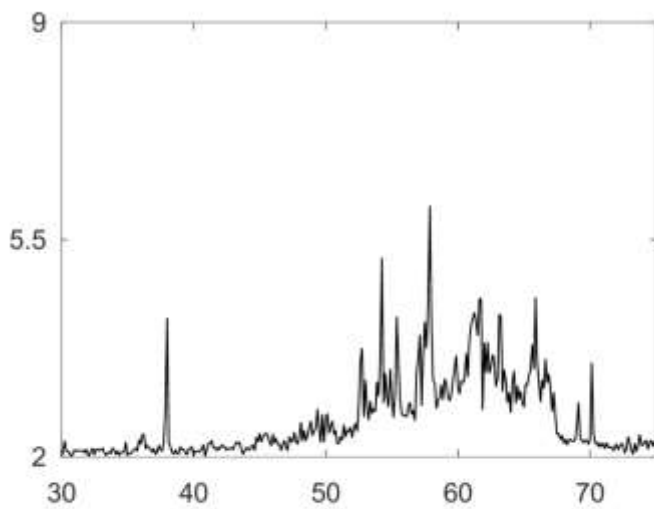
39



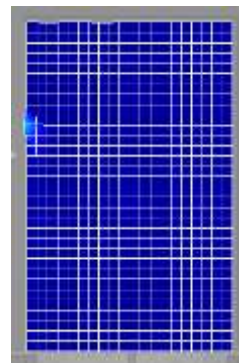
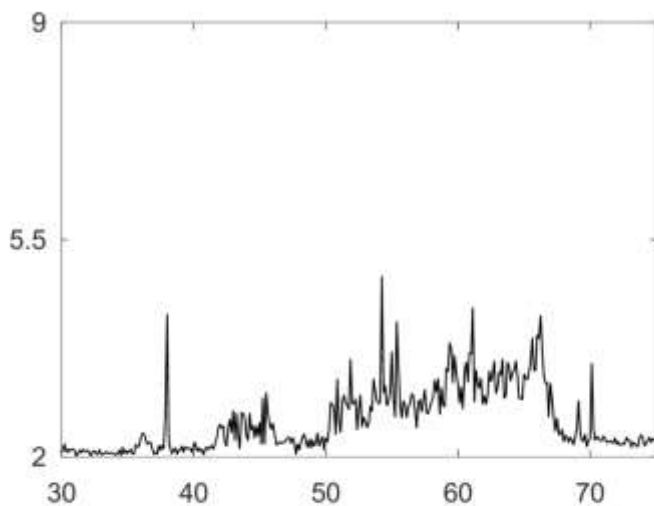
40



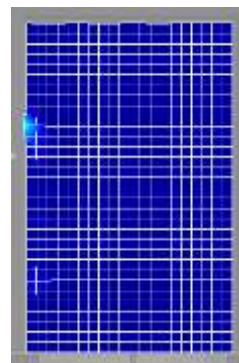
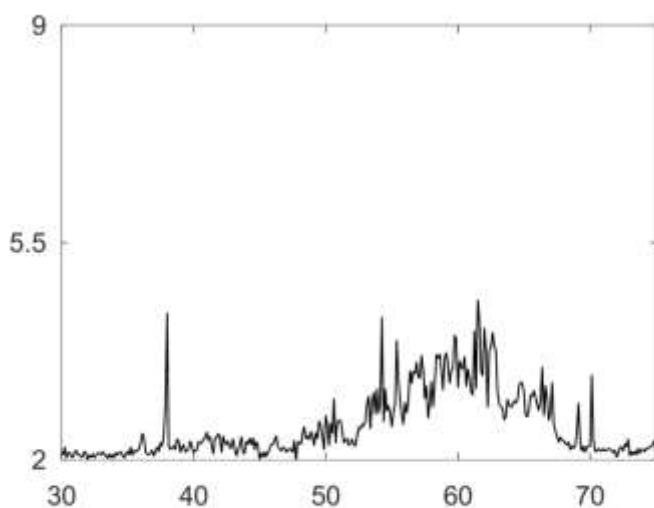
41



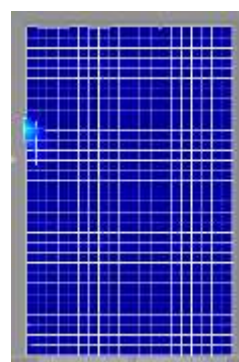
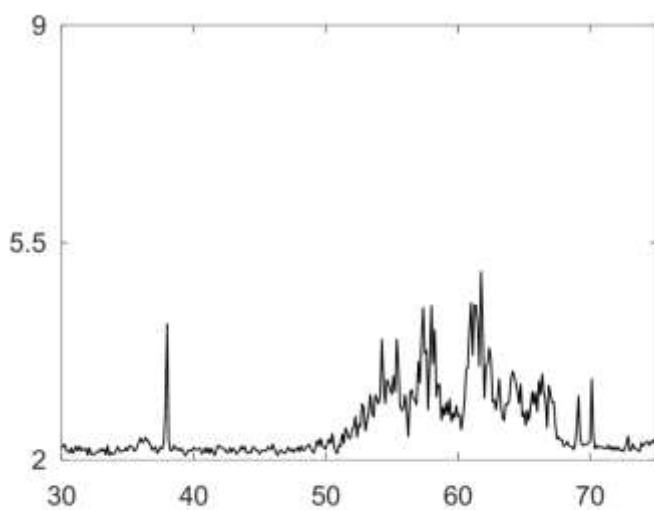
42



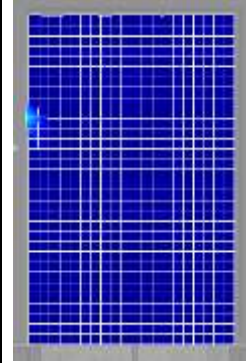
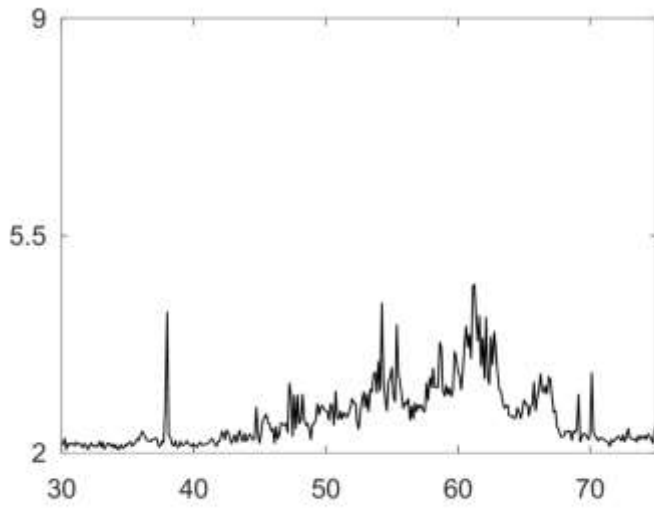
43



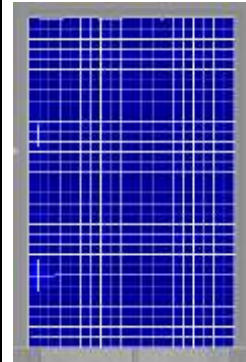
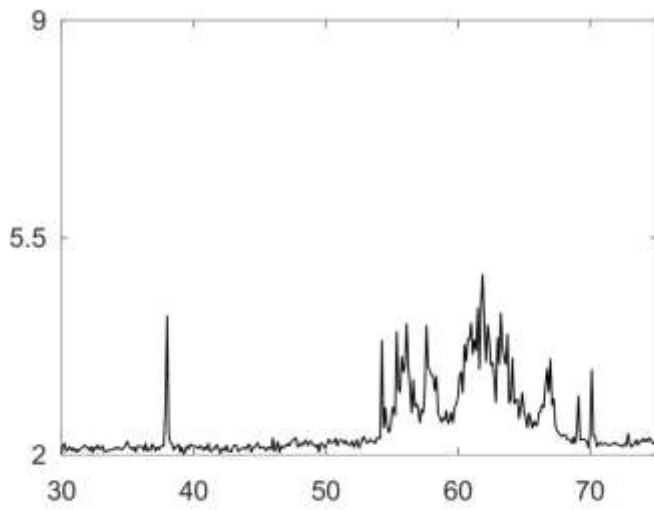
44



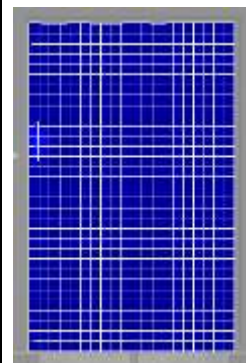
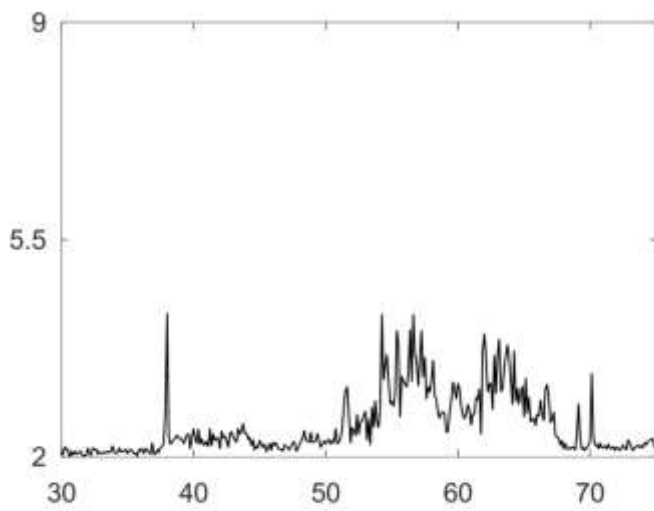
45



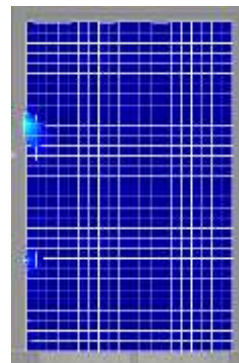
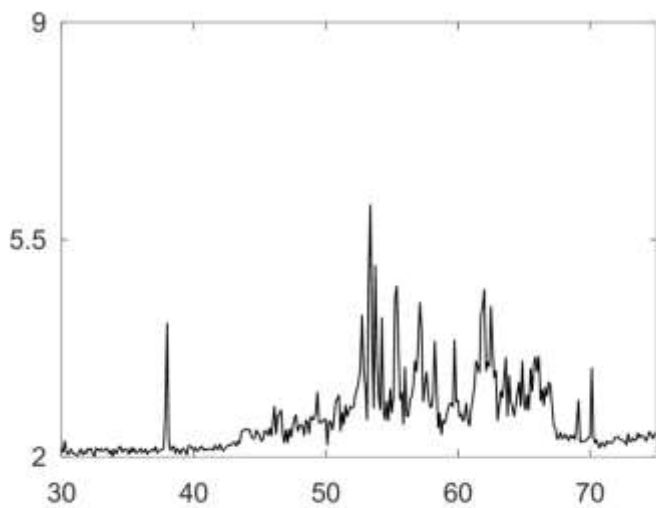
46



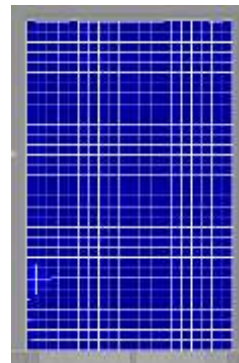
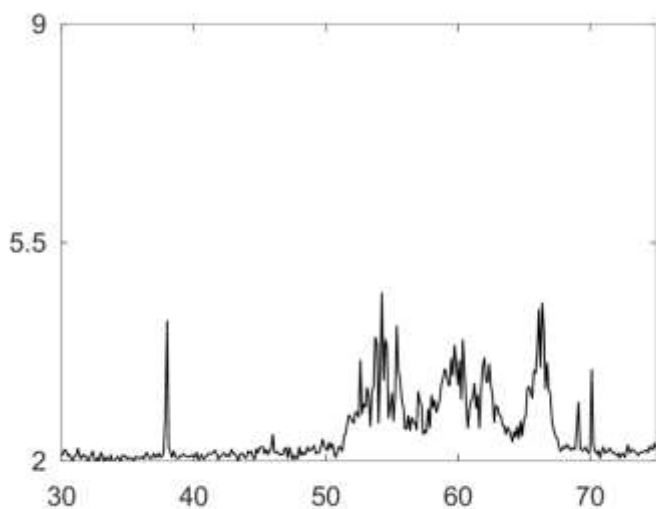
47



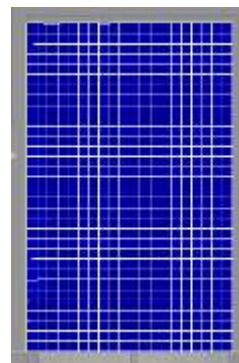
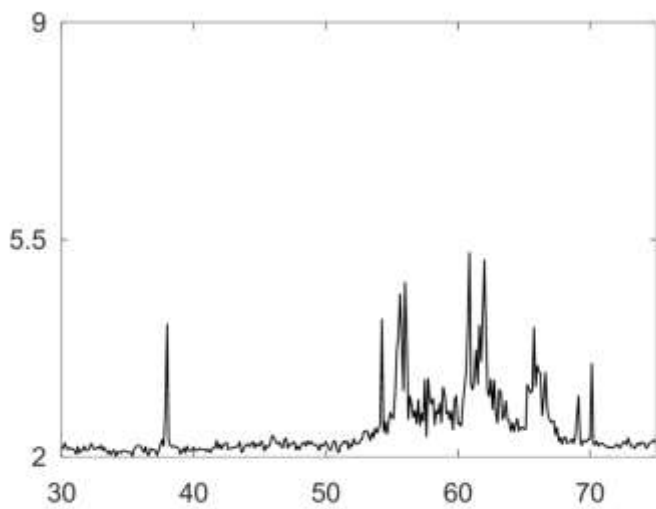
48



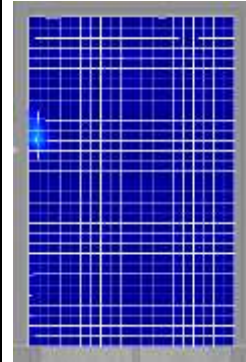
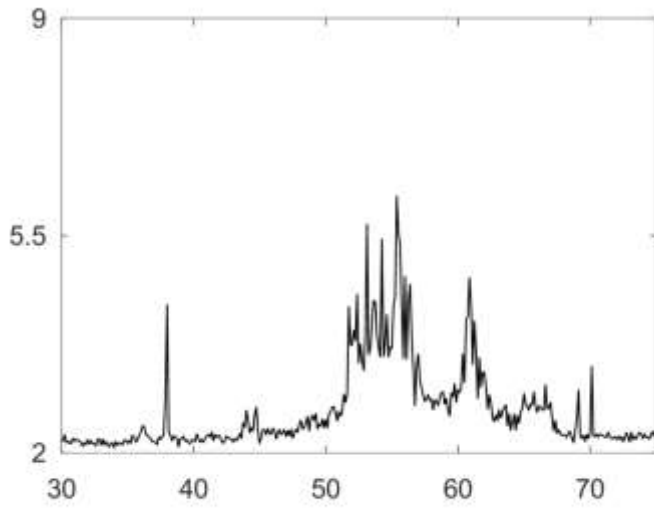
49



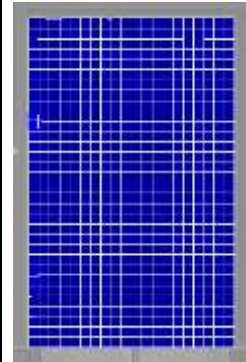
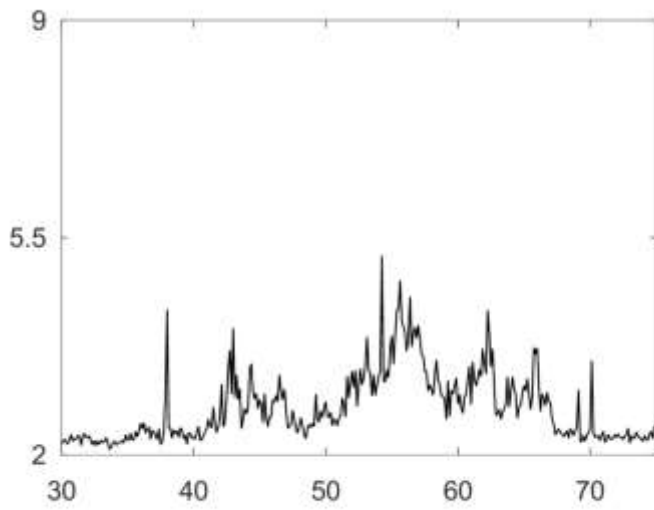
50



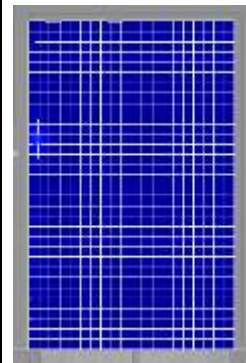
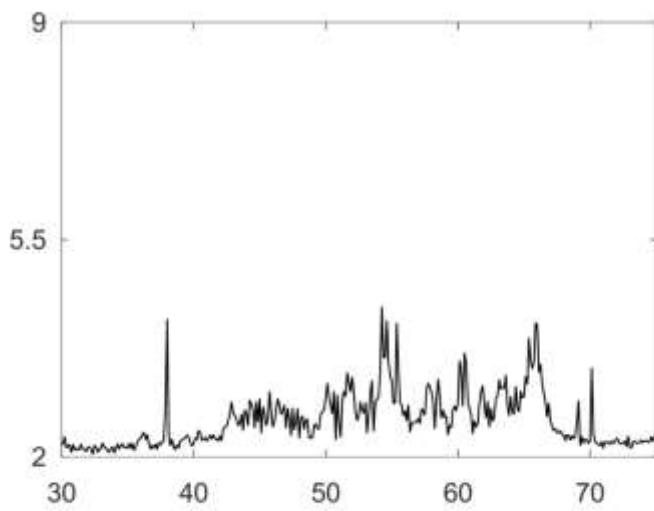
51



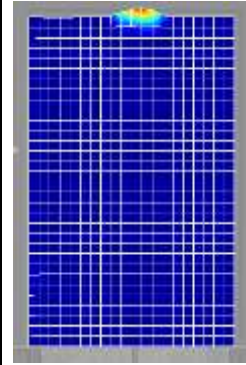
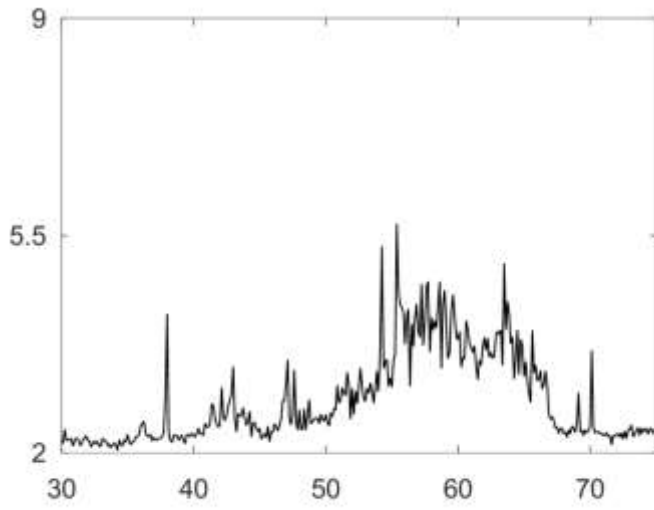
52



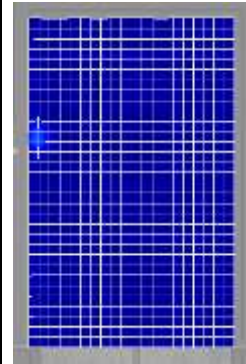
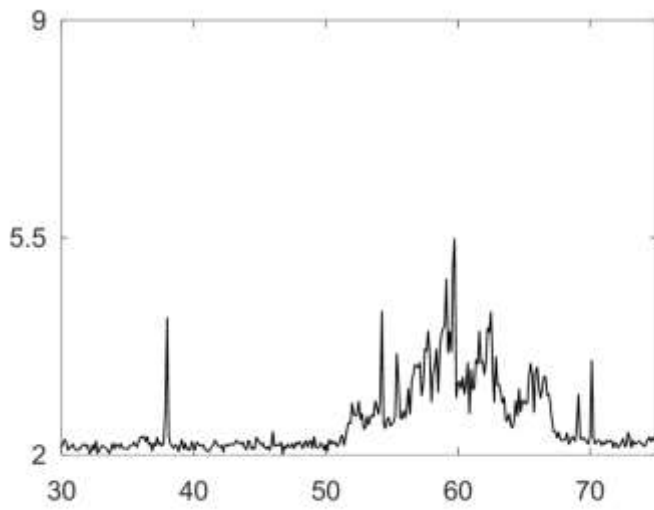
53



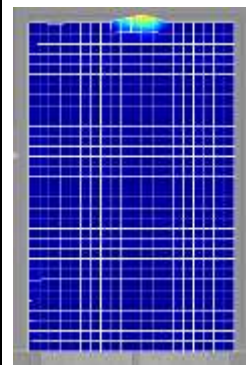
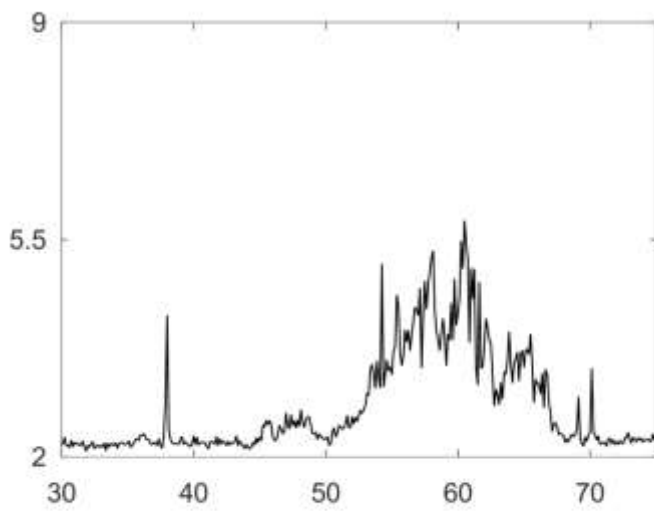
54



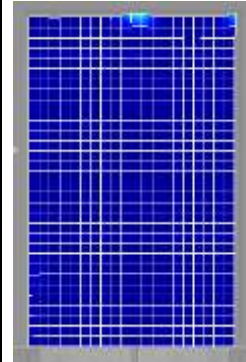
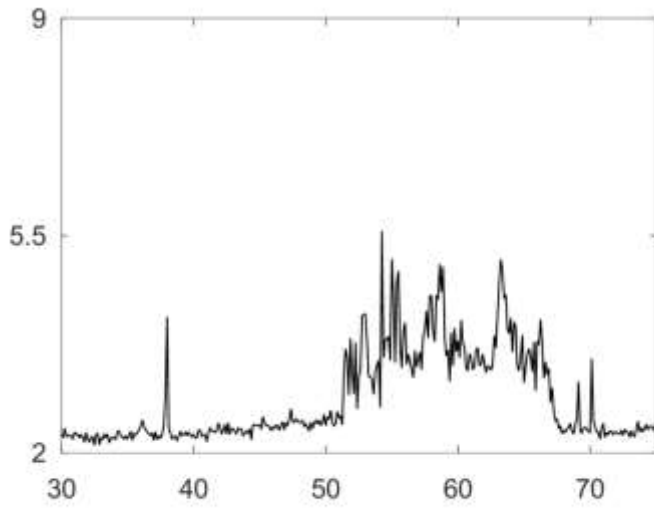
55



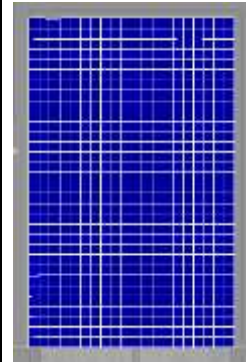
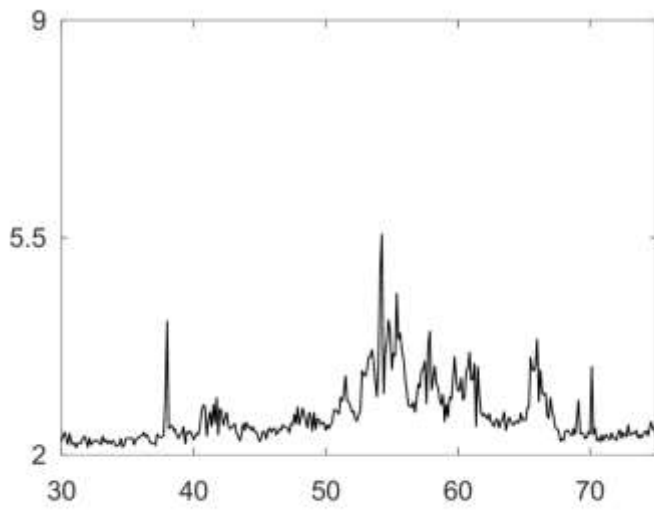
56



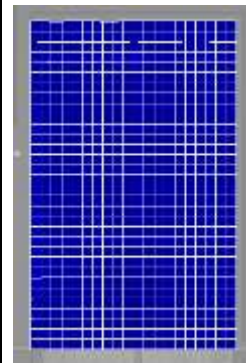
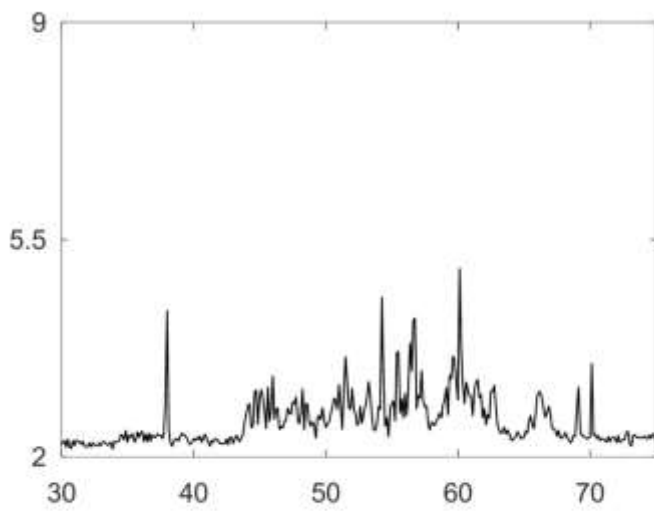
57



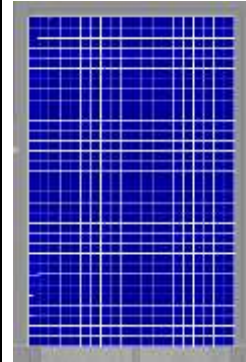
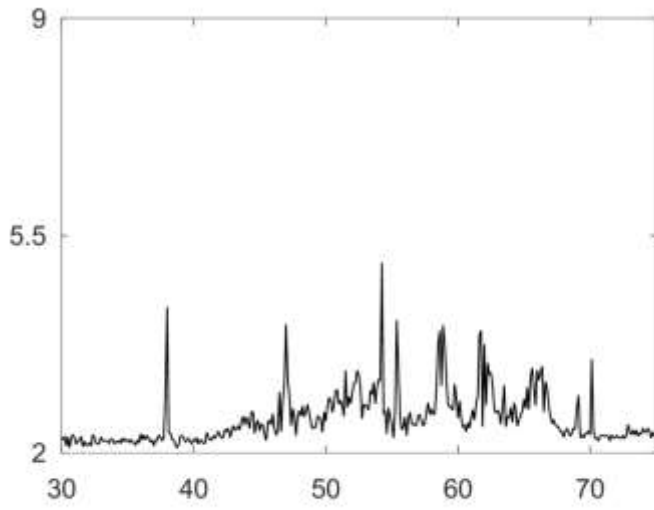
58



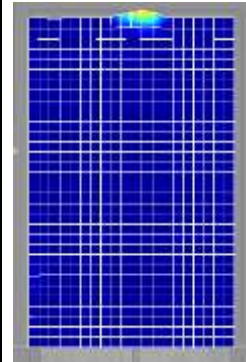
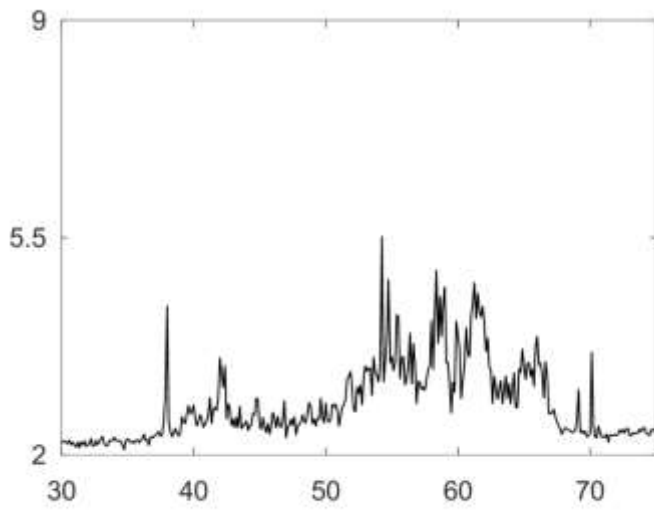
59



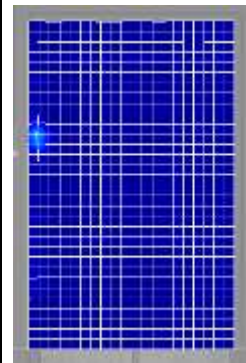
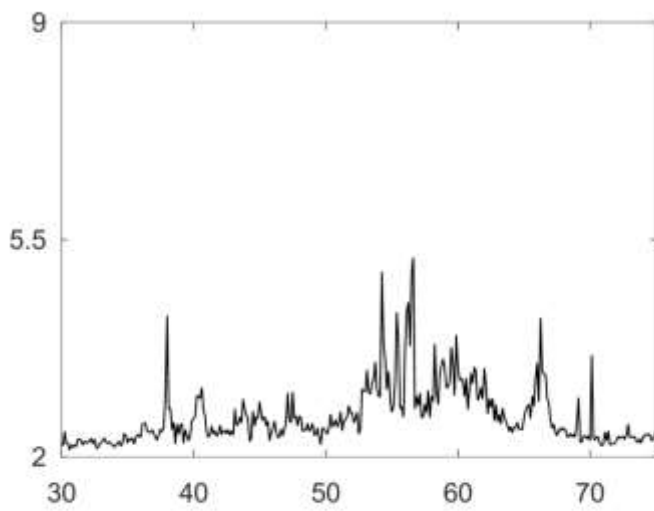
60



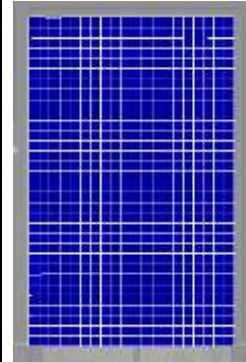
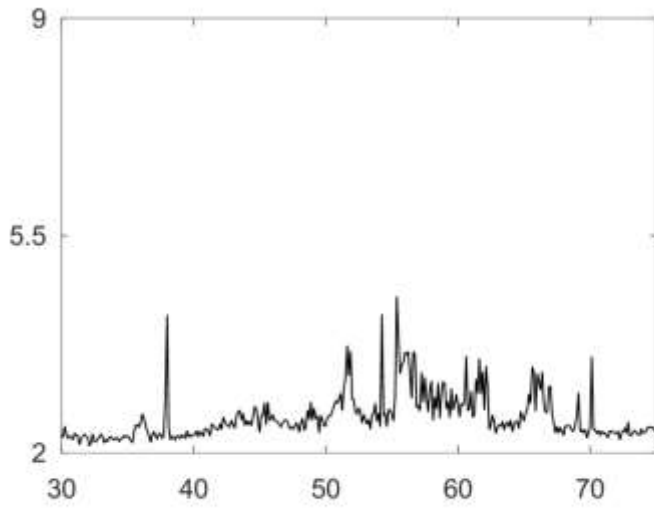
61



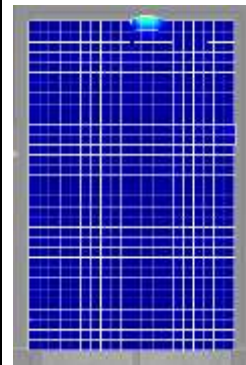
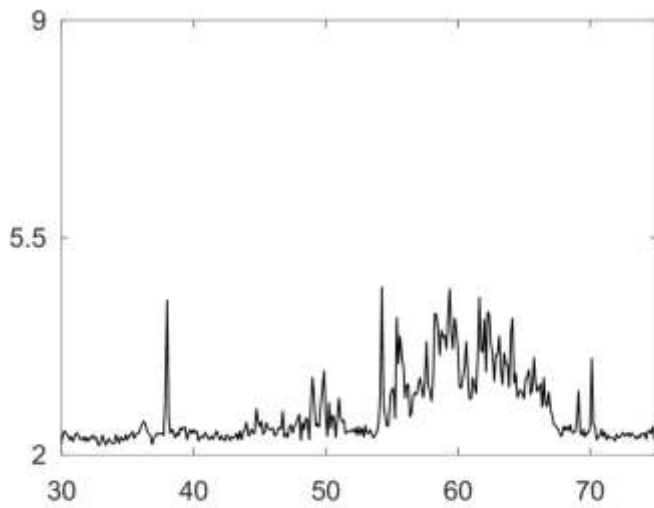
62



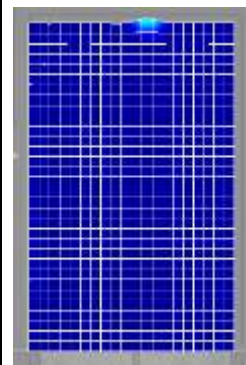
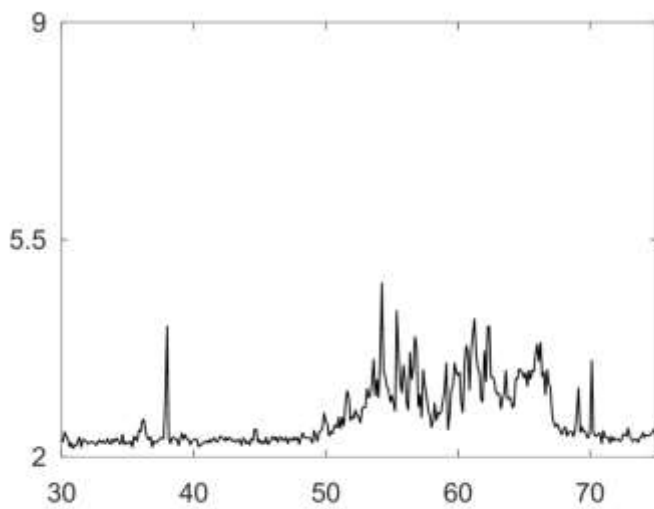
63



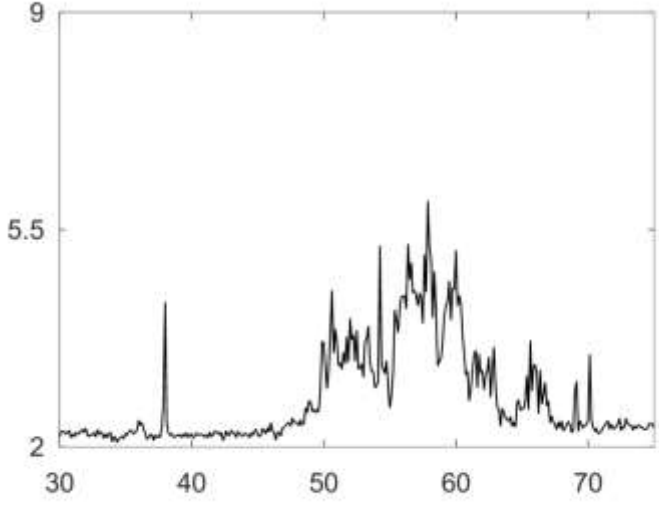
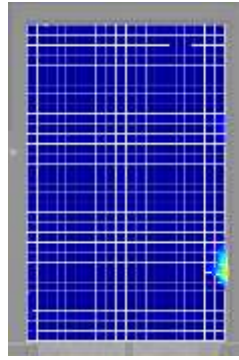
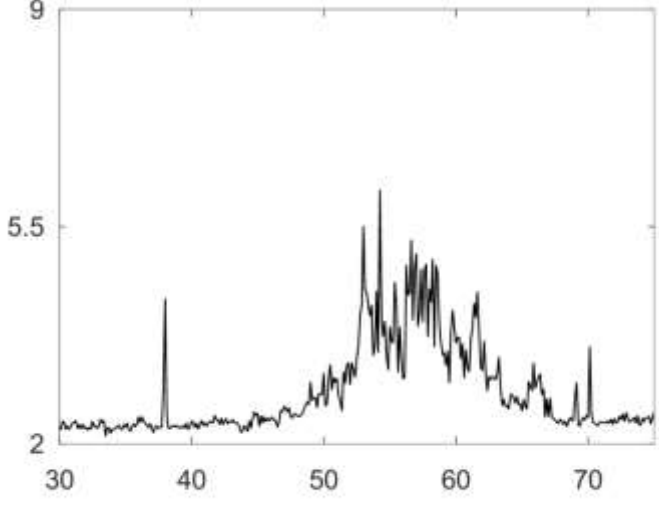
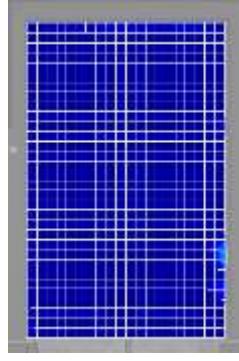
64



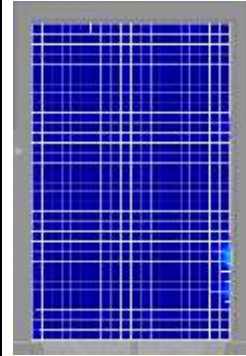
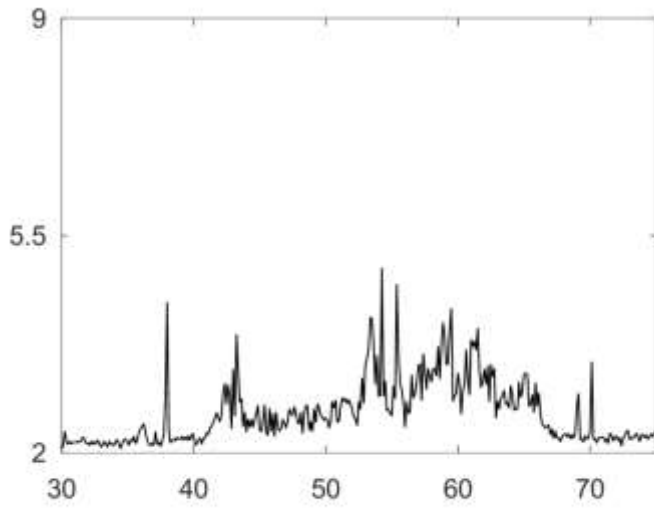
65



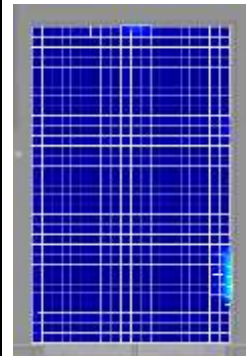
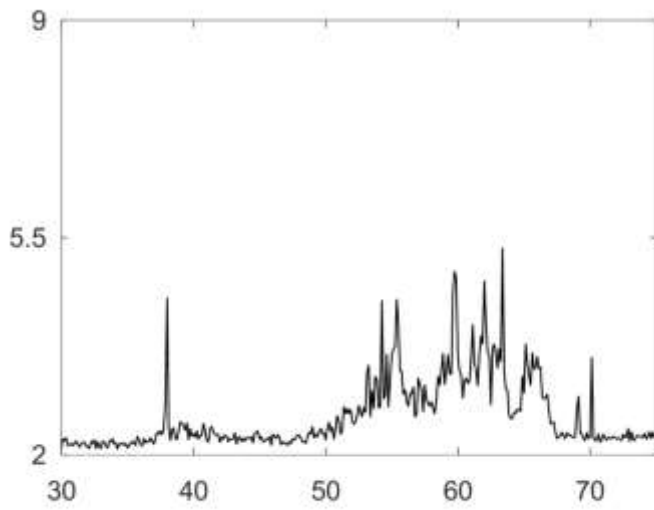
Run 4

Time	Displacement (in pm) vs. Frequency (in kHz)	RMS Surface Displacement 1.2 nm  0 nm
1		
2		

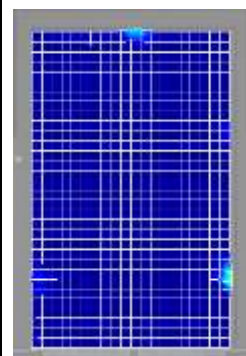
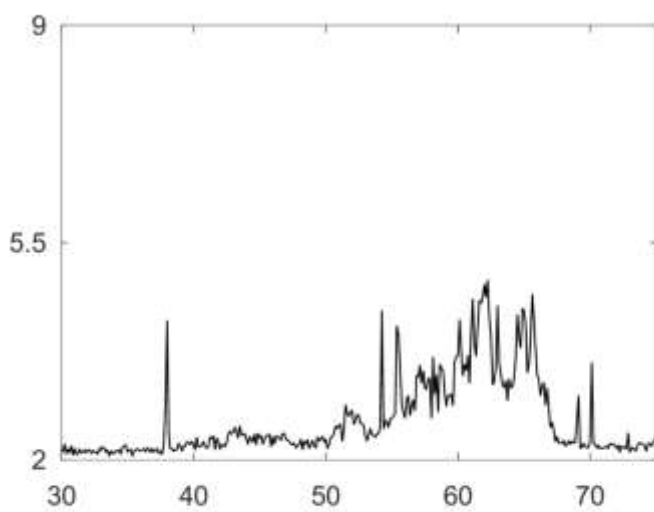
3



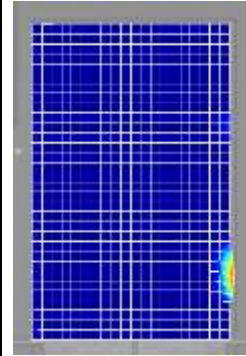
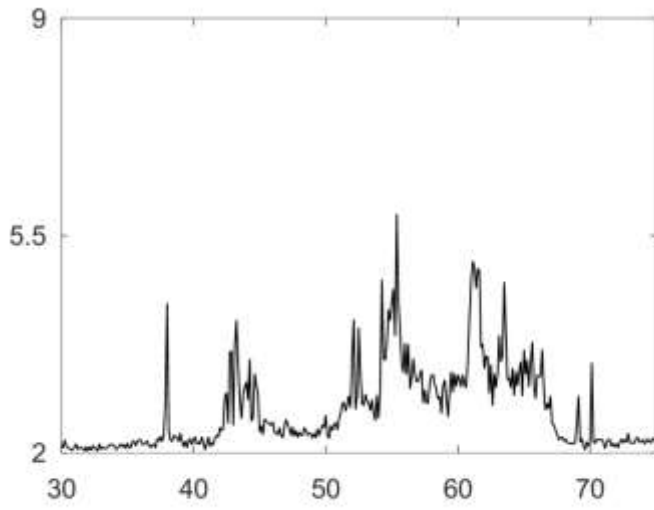
4



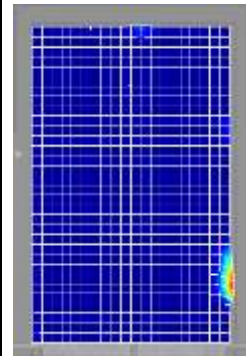
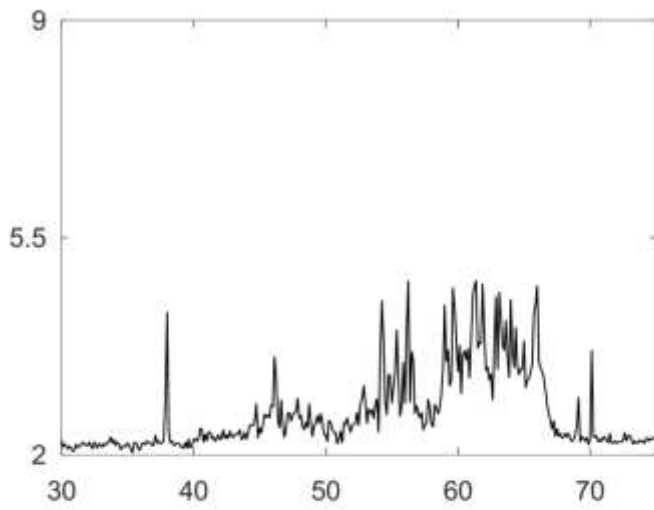
5



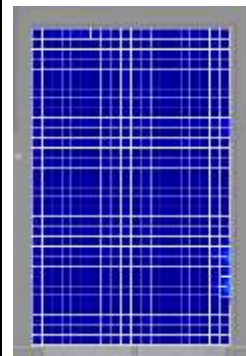
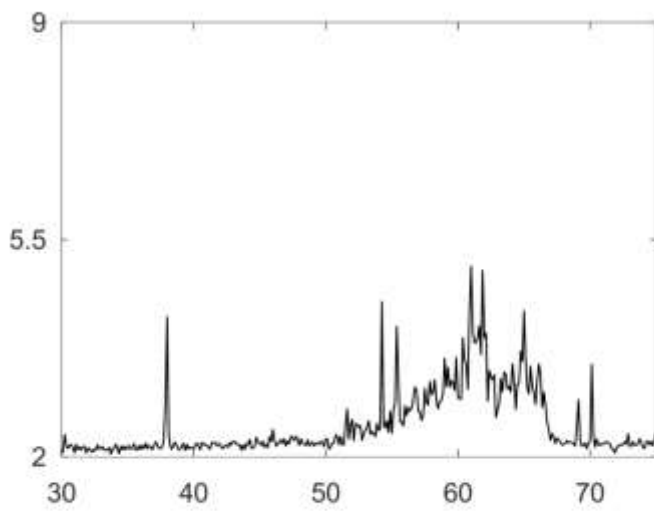
6



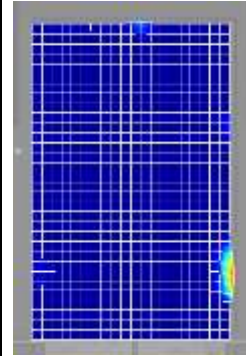
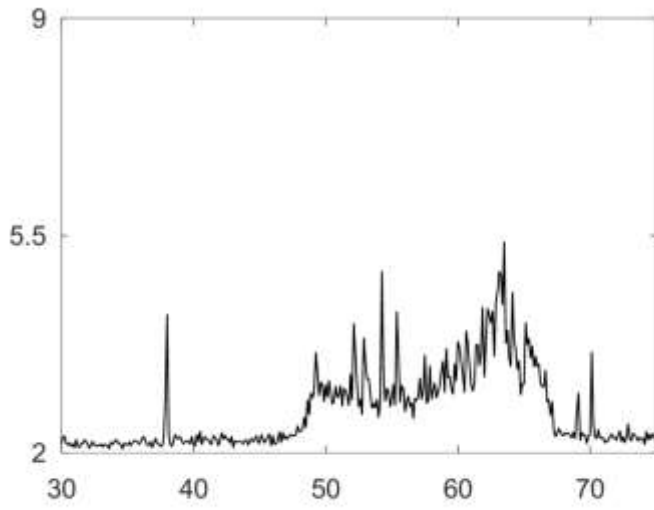
7



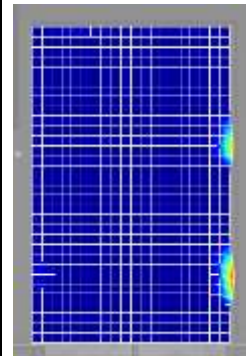
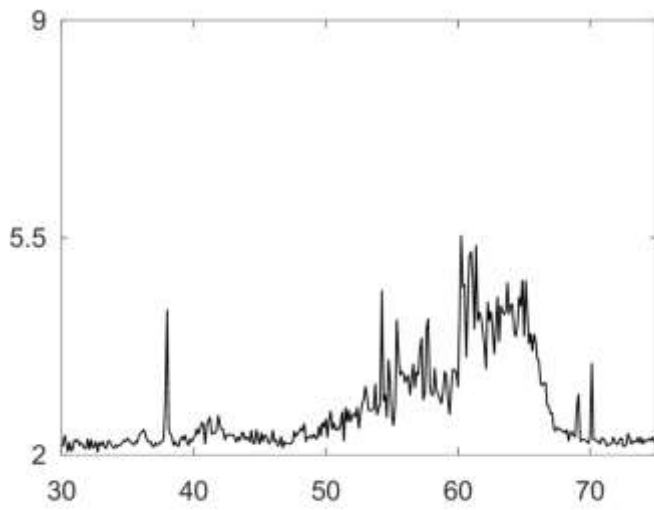
8



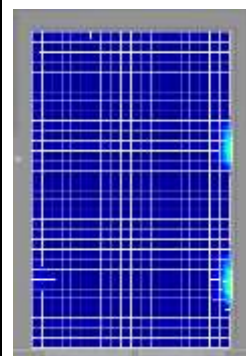
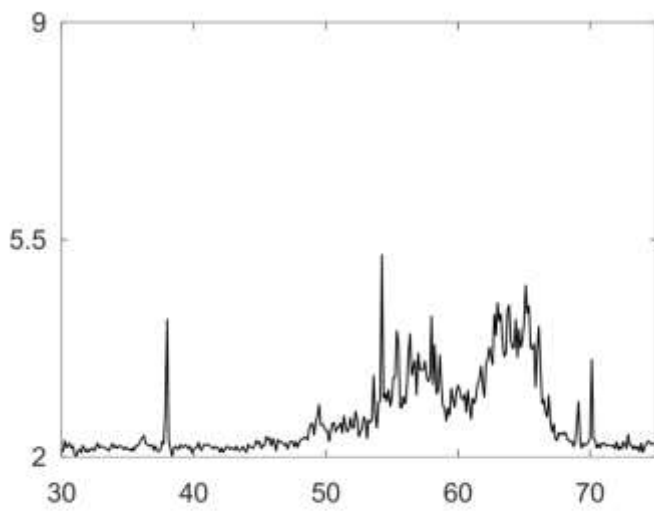
9

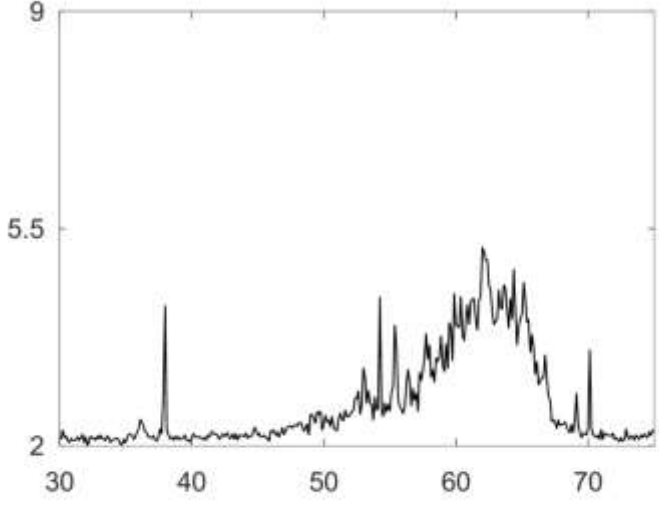
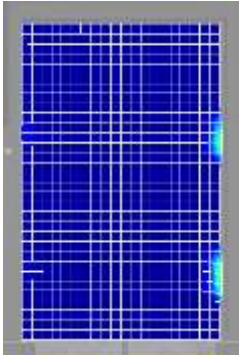
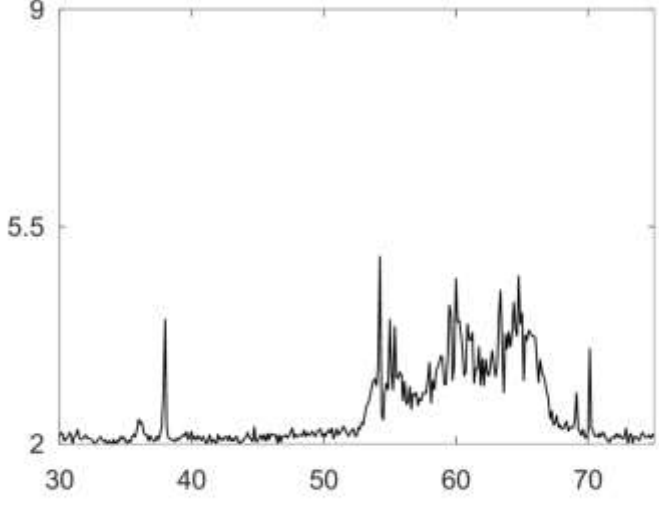
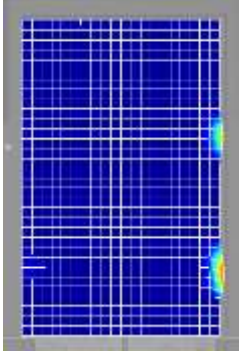
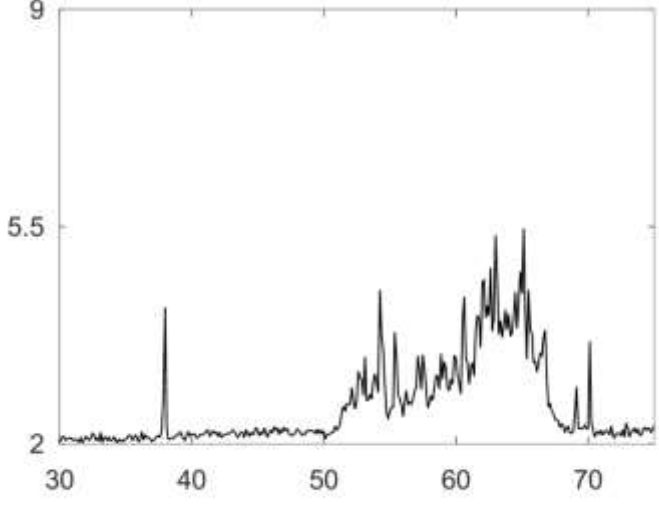
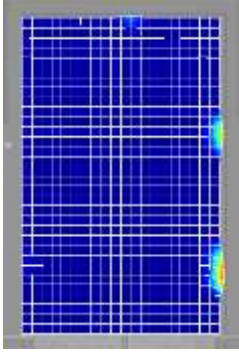


10

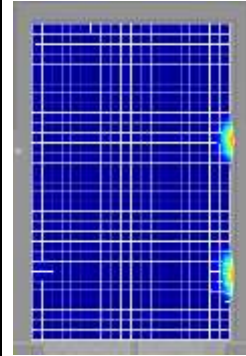
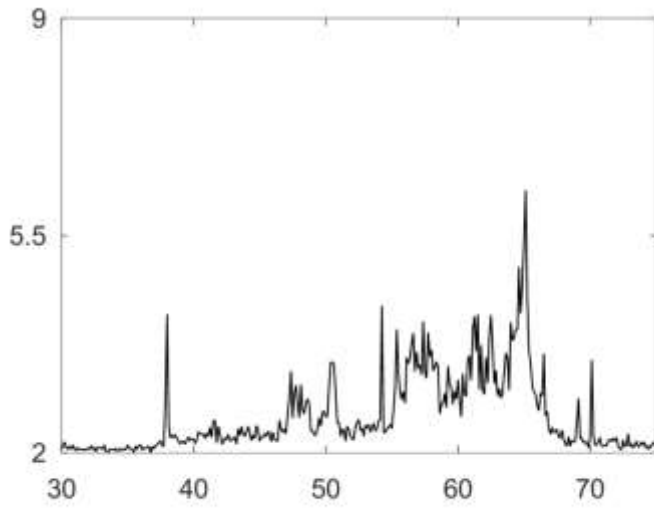


11

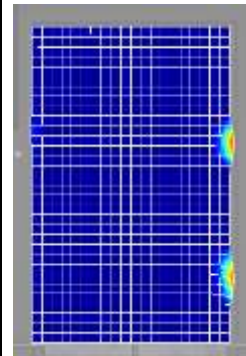
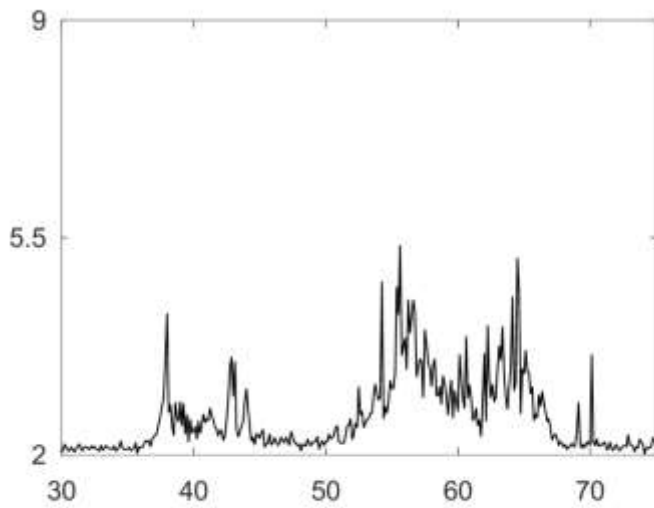


<p>12</p>	 <p>The line graph for row 12 shows a signal on a coordinate system where the x-axis ranges from 30 to 70 and the y-axis ranges from 2 to 9. A sharp peak is visible at approximately x=38 with a height of about 4. A broad, noisy peak is centered around x=65, reaching a maximum height of approximately 5.5.</p>	 <p>The heatmap for row 12 displays a grid of data points. A vertical band of high intensity (yellow and red) is located on the right side of the plot, corresponding to the x-axis values between 60 and 70. The rest of the plot is mostly blue, indicating low intensity.</p>
<p>13</p>	 <p>The line graph for row 13 shows a signal on a coordinate system where the x-axis ranges from 30 to 70 and the y-axis ranges from 2 to 9. A sharp peak is visible at approximately x=38 with a height of about 4. A broad, noisy peak is centered around x=65, reaching a maximum height of approximately 5.5.</p>	 <p>The heatmap for row 13 displays a grid of data points. A vertical band of high intensity (yellow and red) is located on the right side of the plot, corresponding to the x-axis values between 60 and 70. The rest of the plot is mostly blue, indicating low intensity.</p>
<p>14</p>	 <p>The line graph for row 14 shows a signal on a coordinate system where the x-axis ranges from 30 to 70 and the y-axis ranges from 2 to 9. A sharp peak is visible at approximately x=38 with a height of about 4. A broad, noisy peak is centered around x=65, reaching a maximum height of approximately 5.5.</p>	 <p>The heatmap for row 14 displays a grid of data points. A vertical band of high intensity (yellow and red) is located on the right side of the plot, corresponding to the x-axis values between 60 and 70. The rest of the plot is mostly blue, indicating low intensity.</p>

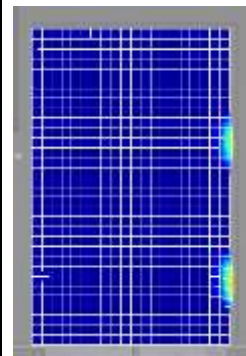
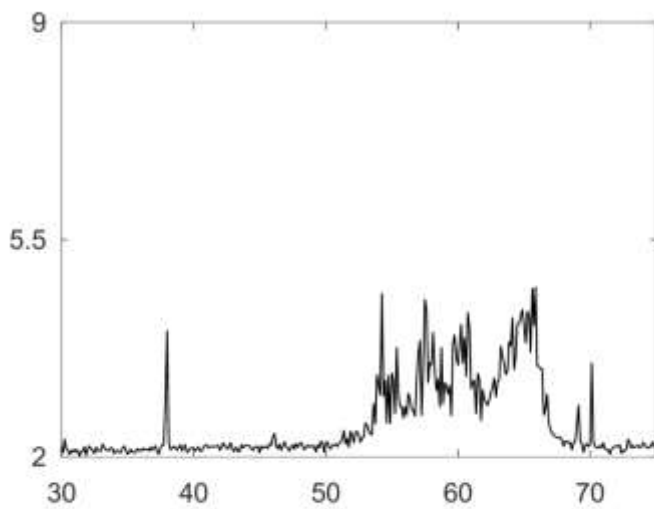
15

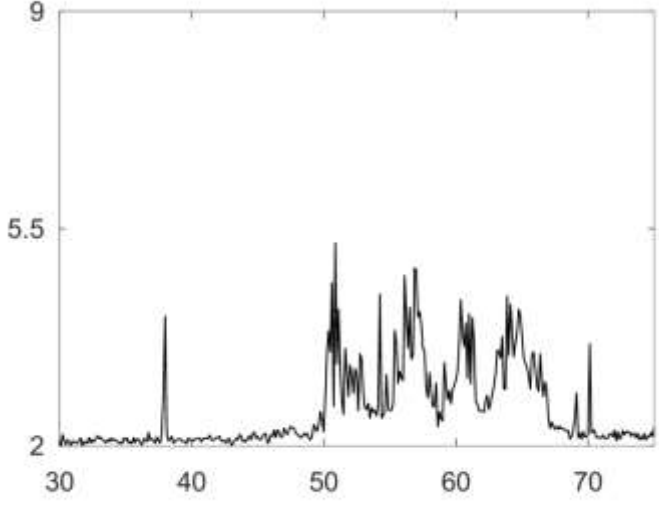
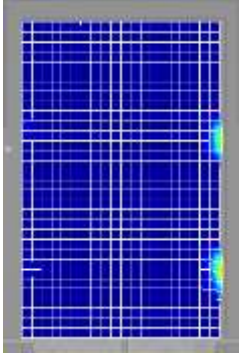
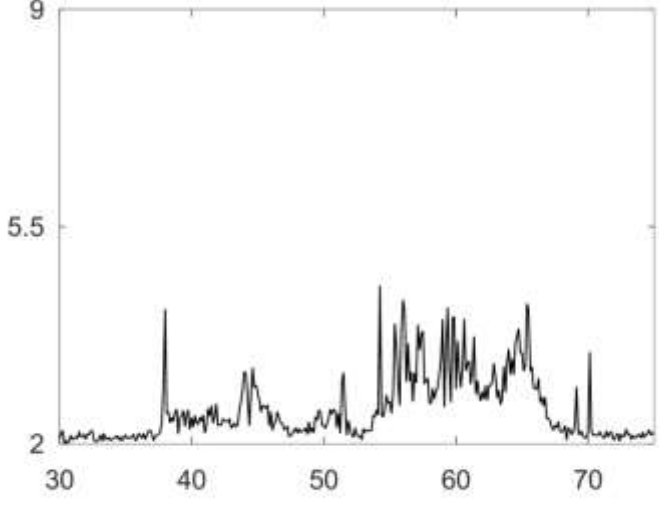
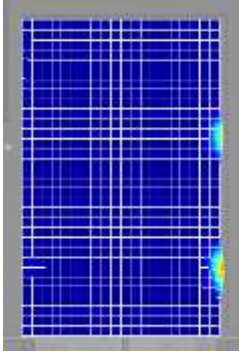
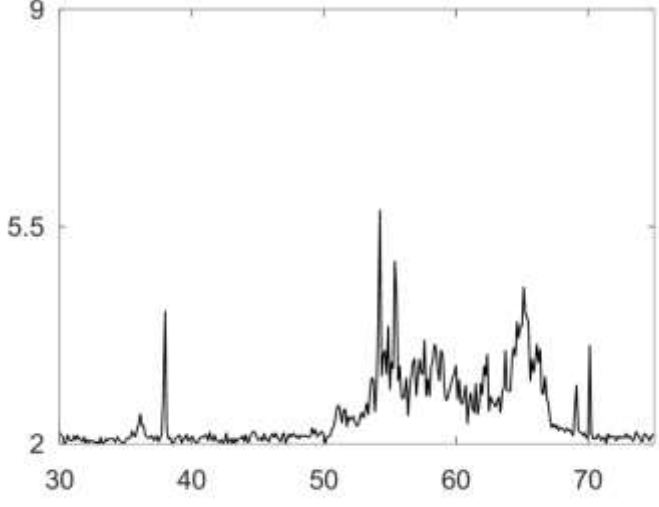
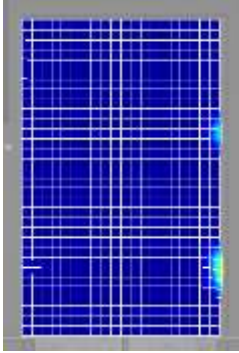


16

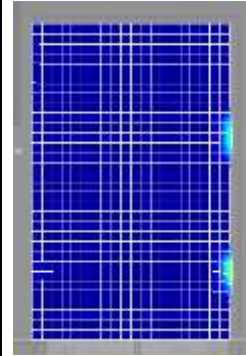
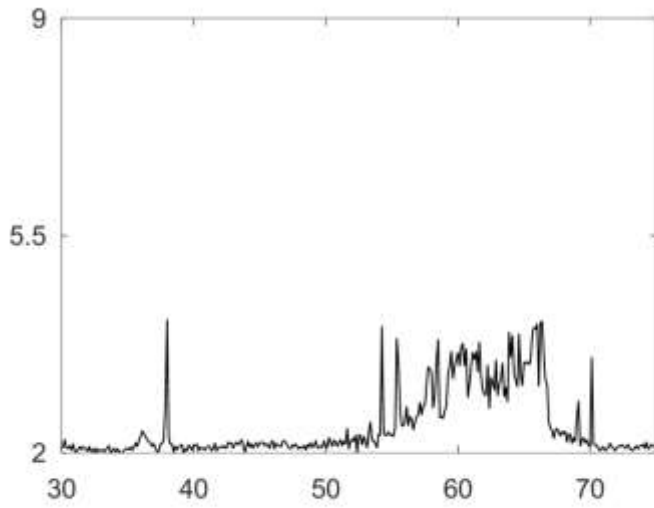


17

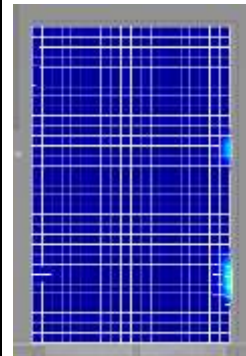
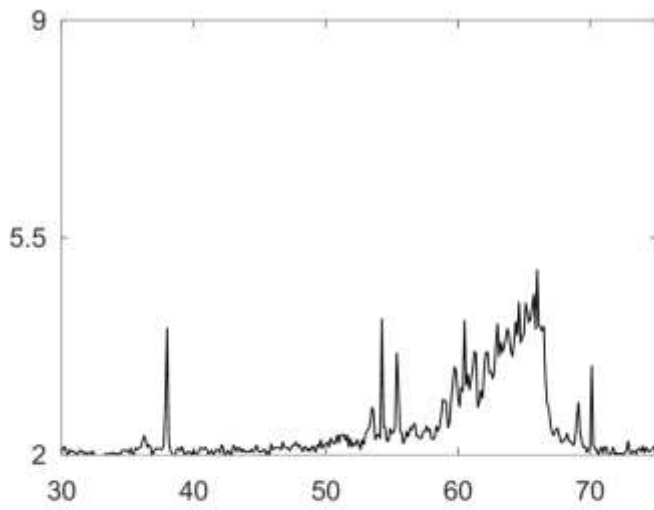


18	 <p>The line graph for row 18 shows a signal on a coordinate system where the x-axis ranges from 30 to 70 and the y-axis from 2 to 9. A sharp peak is visible at approximately x=38. A broader, more complex peak structure is centered around x=50-70, with a maximum value of about 5.5.</p>	 <p>The heatmap for row 18 displays a grid with a vertical band of activity on the right side, corresponding to the x-axis range of 50-70. The activity is represented by a gradient from blue to yellow, indicating intensity.</p>
19	 <p>The line graph for row 19 shows a signal on a coordinate system where the x-axis ranges from 30 to 70 and the y-axis from 2 to 9. A sharp peak is visible at approximately x=38. A broader, more complex peak structure is centered around x=50-70, with a maximum value of about 5.5.</p>	 <p>The heatmap for row 19 displays a grid with a vertical band of activity on the right side, corresponding to the x-axis range of 50-70. The activity is represented by a gradient from blue to yellow, indicating intensity.</p>
20	 <p>The line graph for row 20 shows a signal on a coordinate system where the x-axis ranges from 30 to 70 and the y-axis from 2 to 9. A sharp peak is visible at approximately x=38. A broader, more complex peak structure is centered around x=50-70, with a maximum value of about 5.5.</p>	 <p>The heatmap for row 20 displays a grid with a vertical band of activity on the right side, corresponding to the x-axis range of 50-70. The activity is represented by a gradient from blue to yellow, indicating intensity.</p>

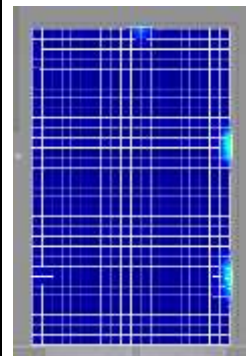
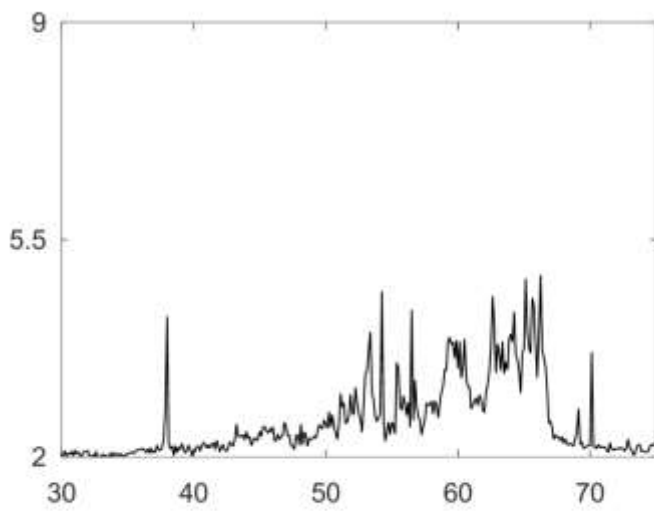
21



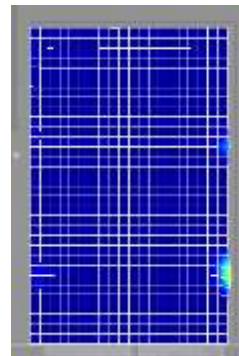
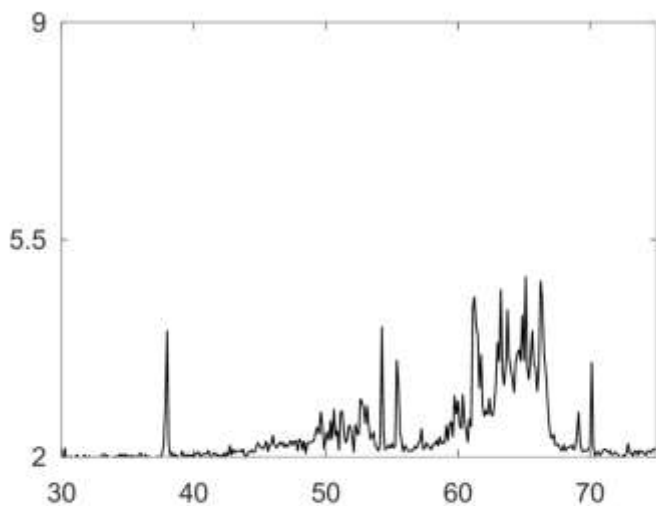
22



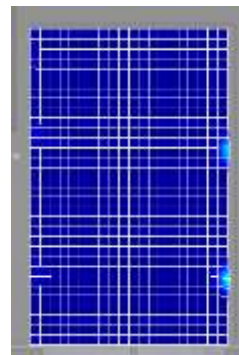
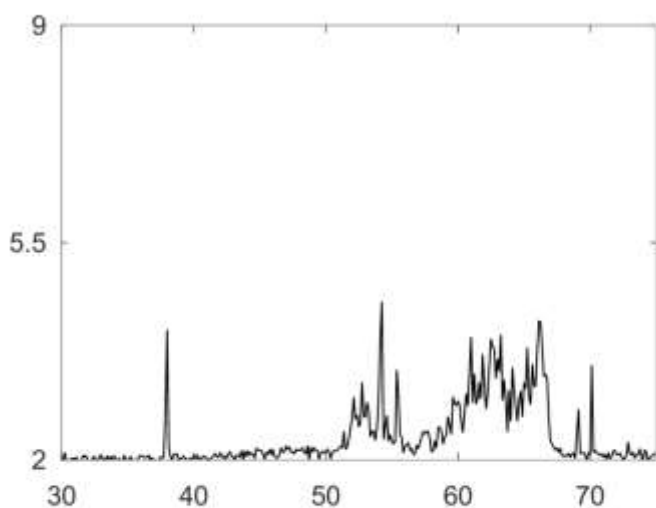
23



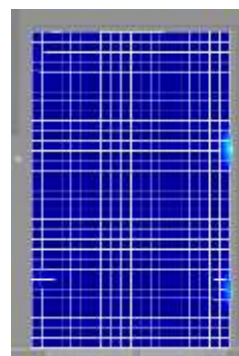
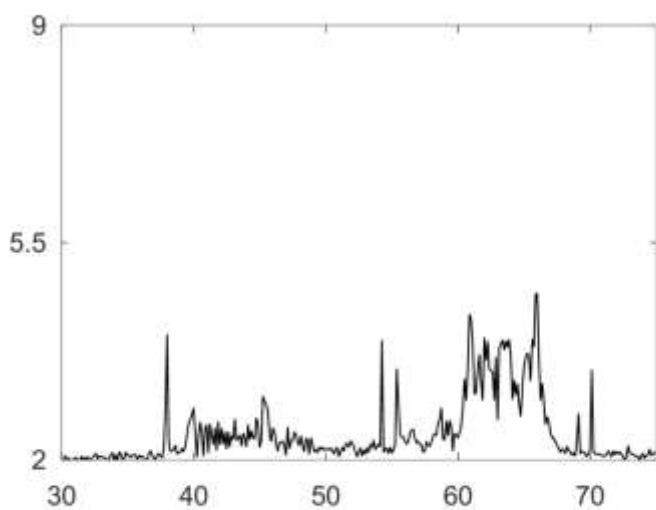
24



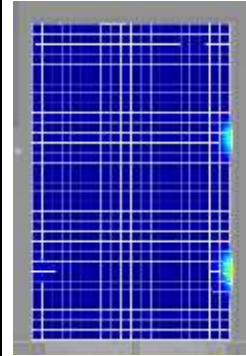
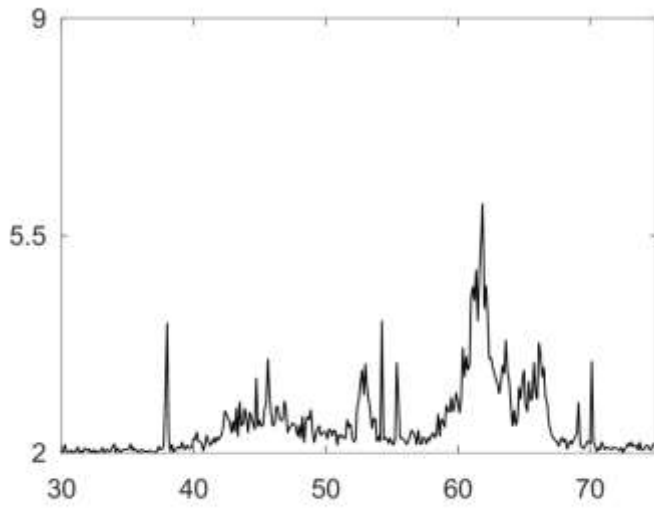
25



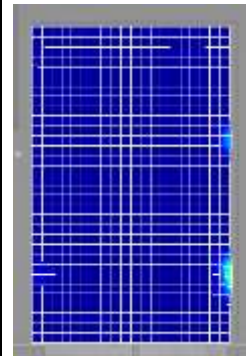
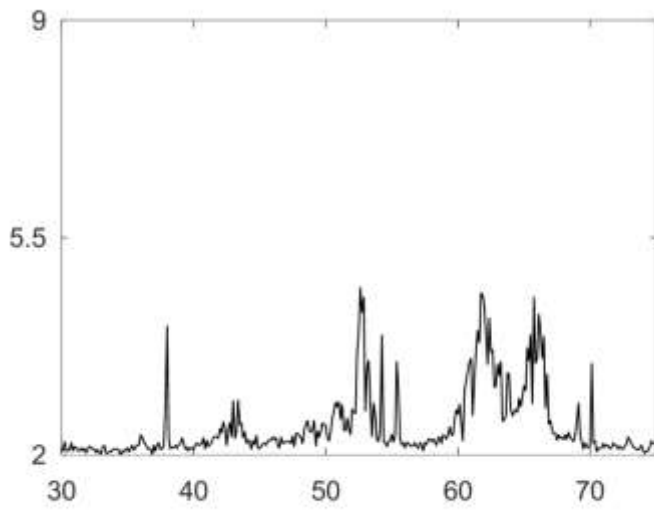
26



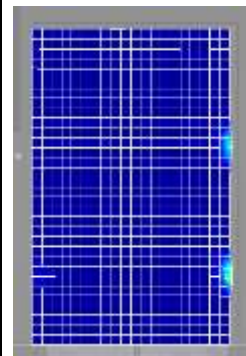
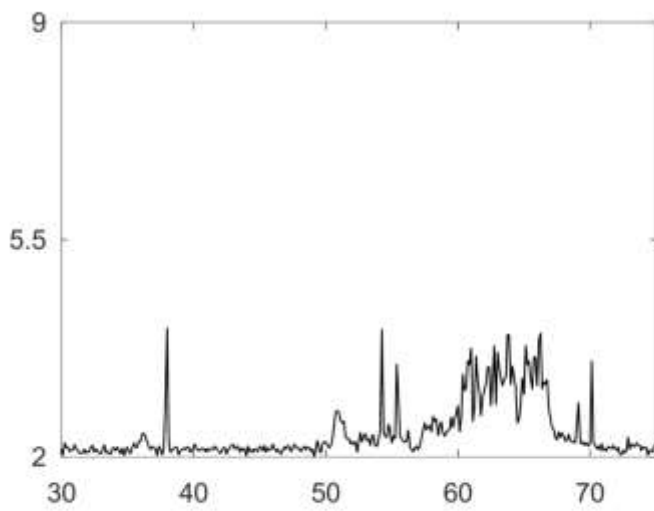
27



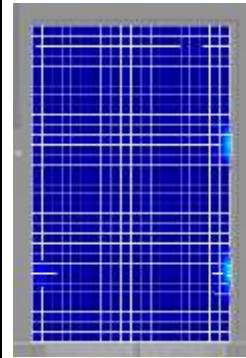
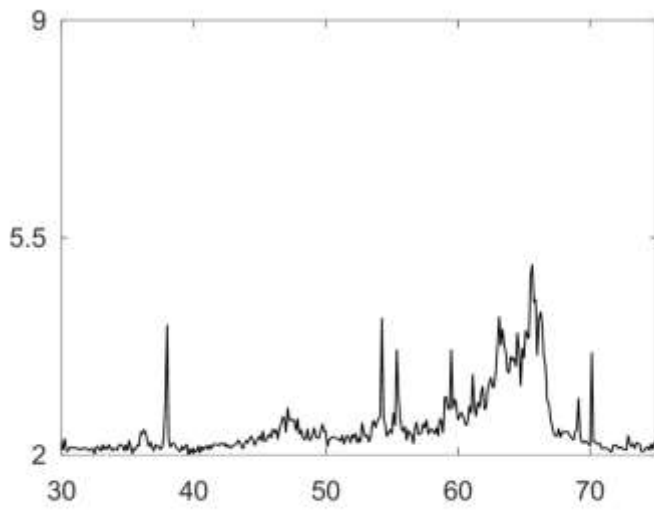
28



29



30



31

